

**A multi-physics-based approach to design of the
smart cutting tool and its implementation
and application perspectives**

Xun Chen

A thesis submitted for the degree of Doctor of Philosophy

College of Engineering, Design and Physical Science
Brunel University

June 2016

Abstract

This thesis presents a multi-physics-based approach to the design and analysis of smart cutting tools for emerging industrial requirements, within an innovative design process. The design process is in stages according to design specifications and requires analysis, conceptual design, detailed design, prototype production and service testing. The research presented in the thesis follows the design process but focuses on the detailed design of the smart turning tool, including mechanical design, electrical wiring and sensor circuitry, embedded algorithms development, and multi-physics-based simulation for the tool system integration, design analysis and optimisation.

The thesis includes the introduction of the research background, a critical literature review of the research topic, a multi-physics-based design and analysis of the smart cutting tool, a mechanical structural detail design of the prototype smart turning tool, the electrical system design focusing on cutting force measurement and embedded wireless communication features, and the final experimental testing and calibration of the smart cutting tool. The contributions to knowledge are highlighted in the conclusions chapter towards the end of the thesis.

The research proposes multi-physics-based design and analysis concepts for a smart turning tool, which can measure the cutting forces on a 0.1 N scale and can also be used to monitor the tool condition, particularly for ultraprecision and micro-machining purposes. The smart turning tool is a sensed tool, constructed with wireless and plug-and-produce features.

The tool design modelling and simulation was undertaken within a multi-physics modelling and analysis environment-based on COMSOL. This integrates the piezoelectric physics with mechanical structural design and radio frequency electronic communications of cutting force signals. The multi-physics simulation method takes

Abstract

account of all design-mechanics-physics-electronics analysis and transformations simultaneously within one computational environment, including FEA analysis, modal analysis, structural deformation, lead piezoelectric effect and wireless data/signal simulation. With the multi-physics simulation developed, the integrated design of the smart turning tool and its performance can be physically analysed and optimised in a virtual environment.

The tool design process follows the total design methodology, which can be strictly executed in several design stages. Both mechanical and electrical design of the smart cutting tool are embodied into the tool detail design. The tool mechanical structure is systematically built from the selection of the tool material, through the structure analysis and further progressed with static force – strain/stress transformation, equivalent force measurement and calibration. The electrical circuitry was systematically developed from developing the customised charge amplifier, detail design of the main circuitry and coding development procedure, preliminary PCB fabrication and multi-sensor port PCB development, as well as the real-time cutting force monitoring programming and interface coding. The experiment calibrations and cutting trials with the tool system are also designed in light of the total design methodology. The experiment procedure for using the smart turning tool is further presented in two different sections.

The thesis concludes with a further discussion on the main research findings, which are further supported by the highlighted contributions to knowledge and recommendations for future work.

Acknowledgements

I would like to express my special appreciation and thanks to my supervisor Professor Kai Cheng, who has been a tremendous mentor for me. I would like to thank him for encouraging my research and allowing me to develop the research scientist career. His advices on both the research as well as on my career have been priceless. I would especially like to thank lecturers, technicians and other staff who work in the AMEE department at Brunel University London. All have been there to support me from the beginning of my PhD study journey and throughout my PhD project process.

A special thanks to my family; words cannot express how grateful I am to my parents for all of the sacrifices that they have made on my behalf. Their prayer for me was what sustained me thus far. I would also like to thank all of my friends who supported me in writing, and encouraged me to strive towards achieving my goals.

Table of contents

Table of contents

Abstract	i
Acknowledgements	iii
Table of contents	iv
Abbreviations	ix
Nomenclature	x
List of Figures	xii
List of Tables.....	xvi
Chapter 1 Introduction.....	1
1.1. Research background	1
1.2. Development of smart cutting tools	3
1.3. Aim and objectives of the research	5
1.4. Research challenges, development and advances from this research.....	6
1.4.1. Scientific challenges.....	6
1.4.2. Technological challenges	7
1.4.3. Development and advances from this research.....	8
1.5. Scope of this thesis	12
Chapter 2 Literature review	14
2.1 Evolution of the cutting condition monitoring	14
2.1.1 Workpiece inspection.....	16
2.1.2 Dynamometers	17
2.1.3 Sensored tools and smart cutting tools.....	19
2.2 Condition monitoring in the machining process	20
2.2.1 Acoustic emissions.....	21

Table of contents

2.2.2	Temperature	23
2.2.3	Cutting forces	24
2.2.4	Vibrations in the machining process	27
2.2.5	Other physical phenomena in the machining system.....	28
2.3	Tool condition monitoring systems	31
2.3.1	Tool wear and the associated key factors.....	33
2.4	Sensored cutting tools and their development.....	34
2.4.1	Review of sensor tools in tool condition monitoring.....	35
2.4.2	Smart machining and smart cutting tools.....	36
2.5	Piezoelectric material applications in sensors and actuators.....	37
2.5.1	Sensing unit and force measurement.....	38
2.5.2	Actuators	38
2.6	Smart system and smart cutting tool	39
2.7	Summary	40
2.7.1	The knowledge gaps identified	41
2.7.2	Research and development needs for smart cutting tools	42
Chapter 3 Multi-physics-based approach to design and analysis of the smart cutting tool		44
3.1.	Introduction	44
3.2.	Design methodology.....	46
3.3.	Integrated multi-physics based approach to modelling and analysis	50
3.3.1.	Evaluation of design constraints	50
3.3.2.	FEA analysis of the tool mechanical structure.....	55
3.3.3.	Modal analysis	57
3.4.	Simulation development.....	58

Table of contents

3.4.1. Multi-physics process and the F-V-E algorithms.....	59
3.5. Machining environment and its effect.....	63
3.6. Simulation of the antenna transmitted efficiency using analogue signal (factory) environment.....	64
3.7. Summary	66
Chapter 4 Development of the prototype smart cutting tool	69
4.1 Introduction and the design process	69
4.2 Conceptual design process	71
4.2.1 Design requirements.....	71
4.2.2 Tool conceptual design and configuration	72
4.3 Detailed design	73
4.3.1 Material selection.....	73
4.3.2 Structural design.....	74
4.3.3 The piezoelectric film sensors and integration.....	78
4.4 The sensors calibration on integrated prototype.....	85
4.4.1 Data acquisition and calibration platform build up.....	86
4.5 Conclusion.....	88
Chapter 5 Electrical system design for smart cutting tools.....	90
5.1 Introduction	90
5.2 Design overview	90
5.2.1 Design requirements and aim of the design related to simulation	91
5.3 Design of the charge amplifier and Bluetooth adaption.....	92
5.3.1 Component selection and justification.....	92
5.3.2 Charge amplifier design overview	96
5.3.3 Amplifier design.....	97

Table of contents

5.3.4	Circuitry sketch and preliminary board design	99
5.3.5	Final circuit board design.....	105
5.3.6	Force measuring resolution scale	109
5.4	Testing and calibrations.....	111
5.4.1	Circuitry testing.....	112
5.4.2	Test with PC communication and receiver program design	114
5.5	Conclusion.....	114
Chapter 6 Performance testing of the smart cutting tools		116
6.1	Smart cutting tool calibration supplementary.....	116
6.1.1	Experiment process design.....	117
6.1.2	Bench calibration set up	118
6.1.3	Dynamic responses test	119
6.2	Experiment set up on 1st attempt of cutting trial	120
6.2.1	Work-piece material and cutting parameter	122
6.2.2	Dynamometer	123
6.2.3	Data acquisition.....	124
6.2.4	Dynamic performance of the smart cutting tool	124
6.2.5	Static force response	125
6.3	Experiment on Moore 250UPL ultraprecision turning machine	127
6.3.1	Work-piece material and cutting parameters	128
6.3.2	Tool signal stability control test.....	129
6.3.3	Cutting force analysis.....	130
6.3.4	Work-piece inspection	131
6.4	Summary	133
Chapter 7 Conclusions and recommendations for future work.....		134

Table of contents

7.1	Conclusions	134
7.2	Contributions to knowledge	135
7.3	Recommendations for future work	137
	References:	139
	Appendix A: A list of publications arising from the research.....	152
	Appendix B: Key equipment used for this research.....	153
	Appendix C: Components data sheet for the smart cutting tool.....	159
	Appendix D: Program codes developed for the smart cutting tool	162
	Appendix E: Schematic diagram for the smart cutting tool	180
	Appendix F: Pro-Engineer CAD plotting for the smart cutting tool - top and bottom parts	181

Abbreviations

AE	Acoustic emission
CCD	Charge-coupled device
CPS	Cyber physical systems
FEA	Finite element analysis
IDE	Integrated development environment
IOT	Internet of things
LDO	Low drop out
MEMS	Microelectromechanical System
Op-amp	Operational amplifier
PCB	Printed circuit boards
PCBN	Polycrystalline cubic boron nitride
PI	Physik Instrumente
PZT	Lead, zirconium and titanium
RPM	Revolutions per minute
SAW	Surface acoustic waves
TCM	Tool condition monitoring
TFTS	Thermocouple
USART	Universal Synchronous Asynchronous Receiver Transmitter
VAM	Vibration assistance machining

Nomenclature

Nomenclature

C_{ADC}	Resolution of analogue to digital convertor
$[C^E]$	Stiffness matrix evaluated at constant electric field
C_S	Capacitor in charge amplifier (F)
C_s	Capacitor in charge amplifier (F)
D	Electric displacement vector
$[e]^t$	Piezoelectric matrix relating stress/electric field
$[\epsilon^S]$	Dielectric matrix evaluated at constant strain
$[e]$	Piezoelectric matrix relating stress/electric field
E	Electric field vector;
F	Cutting force (N)
g_{33}	Piezoelectric voltage constant
K	Spring constant
Q	Electron charges (C)
R_b	Resistance in charge amplifier (Ω)
R_f	Resistance in charge amplifier (Ω)
R_{in}	Resistance in charge amplifier (Ω)
R_s	Resistance in charge amplifier (Ω)
S	Strain vector
T	Stress vector
T_C	Mechanical pressure on piezoelectric surface (N/m^2)

Nomenclature

V_{ref}	Reference voltage in circuitry design
V_{Ff}	Voltage of feed direction from piezoelectric sensor (v)
V_{Fr}	Voltage of radial direction from piezoelectric sensor (v)
V_{Fvp}	Voltage of vertical piezoelectric sensor (v)
V_{cf}	Voltage of cutting force direction from piezoelectric sensor (v)
V_{out}	Voltage output from circuit board (v)
V	Voltage (v)
Vdd	Drain negative power (v)
Vss	Power supply (v)
Vt	Variation voltage in design of charge amplifier (v)
X	Displacement ($\mu\mathbf{m}$)
Z_f	Impedance of the charge amplifier (Ω)

List of Figures

Figure 1.1: An overview of the future industry applied with smart manufacturing systems	2
Figure 1.2: The role of the smart cutting tool in smart manufacturing	3
Figure 1.3: Smart cutting tools development	4
Figure 1.4: Diamond tool wear examples - SEM photographs of the cutting edge	7
Figure 1.5: Development of force-based smart cutting tools	8
Figure 1.6: Radio frequency signal-based smart cutting tool	9
Figure 1.7: The SAW-based smart cutting tool	10
Figure 1.8: Bluetooth-based smart cutting tool.....	11
Figure 1.9: The scope of the PhD thesis	12
Figure 2.1: Product quality key factors in machining process [Park and Tran, 2014]....	15
Figure 2.2: Overview of machining condition monitoring methods.....	16
Figure 2.3: Kistler Minidyn type 9256C	18
Figure 2.4: Machine process condition monitoring methods.....	20
Figure 2.5: Acoustic emission sensor.....	21
Figure 2.6: Cutting moment captured by the infra-red temperature camera.....	24
Figure 2.7: Cutting force components on a single point tool during turning [Dimla and Lister, 2000]	26
Figure 2.8: Force time diagram for static and dynamic force [Dimla and Lister, 2000]	27
Figure 2.9: Physical phenomenon occurring in machining [Bhuiyan and Choudhury, 2014]	32
Figure 2.10: Tool wear forms in orthogonal metal cutting [Dimla and Lister, 2000]	34
Figure 2.11: SAW-based smart cutting tool.....	35
Figure 2.12: Piezoelectric effect on piezoelectric cylinder	37
Figure 2.13: A pyramid of smart manufacturing system	39
Figure 2.14: Literature review steps.....	42
Figure 2.15: Plug-and-play software development environment [Byrne et al., 1995]....	43

List of figures

Figure 3.1: Comparison of the development of a smart cutting tool versus the MEMS	45
Figure 3.2: One scenario of applying the smart cutting tool in the machining system...	46
Figure 3.3: Flowchart of smart cutting tool mechanical design process.....	49
Figure 3.4: Multi-physics approach design specifications.....	50
Figure 3.5: 3D illustration of the smart cutting tool mechanical design. (a) Force load point (b) Fixed surface; (c) Piezoelectric ceramic demonstration; (d) Overview of the tool	53
Figure 3.6: Surface displacement under 10 N, Y direction without piezoelectric ceramic (a); Y direction with piezoelectric ceramic (b); X direction without piezoelectric	55
Figure 3.7: Fundamental natural frequency (a) and second step natural frequency (b)..	57
Figure 3.8: Flow chart of the simulation approach	58
Figure 3.9: Force to voltage transformation cutting force direction (a). Feed force direction (b).....	59
Figure 3.10: Linear relationship between the simulated cutting force and the sensor voltage output (a) and with radial force 1 N simultaneously (b) Linear relationship between the simulated feed force and the sensor voltage output (c) with radial force 1 N associated (d).....	61
Figure 3.11: Real Bluetooth module and 3D model antenna under COMSOL	64
Figure 3.12: Machine environment simulation for dipole antenna transmission efficiency.....	65
Figure 3.13: Electric field result in machining environment	66
Figure 3.14: Physical couplings in smart cutting tool.....	67
Figure 4.1: Design process for the smart cutting tool	70
Figure 4.2: Detail design of the smart cutting tool.....	73
Figure 4.3: Tool design and configurations mechanical	74
Figure 4.4: The design configuration of the smart cutting tool 3D model (a) and the design configuration of the smart cutting tool prototype (b)	76
Figure 4.5: The design of upper part (left) and base part (right) of the smart cutting tool	77
Figure 4.6: Diamond micro-cutting tool and diamond smart cutting tool comparison...	77
Figure 4.7: The bench test of the piezoelectric ceramic response.....	78

List of figures

Figure 4.8: Force response result of the piezoelectric sensor (a) demonstration compared with capacitive sensor (b).....	80
Figure 4.9: The material data of piezoelectric ceramic.....	81
Figure 4.10: 2D plot of stress deformation, 1 N force on cutting force direction (top), and 1 N force on feed force direction (bottom).....	82
Figure 4.11: The linear ratio relationship between force sensors and piezoelectric reference voltage	84
Figure 4.12: Preliminary dynamic response calibration set up.....	86
Figure 4.13: Smart cutting tool calibration platform	86
Figure 4.14: (a) Linear relationship between the emulated cutting force and the sensor 1 voltage output; (b) Linear relationship between the emulated feed force and the sensor 2 voltage output; (c) Hysteresis at the sensor 1 with loading and unloading test	88
Figure 5.1: Electrical design of the smart cutting tool for real-time monitoring	91
Figure 5.2: The theoretical equivalent circuit model for a piezoelectric material	97
Figure 5.3: The charge amplifier design sketch.....	97
Figure 5.4: Charge amplifier design circuit diagram	99
Figure 5.5: Circuit diagram of the microcontroller and Bluetooth	101
Figure 5.6: Preliminary circuitry on a breadboard.....	102
Figure 5.7: 1st attempt single sensor input circuit board	103
Figure 5.8: 2nd attempted circuit diagram of the microcontroller and Bluetooth	106
Figure 5.9: CAD sketch of the PCB routing	107
Figure 5.10: 2nd attempt on the circuit board with three sensor input in used	108
Figure 5.11: Flow chart of the cutting force converted to digital signal process.....	109
Figure 5.12: The prototype cutting tool with the wireless system embedded.....	112
Figure 5.13: A test example sensor response for 1.5 N	113
Figure 5.14: The receiver program interface.....	114
Figure 6.1: The smart cutting tool calibration process flow-chart.....	117
Figure 6.2: Dynamic force sensing test.....	118
Figure 6.3: Dynamic response to the square and sinusoidal force modes by the smart cutting tool and Kistler MiniDyn dynamometer respectively: (a) at the low frequency of 4 Hz; and (b) at the high frequency of 100 Hz.....	120

List of figures

Figure 6.4: Cutting trials setup with the smart cutting tool on a self-developed customised cutting machine	121
Figure 6.5: Construction of Kistler 9256C dynamometer.....	123
Figure 6.6: Dynamic force response in 1 st cutting trial attempt.....	125
Figure 6.7: The smart cutting tool's reading of cutting force respectively for (a) - Aluminium T 6082, (b) - Single crystal Silicon, (c) - Titanium 6Al-4V.....	125
Figure 6.8: Comparison of cutting forces and feed force measured by the smart turning tool and Kistler MiniDyn dynamometer	126
Figure 6.9: Cutting trials setup with the smart turning tool	127
Figure 6.10: Wireless cutting force real-time monitoring.....	129
Figure 6.11: Representative comparison of the cutting force data from smart cutting tool (Blue) and Kistler dynamometer (Red) in one cut. Cutting force (a) and radial force (b)	131
Figure 6.12: Example of workpiece manufactured by the smart cutting tool.....	132
Figure 6.13: Surface roughness profile from Zygo 3D profiler	132

List of Tables

Table 3.1: The simulated cutting force correlated to the piezoelectric sensor result	60
Table 3.2: The simulated feed force correlated to the piezoelectric sensor result	62
Table 3.3: The simulated result of the coupling forces on vertical piezoelectric sensor	62
Table 4.1: Smart cutting tool sensor voltage output with regulated piezoelectric ceramic reference voltage output	83
Table 6.1: Material characteristics of the workpiece in cutting trial.....	122
Table 6.2: Cutting parameters on Moore 250UPL lathe machine	128
Table 7.1: Assessment and comparison of three smart cutting tools	135
Table 7.2: The standard technical data for the smart cutting tool.....	136

Chapter 1 Introduction

This chapter provides the overview of the research with particular focus on the science and technical challenges of the project and its industrial specification. The main scope of this chapter is further highlighted in the aims and objectives of the research as identified in the thesis structure and research scope.

1.1. Research background

At the end of the 18th century, when the water steam engine was developed, mankind stepped into an industrial revolution. It was the first of several such revolutions and may be called Industrial 1.0. Industrial 2.0 and 3.0 followed in the 1870s and 1970s respectively. Over the last two decades, with the advance of ICT and web-based technology, a group of engineers and academic scientists have developed a concept of integrating all levels of the information systems in the industry, as presented at the National Academic Science and Engineering Conference at Germany. This concept is working with Internet of Things (IoT). Working on cyber-physical systems (CPS) and aiming for further smart manufacturing is seen as the beginning of Industrial 4.0; the new industrial revolution is leading the world into another stage in humans' industrial manufacturing history [Kagermann et al., 2014].

The new smart manufacturing system must integrate with information communication technology. It includes, but is not limited to, the following aspects as shown in Figure 1.1: smart logistics, smart production, smart mobility, monitoring information, big data and personal digital products.

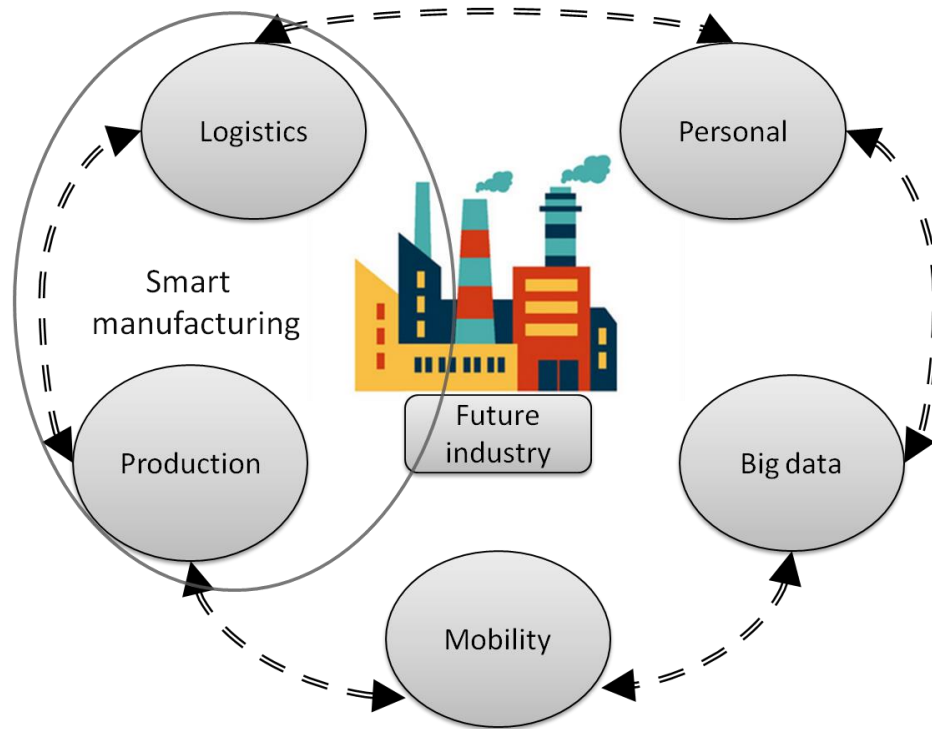


Figure 1.1: An overview of the future industry applied with smart manufacturing systems

In 2008, Edward Lee proposed the concept of cyber physical systems (CPS). Cyber physical systems are an integration of computation and physical process. Embedded computers and networks monitor and control the physical processes, usually with feedback loops where physical processes affect computations and vice versa [Edward, 2008]. To satisfy the increased production demands in this new industrial revolution, the whole manufacturing system has to become smart enough to be evaluated into smart manufacturing. Hence, in the aspect of precision manufacturing engineering, smart machining is our essential current topic. In smart machining, the technology related to manufacturing process monitoring has a very important role in today's manufacturing. A smart cutting tool is a key concept in machining manufacturing engineering. From Figure 1.2, it can be seen that the smart cutting tool fits all the features of smart machining at operational level. The integration of the information at the very front end of production is called the operational level of smart machining.

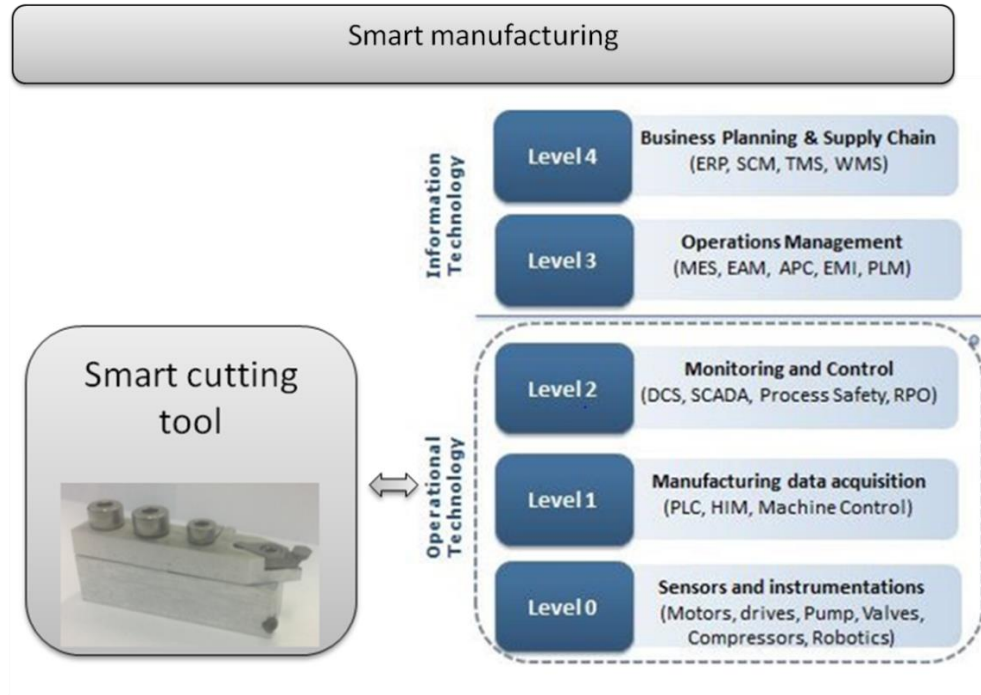


Figure 1.2: The role of the smart cutting tool in smart manufacturing

1.2. Development of smart cutting tools

Nowadays in the world market, there are various commercialised force sensors in manufacturing industry. Technicians aim to use these force sensors to optimise the efficiency of production. All the designed tools were-based on force monitoring. Various ‘manufacturing systems’ were designed as ‘Real-time cutting tool condition monitoring’ in order to reduce production costs and enhance production efficiency.

The in-process monitoring systems generally contain sensors, and allied data transfer, signal processing, status recognition functions and response control algorithms. There are various methods for monitoring the cutting condition, such as force measurement, temperature measurement, acoustic emission, etc. Force-based smart cutting tools mostly use strain gauges to detect in traditional manufacturing machines, but piezoelectric ceramics have become more popular in the last decades.

A smart cutting tool should be a ‘plug-and-produce’ device similar to an USB device on a computer. It has the ability to be used on different computation platforms while physically working inside the machine. The smart cutting tool’s development chart was given in Figure 1.2.

During the period of research, we have used both wire and wireless data transmission for analysing the cutting process in order to optimise the cutting result during the machining process and extend the diamond tool life.

This thesis will focus on the most recent wireless smart cutting tool’s design and its implementation with application perspectives.

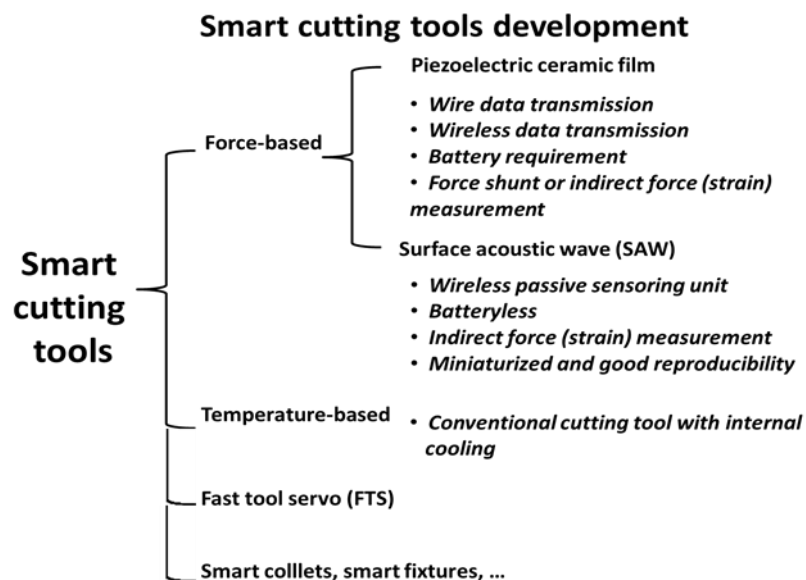


Figure 1.3: Smart cutting tools development

A smart cutting tool is not only limited by measuring forces or temperature. It must include ‘plug-and-produce’ ability, which means that the unit is easy to install and can be instantly used on different machine and computational platforms. The key feature is to have the ability to monitor the cutting condition in real time. In other words, when the machining goes abnormal during the manufacturing process, the smart cutting tool

reports to users or control systems to correct the machining procedure with continuation or cancel the current machining process to prevent a greater loss.

Manufacturing process monitoring technology has taken on a very important role in today's manufacturing. There are various methods to monitor the cutting condition, such as force measurement, temperature measurement, acoustic emission, etc. The force measurements used are often stress measurements in industries and research, but in this smart cutting tool experiment, direct force measurement was used. An accurate, high performance sensor for ultraprecision machining is difficult to produce because the cutting force, power and acoustic emissions are very minor in comparison with conventional machining processes.

The latest designed smart cutting tool was formed with two parts: mechanical structure and electronic circuitry. The simulation will be explained in the following chapter using the COMSOL multi-physics structural system to analyse the mechanical design and the process from the cutting force (N) and electrical signal (V) from the sensing unit.

1.3. Aim and objectives of the research

This research aims to investigate an industrially feasible approach to designing and analysing the smart cutting tool, which can measure and diagnose the cutting forces in real time, with a high resolution reaction during the cutting process and mobility of usage.

The distinct objectives of this research are to:

- Carry out a critical review of the state of the development of the smart cutting tool;
- Investigate a multi-physics-based approach to modelling the smart cutting tool, from the mechanical design to the wireless signal analysis at the control end;
- Develop a prototype of the smart cutting tool for cutting trial experiment;

- Undertake further comparative investigation on smart cutting tools, including RF cutting tool, SAW cutting tool and BT smart cutting tool; and
- Carry out well-designed cutting trials using the smart cutting tools, with in-depth analysis of results and discussion.

1.4. Research challenges, development and advances from this research

1.4.1. Scientific challenges

In the cutting process, the diamond cutting tools are in direct contact with the workpieces, which are often titanium, silicon, aluminium and other metallic materials. Although diamond is the strongest structural material in the world, it will get worn because of the repetitive process and fatigue. Also, in micro-cutting, tool wear occurs for one more reason than in traditional cutting, namely atomic fracture. In Figure 1.4, the tool wear pictures were taken using a large magnification microscope. This shows the tiny breakages that would hardly be noticed during the machining process, and normally the workpiece would fail the quality test afterwards. Importantly, time and money has been wasted.

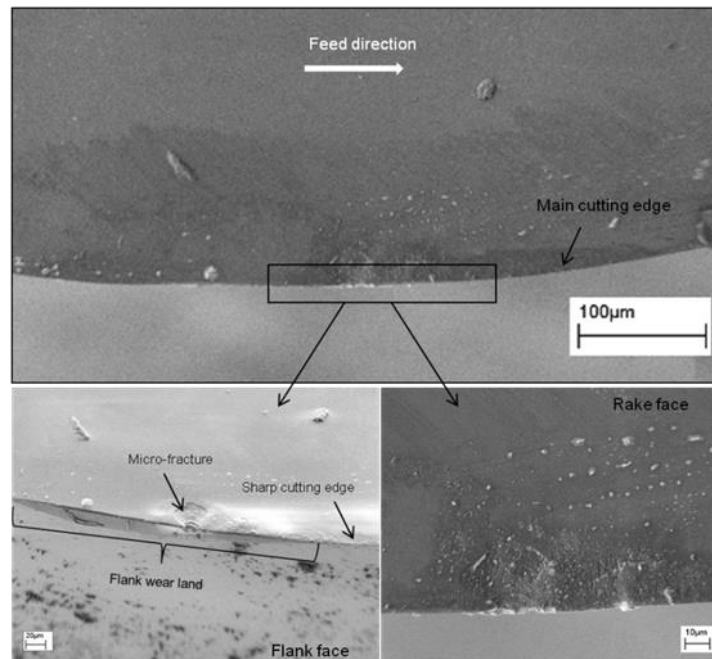


Figure 1.4: Diamond tool wear examples - SEM photographs of the cutting edge

Scientists have been thinking over and over again about possible detecting methods, and various algorithms have been built-based on the cutting forces or cutting temperature to couple with the tool wear. This smart cutting tool is designed-based on real-time online cutting condition monitoring of cutting force.

1.4.2. Technological challenges

A force-based smart cutting tool should contain the features of being intelligent, secured, managed and connected. Also, it has requirements of sensitivity, cross-talk, measuring range, responding bandwidth, operating temperature range, plug-and-produce and most importantly size and weight.

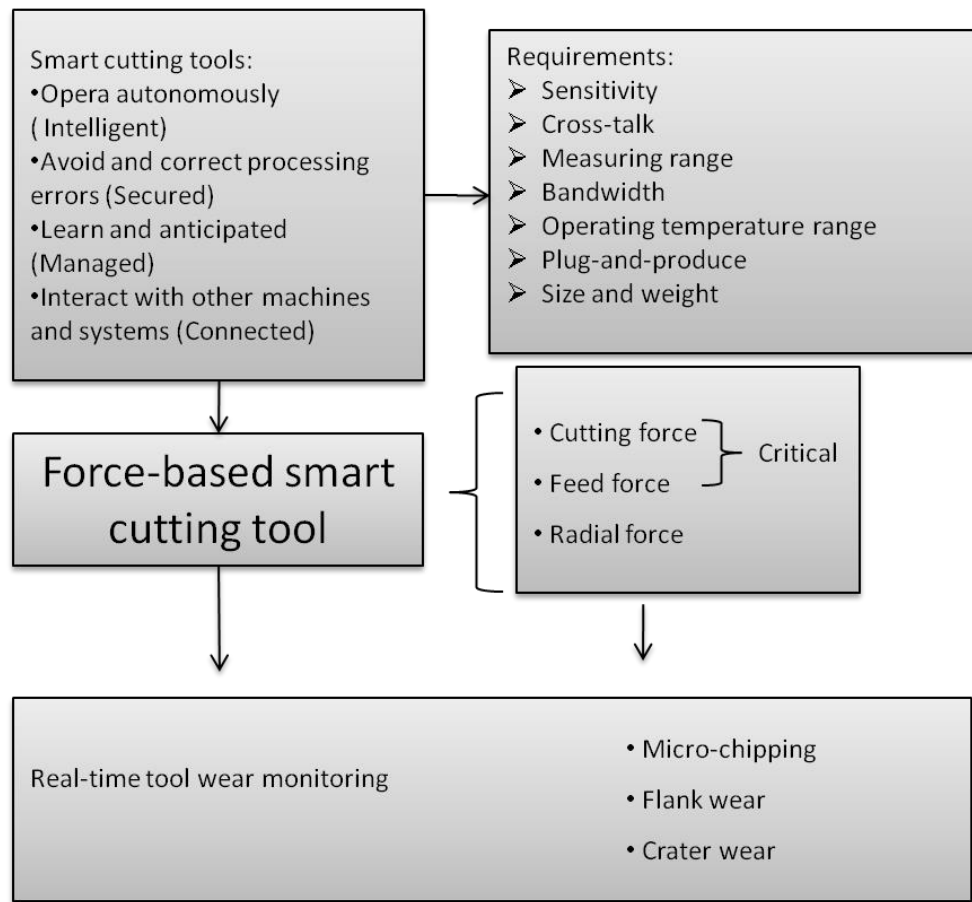


Figure 1.5: Development of force-based smart cutting tools

In micro-machining, the smart cutting tool should have an accurate high performance sensor for ultraprecision machining, and this is difficult to produce because the cutting force, power and acoustic emissions are extremely small in comparison with conventional machining processes. Because physical changes are tiny, the electrical signals are weak and small when transmitted from the sensor, which could lead to inappropriate reading through touching the wires. Wireless technology could be the best solution to this issue.

1.4.3. Development and advances from this research

The author has successfully developed several wireless cutting tools that are used on a manufacturing machine [Wang et al., 2014; Chen, 2014], with in addition a paper

published on the following projects:

- Wireless sensing unit-based smart cutting tool (1st smart cutting tool);
- Surface acoustic wave (SAW)-based smart cutting tool (2nd smart cutting tool);
and
- Bluetooth-based smart cutting tool (3rd smart cutting tool).

The smart cutting tool design started from a radio frequency signal wireless sensor-based cutting tool, which was a cooperation with Renishaw in 2011. It was focused on cutting force monitoring perspective on the CNC cutting machine.

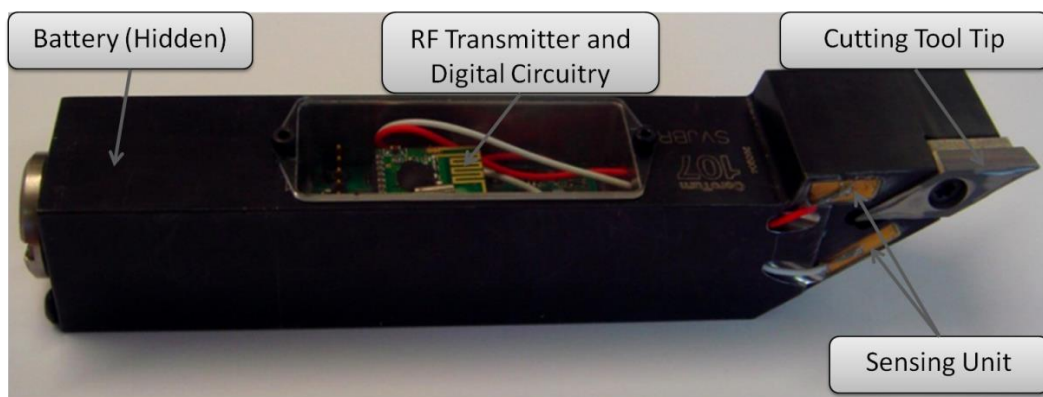


Figure 1.6: Radio frequency signal-based smart cutting tool

The idea of developing this smart cutting tool were because the use of commercial dynamometers to determine the cutting forces is limited by several aspects: high costs, poor performance in certain environments and possibility of interference with cutting dynamics.

The first smart cutting tool was designed using a single layer piezoelectric ceramic for a sensing unit to detect the cutting forces. It measures the strain and is limited on sensitivity and noise elimination as it is using radio frequency wireless technology.

The second smart cutting tool was-based on surface acoustic waves that are used to

determine the cutting force and feed force on cutting machines. The tool was not qualified for micro-manufacturing force process monitoring due to its force resolution being unable to meet the requirement for micro-machining.

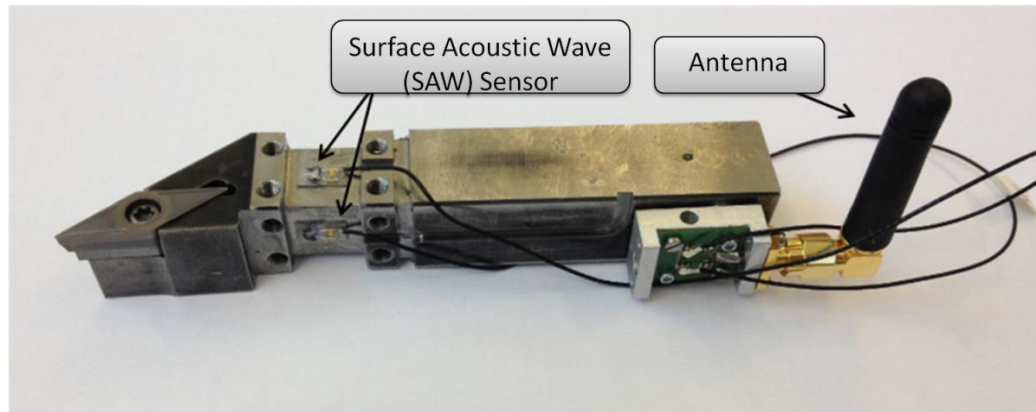


Figure 1.7: The SAW-based smart cutting tool

It is also a strain gauge method using surface acoustic wave (SAW) strain sensor. This smart cutting tool is capable of measuring the cutting force and feed force on-line. Surface acoustic waves are ultrasonic waves propagating along the surface of solids; the transmission and reception principles are based on piezoelectric transducers. This was the author's first attempt at designing a smart cutting tool applied in harsh cutting environments [Wang et al., 2014]. Because of the limitation of using surface acoustic waves (SAW), the monitoring process is unable to visualise in real time as well; also the wireless range is limited and there is a power supply issue for continuously measuring. Hence the idea of investigating a new approach to monitor the cutting process has been proposed in response to these problems.

Therefore, the latest research of the third smart cutting tool-based on a Bluetooth transmission approach was designed to focus on micro-cutting force monitoring, with small force resolution and high-frequency sensitivity. This prototype has the best operation range and smallest force resolution.

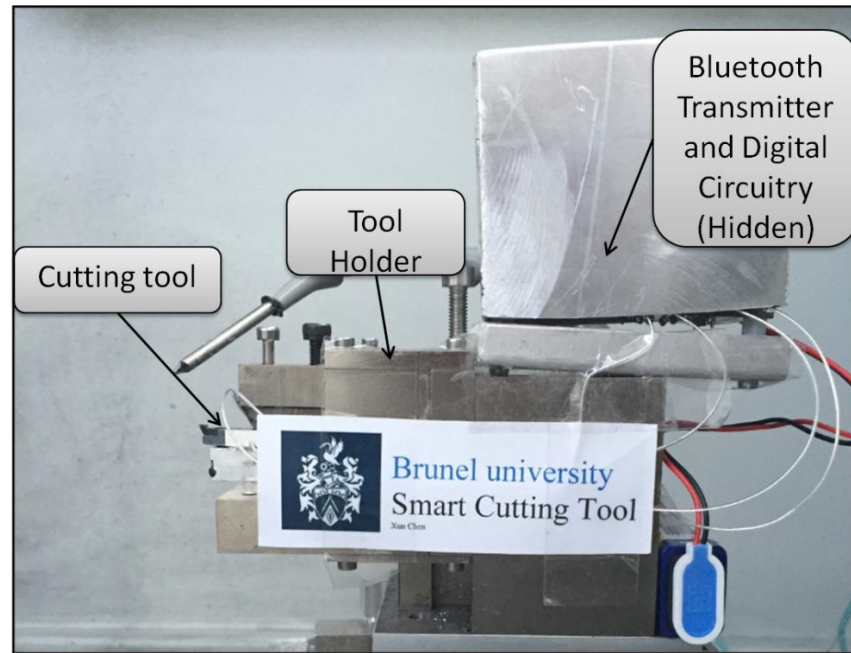


Figure 1.8: Bluetooth-based smart cutting tool

The idea of designing this Bluetooth technology-based smart cutting tool was to optimise it greatly compared with the previous smart cutting tools. The maximum sampling rate of the SAW strain sensors from previous research is 150 Hz and the interrogation distance is much shorter between the antenna and the interrogator than for Bluetooth.

This new smart cutting tool has a strong response in any cutting environment, longer operation distance and a more precise sensitivity. All these features are aimed to apply this smart cutting tool to micro-cutting environments.

Bluetooth-based wireless smart cutting tools are invented by focusing on the concept of 'plug-and-produce', meaning that they are adaptable devices that could fit to any manufacturing machine and operate it. Also, most electronic devices with Bluetooth connection, such as a tablet PC, smart phone, iPad, etc., could be at the receiver end.

1.5. Scope of this thesis

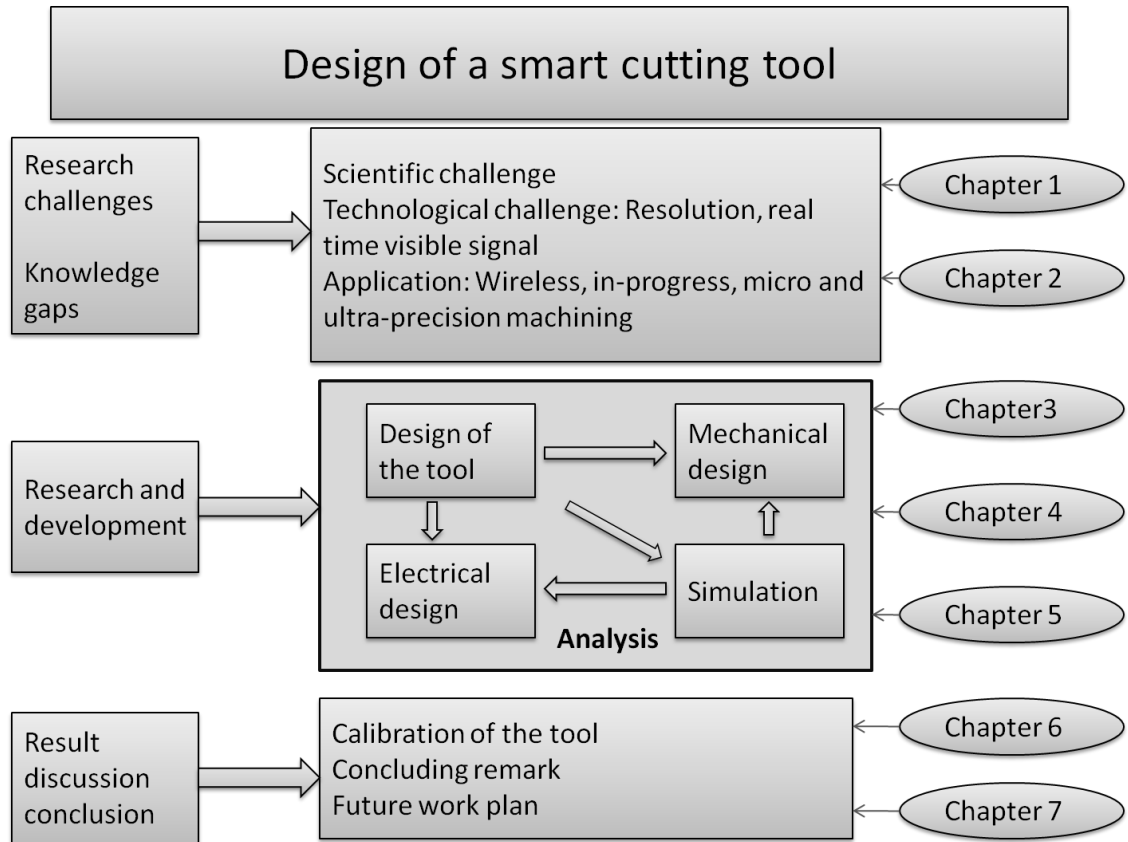


Figure 1.9: The scope of the PhD thesis

The thesis comprises seven chapters, which are structured as illustrated in Figure 1.9.

Chapter 1 introduces the background to the research. It further presents the scientific and technological challenges of the research project, and the main aim and objectives of this PhD research and the final dissertation scope are determined.

Chapter 2 critically reviews the present and previous researches in tool condition monitoring methods, and also sensor tools developed for the condition monitoring with the purpose of identifying the knowledge gap and reasoning for the design of this smart cutting tool.

Chapter 3 demonstrates the design of modelling and simulation of the smart cutting tool and its performance analysis by using the multi-physics approach via COMSOL multi-physics software, explaining the design process in simulation and optimising the tool design. The simulation can be broken down in to three main parts: mechanical, electrical and implementation. The modelling approach integrates cutting force, electron charges and radio wave models,-based on a novel mechanism and machining environment.

Chapter 4 illustrates the prototype design process from conceptual design to detailed design, and then to the manufacturing process, along with the calibration to testify the accuracy and reliability of the prototype.

Chapter 5 demonstrates the electrical system design process of the smart cutting tool, carefully from conceptual design to detail design, and the prototype manufacture process. The methods to achieve the smart cutting tool's core features in the abilities of wireless and real-time monitoring are explained in detail.

Chapter 6 presents the design of the experiment procedure and in brief the experiment step by step. The supplementary calibration of the smart cutting tool of previous chapters is explained. The experiment procedure is divided into two sections, with the second section also separated in to another two sections. The cutting trial successfully proves that the proposed smart cutting tool was fully calibrated and ready to use.

Chapter 7 draws conclusions from the research and presents a summary of the thesis and contribution to knowledge with complete user instructions for the new designed smart cutting tool. It also makes recommendations for future work and the expected results are explained.

Chapter 2 Literature review

Smart cutting tools have been spawned from the new development and integration of sensing technology and a tool condition monitoring (TCM) system. In this chapter, the study of cutting condition monitoring leads to TCM. The representative physical phenomena and their experimental methods are reviewed in this chapter. Several different sensor tools are considered and the concept of the smart cutting tool is reviewed briefly. The technologies of piezoelectric materials are also introduced.

2.1 Evolution of the cutting condition monitoring

Throughout the process of machining, cutting condition monitoring was a big topic and still is, both academically and industrially. In this section the evolutions of the cutting condition monitoring methods are reviewed.

Machining process is the name for the metal part removal process in industry. Cutting condition monitoring is highly related to machining process. Park and Tran [2014] have summarised the core parameters affecting the workpiece quality in machine processing. As Figure 2.1 shows, in the machine process, condition monitoring contains the controls of cutting parameters such as feed rate, cutting speed, depth of cuts and environment factors, such as cooling and lubrication, and chip flows, etc. [Park and Tran, 2014]. Condition monitoring is basically detecting, collecting and analysing these signals, and the signals must be captured in order to use appropriate methods for the collecting and analysis afterwards.

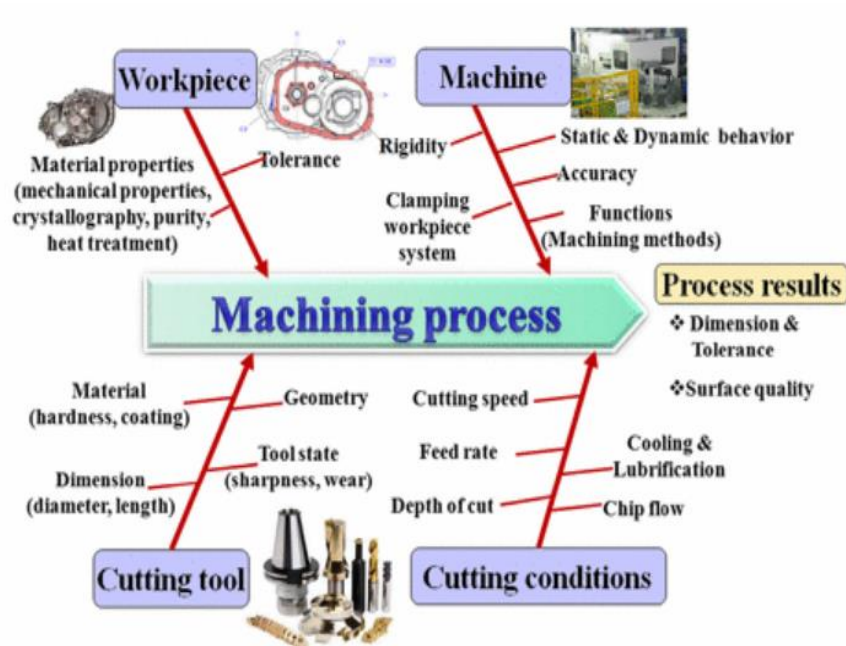


Figure 2.1: Product quality key factors in machining process [Park and Tran, 2014]

Condition monitoring is the key factor that affects the robustness and reliability during the machining process. In order to avoid or predict the failure of the finished products, the condition monitoring system should combine information from several sources to improve the detection of instabilities during the machine process. At the very beginning, also the traditional way at present, engineers used the finished workpiece to optimise the tool wear or tool breakage. However, this inspection took place after the machining process. It is very uneconomical, when the workpiece may be giant in size and weight. Hence, condition monitoring theory was established in process cutting.

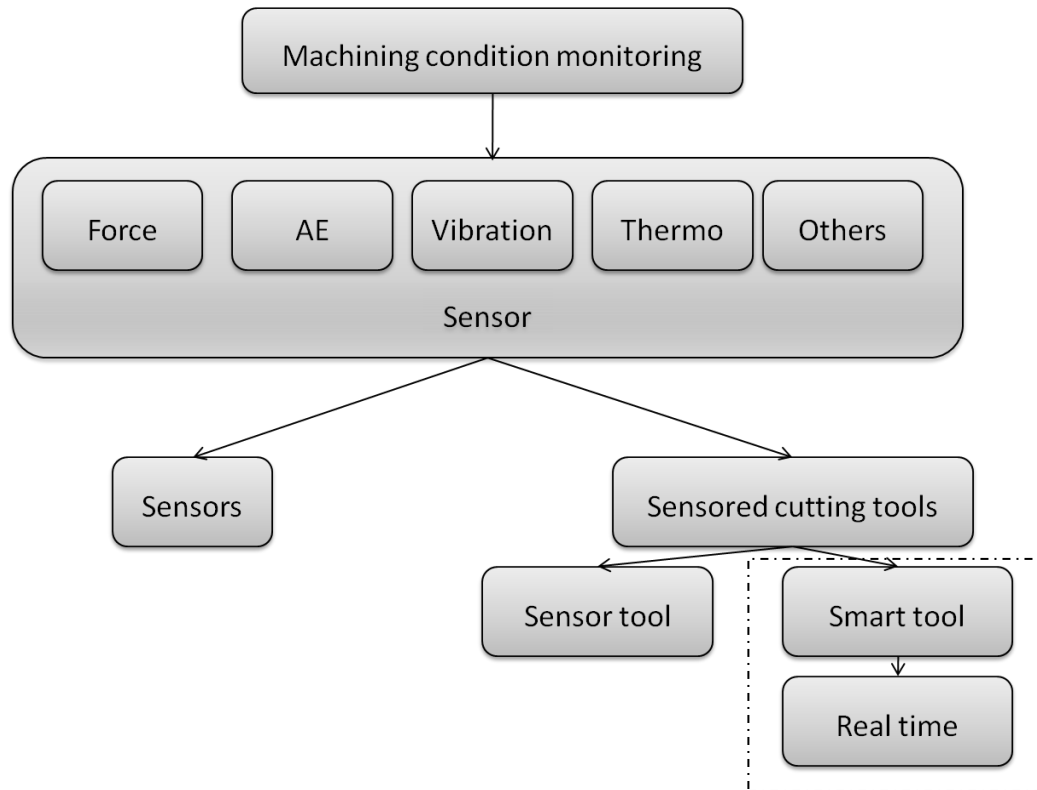


Figure 2.2: Overview of machining condition monitoring methods

In process cutting, condition monitoring requires a faster response time for measuring compared with the workpiece inspection methods. Various kinds of dynamometers and sensor tools have been starting to appear in researchers' experiments.

2.1.1 Workpiece inspection

In the traditional method, tool wear was able to be analysed at the same time as workpiece inspection after the machining process. Tool wear of the chemical-etched surfaces was visually indicated when a finished workpiece was found to have a failed surface, as presented by Lee et al. [2006] in Chapter 2 of the book *Condition Monitoring and Control for Intelligent Manufacturing* [Lee et al., 2006; Wang et al., 2006].

The most important relation of workpiece and tool failure is the material hardness of the workpiece and tool itself. Özel et al. [2004] studied the effects of workpiece

hardness, cutting tool geometry, feed rate and cutting speed on surface roughness and found them to be statistically significant. But it is worth mentioning that these effects also act on cutting force and other parameters [Özel et al, 2004]. Vamsi Krishna et al. [2009] had also developed a novel model for tool wear and surface roughness prediction in a steel turning environment with lubricant cooling.

The tool life can be ended by tool failure and edge failure due to gradual wear and chipping. The degradation in surface finish of the workpiece can prove that a cutting tool is coming to the end of its life. Characterisation of the machined workpiece surface topography is the evidence of the machining process and, to be specific, the present health condition of the cutting tool. The structural changes of the machined workpiece have become significant if the present tool is approaching the end of its life cycle. Kurada has pointed out that either monitoring the cutting tool directly or inspecting the machined workpiece can achieve the same goal [Kurada and Bradley, 1997].

2.1.2 Dynamometers

Besides the workpiece inspection method, the dynamometer is nowadays more commonly in used in machining. Traditional dynamometers are torque or force measurements. But in recent researches, force measurement dynamometers are more popularly used in the literature. Many researches are using dynamometers as the experimental approach in tool condition monitoring systems [Čuš, 2010; Yaldiz, 2006; Dimla, 1999].

The sensing unit of a dynamometer can be either a strain gauge, or piezoelectric materials. Strain gauge dynamometers are also called analogue dynamometers. But more major dynamometers are based on piezoelectric sensing units.

Kistler was the most famous commercial dynamometer manufacturer, but in 2003, Korkut designed a three dimension of force analogue wireless strain gauge sensing dynamometer [Korkut, 2003]. Unuvar and Saglam used the strain gauge dynamometer to measure cutting force and presented an estimation algorithm of a possibility to set up

a sensor system in milling [Unuvar and Saglam, 2003]. One year previously, Şeker et al. [2002] designed a strain gauge-based dynamometer for measuring cutting forces during machining with linear motion. Charttopadhyay et al. [2000] used the strain gauge-based dynamometer to analyse the cutting force correlation between speed feed rate and depth of cut in milling. Furthermore, Adolfsson and Ståhl [1995] discovered a cutting force model for multi-toothed cutting processes by using the strain gauge sensor-based dynamometer. Concluding from the above, it is quite a coincidence that the strain gauge sensor-based dynamometers are more often in used in milling.

Piezoelectric sensor-based dynamometers are more widely in use in industry, where piezoelectric sensors are more effective for measuring pressure, acceleration, pressure, force and vibration. Figure 2.3 shows the Kistler dynamometer that was used in the thesis experiment as the contrast to reference the designed smart cutting tool's accuracy and stability.

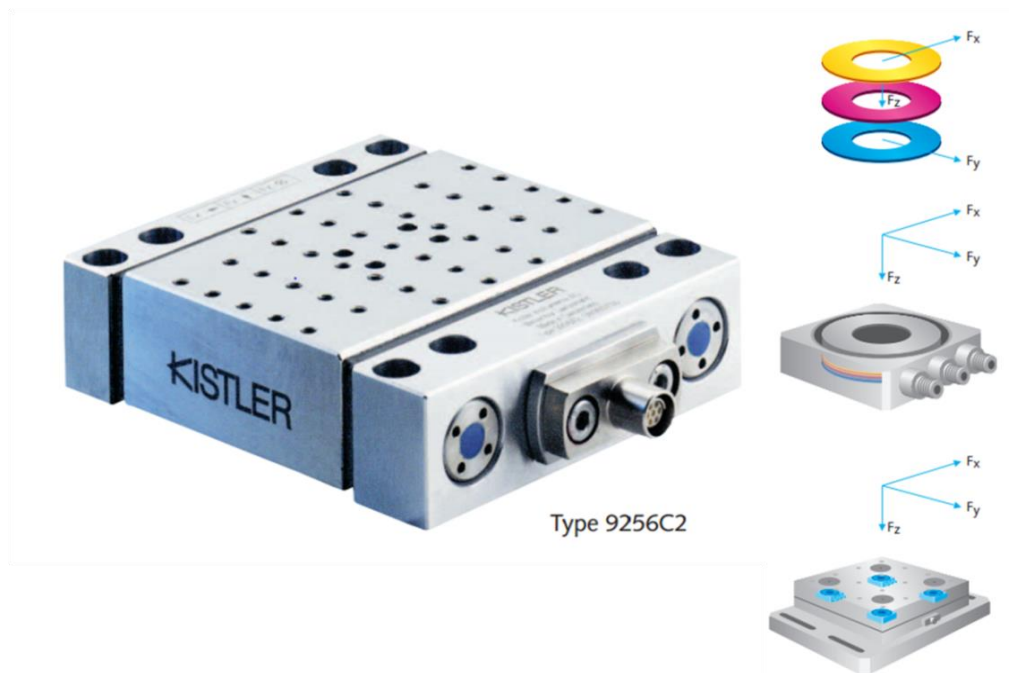


Figure 2.3: Kistler Minidyn type 9256C

Lin [1996] has confirmed that tool wear can be well predicted by experiment using the piezoelectric sensing unit-based sensor. Chung and Geddam [2003] developed a multi-

sensor-based tool wear detection method by using dynamometers as well as AE sensors. Because the characteristics of piezoelectric materials are an advantage when detecting force and vibration, Bhattacharyya et al. [2007] have used a piezoelectric accelerometer to estimate tool breakage and have compared with cutting trials in the real world. Chen et al. have pointed out that the correlation between the cutting force and the flank wear can be used to control the theory of reconstruction of tool wear confirmation by using a piezoelectric sensing unit-based Kistler dynamometer [Chen, 2007]. Girardin et al. have studied and analysed the cutting forces associated with spindle rotation to estimate the tool wear [Girardin et al., 2007]. Kious et al. [2010] have also used the piezoelectric sensing unit-based dynamometer for their research to predict the tool wear by analysing the correlation of the cutting force.

2.1.3 Sensored tools and smart cutting tools

Sensor history can be traced back to the 1930s when the first thermal sensor was invented, and the first pressure sensor was introduced in 1963. The sensor applied to the machining industry for monitoring the machine process was first used back in the 1970s, but it is not possible to confirm who made the first attempt [Texas instrument, 2015].

No exact and reliable mathematical models exist for cutting processes predicting tool wear and tool breakage. Santochi et al. [1996] introduced a new concept of sensor tool which used strain gauges for measuring the forces in turning operations. It was at the time a very inspired sensor tool.

Sensor tools can be separated into two categories: firstly, mechatronic systems including strain gauge methods and thermal methods; and secondly, micro-electron mechanic systems (MEMS). Along with the development of the other technologies, rather than traditional cutting condition monitoring methods, smart cutting tools are the best solution at the present time. Smart cutting tools have several additional advantages beyond sensor tools, which are self-learning, real-time signal analysing, real-time decision-making, and plug-and-produce characteristics.

2.2 Condition monitoring in the machining process

Machine process is the process that transforms the mechanical shape of a work piece into the demanded form. The mass of the metal from the workpieces is removed by the machining process. During this process, various factors can affect the workpiece finish. Engineers and researchers had studied for many years to analyse the consequences and relations between surface finish and machining process. Özel and Karpat found that the surface finishes are able to be predicted without tool wear or tool breakage; however, tool wear and tool breakage exist most of the time [Özel, 2004]. Therefore, machining condition monitoring will be continuously researched by industry and institutes.

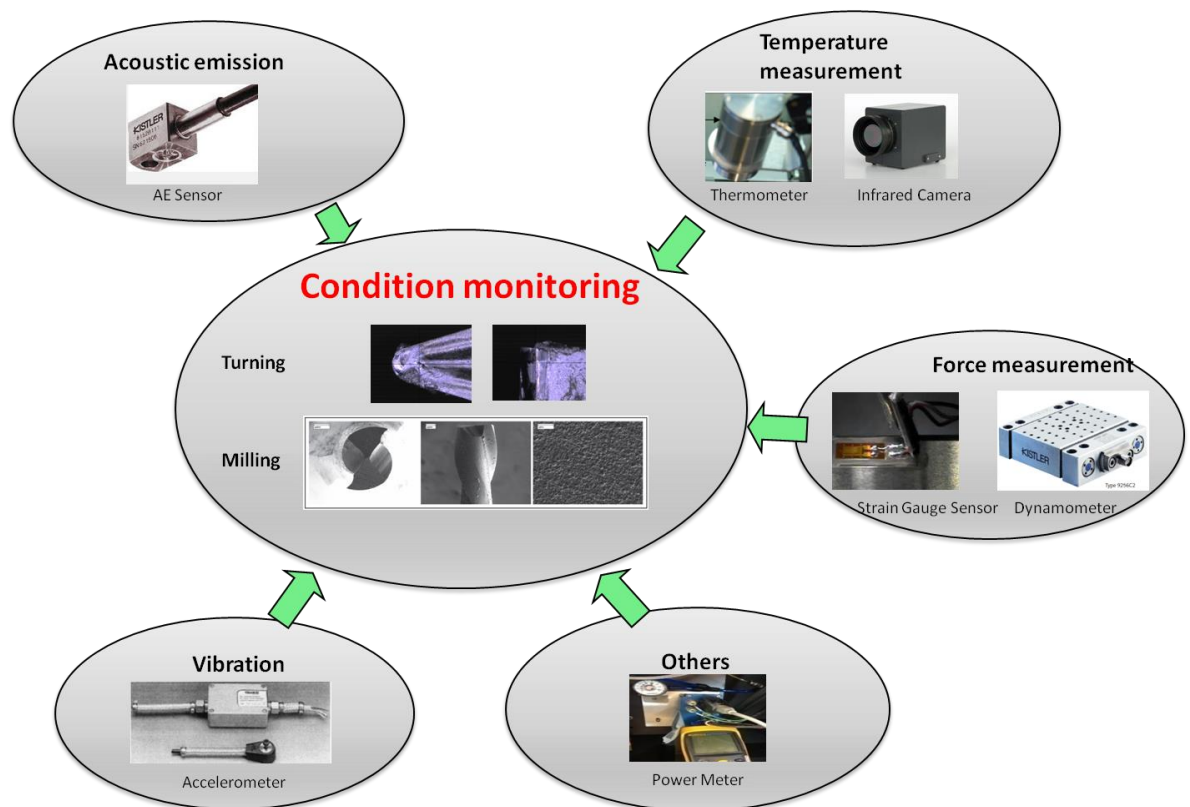


Figure 2.4: Machine process condition monitoring methods

In industries, the goals are to be reliable and highly efficient; hence, force, power and AE sensors are in use most of the time for machining condition monitoring [Byrne et al., 1995]. The ultimate goal for condition monitoring was to meet real automation on

an unmanned production system, and ensure the quality of the workpiece by control of the tool failure. Although tool life varies depending on circumstances, tool wear and tool breakage is eventually unpreventable, and researchers and engineers had to study its prediction via the methods shown in Figure 2.2.

2.2.1 Acoustic emissions

Acoustic emission (AE) is a very common technology applied to the machine process monitoring of tool wear and breakage. Dornfeld [1989] verified that AE source waves are generated over a short time period during material deformation while machining. The principle is a physics phenomenon whereby when a solid material is mechanically transformed, the stress energy release is very fast through radiation of elastic acoustic waves. Figure 2.5 shows the Kistler AE sensor and AE sensor's work philosophy.

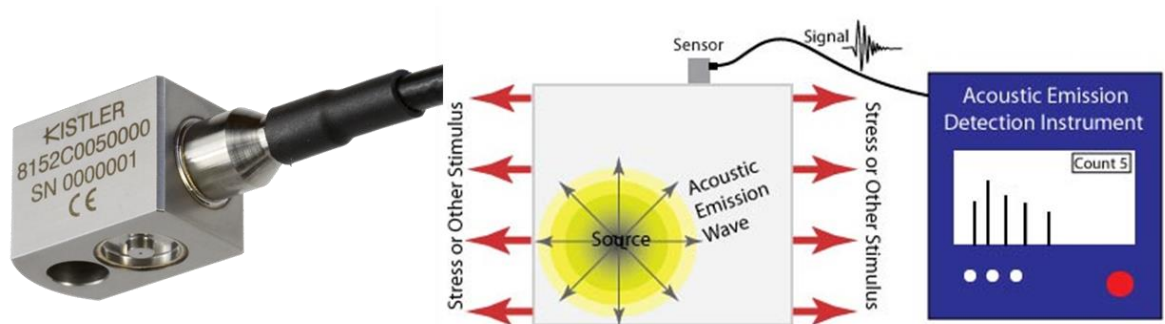


Figure 2.5: Acoustic emission sensor

The AE method applied to machining processes can be traced back to the 1980s. Professor Kannatey-Asibu has summarised the advantage of the AE as a tool wear sensing technique [Kannatey-Asibu, 1987]:

- Its adaptability to computer 'control;
- Its generation by processes in the cutting zone, including the chip tool interface and the tool flank, which have a direct influence on tool wear;
- The ability to detect signals from the cutting process away from the process zone, thus reducing the risk of instrumentation damage from the cutting

environment; and

- The high frequency content of the emission signal, which is well beyond the frequency range of noise from machine tool dynamics and extraneous sources.

Dornfeld [1987] has analysed the several factors that could affect the AE sensor:

- Plastic deformation of the workpiece while cutting process is taking place;
- Chip shearing;
- Frictional contact between the tool flank face and the workpiece resulting in flank wear;
- Frictional contact between the tool rake face and the chip resulting in crater wear;
- Collisions between chip and tool;
- Chip breakage; and
- Tool fracture.

The above factors are also separated into continuous signal and inconstant signal. Continuous AE signals are such as plastic deformation of the work-piece, chip shearing and frictional contacts; inconstant AE signals are such as collisions, chip breakage and tool fracture.

One of the advantages of the AE sensor is that it can be pasted or coated onto the rotating spindle on the machine via fluid and coolant, with controllable interfering of the sensitivity. A significant AE signal could be picked up if the tool is suffering tool wear or tool breakage. Moriwaki and Okushima [1980] claimed a tool breakage detection method in 1980. They discovered the feasibility of the in-process detection of tool wear in cutting machines by combining the AE signal with fractures of the tool materials and measuring the difference of tool materials to analyse the character of the AE signal in the process. Choi et al. [1999] developed a real-time process monitoring system in turning machines with a combination of force sensor and AE sensor. An algorithm is proposed for tool breakage detection by using the designed machine monitoring system.

Relatively speaking, tool breakage and chip breakage are easier to be detected by the abrupt AE signal [Li, 2002]. However, tool wear is not that obvious to be picked up by AE sensors because of the low intensity of the signal during machining process.

2.2.2 Temperature

The most frequently used experimental techniques in tool condition monitoring are heat analysis and cutting force analysis.

Komanduri and Hou [2001] summarised that there are six categories for measuring the heat and temperature during manufacturing process in tribology. They are:

- Thermocouples;
- Infra-red photography;
- Infrared optical pyrometers;
- Thermal paints;
- Materials with known melting temperatures, either in powder form or as a thin film; and
- Change in microstructure with temperature in the case of high-speed steel tools, to name some.

Thermocouples can be embedded thermocouples, dynamic thermocouples or chip–tool thermocouples in the case of cutting; the rest of the categories are simply as listed.

It should be mentioned that each category must be considered in the big picture of the machining environment for the specific situation; each method has its own advantages and disadvantages compared to others, such as the ease of accessibility, spot size, dynamics of the situation, accuracy needed, cost of instrumentation and advancements in technology.

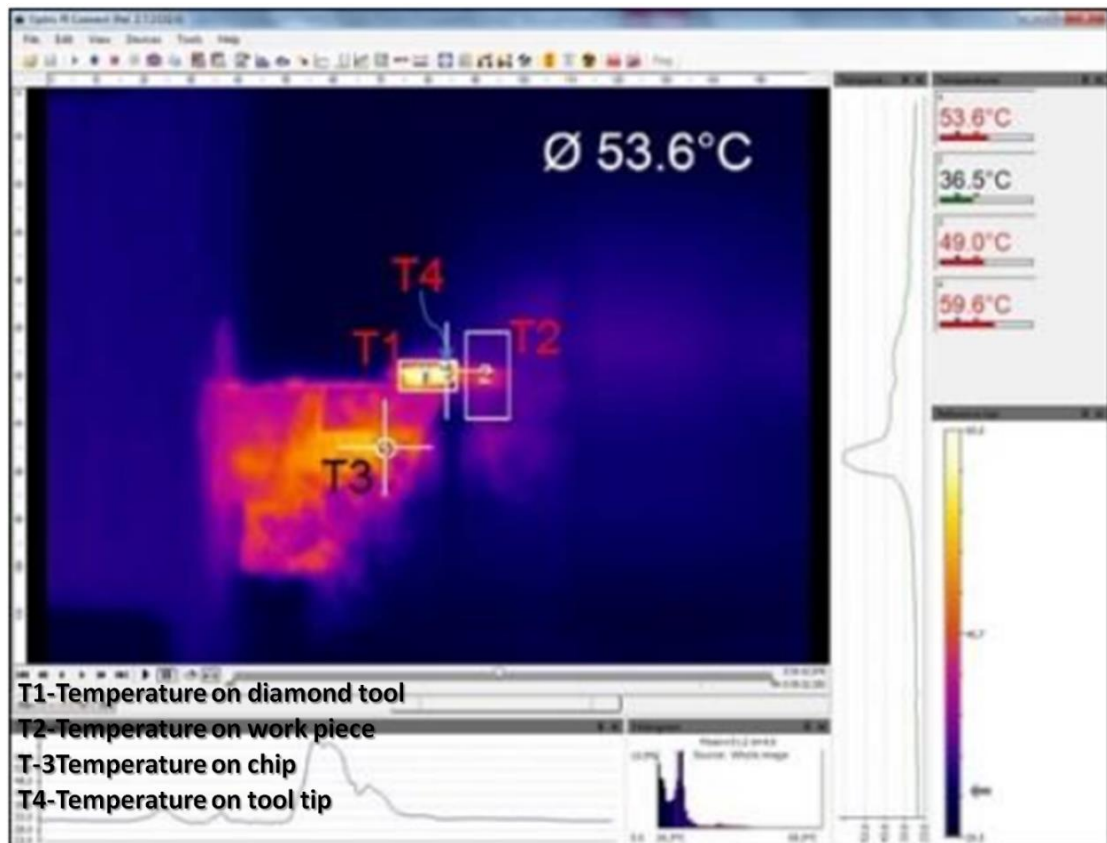


Figure 2.6: Cutting moment captured by the infra-red temperature camera

2.2.3 Cutting forces

The research results from Lan and Dornfeld [1984] show that the cutting force and feed forces are the most sensitive relating to tool wear. Supportively, Oraby and Hayhurst [1990] claimed that cutting forces are actually related to tool wear in machining operations and can be used in predictive tool wear. Hence, cutting forces categorise as one of the most significant parameters which are reliable and act as a robust indicator for tool condition monitoring regarding tool wear.

The relationship between the cutting force and tool wear has been investigated by several researchers [Koren, 1978; De Filippi and Ippolito, 1969; Zorev, 1966]. Cutting force and temperature are the most common physical phenomena in machine process monitoring; the cutting force is relatively important because it is directly related to the material removal motion and also occurs in the whole cutting process. Cutting force monitoring and temperature monitoring are most widely used in tool condition

monitoring because cutting force monitoring has the advantage of quick response, sensitivity and is easy to detect. Compared to temperature, cutting forces are shown at the very beginning of the machining process without any delay. Also the cutting forces are sensitively related to tool wear as the force will change immediately after tool wear or when tool breakage starts. When cutting tool wear or tool breakage occurs, the cutting force signals are clearly visualised on the spectra. The increased force is normally caused by build-up on the tool edge because the contact face increases. The decreased force is normally caused by tool breakage or chipping because the contact face has decreased since the depth of cut is no longer precise. However, the above conclusion has exceptions that depend on the real situation.

Lindstrom and Lindberg's [1987] studies concluded that cutting forces are very good indicators for cutting condition monitoring. The cutting forces are related to the geometry and material characteristic of the tool and workpieces, also coupling with the cutting parameters such as spindle speed, feed rate etc. In Nouni's paper, where measurements were made of the all of the cutting forces and build model coefficients during the cutting processes with a variety of spindle speeds, feed rates and also radial and axial depth of cuts, the change of cutting force signal may be caused by a variation of tool condition such as tool breakage, chatter or tool wear, cutting parameters and noise [Nouni, 2014].

The force monitoring method includes the main cutting force, feed force and radial force.

In Figure 2.7 below, F_t is the cutting force, F_f is the feed force and F_r is the radial force.

These three different directions of the cutting force have different influences with the wear cutting conditions and also at different stages of tool life. The cutting forces are highly related to the machine's process dynamics, which gives cutting force as the best reason to be the most widely used approach in cutting condition monitoring. According to Gould and Lister, cutting force is more influenced by tool wear, and feed force is more influenced by crater wear [Gould, 1988; Lister, 1993].

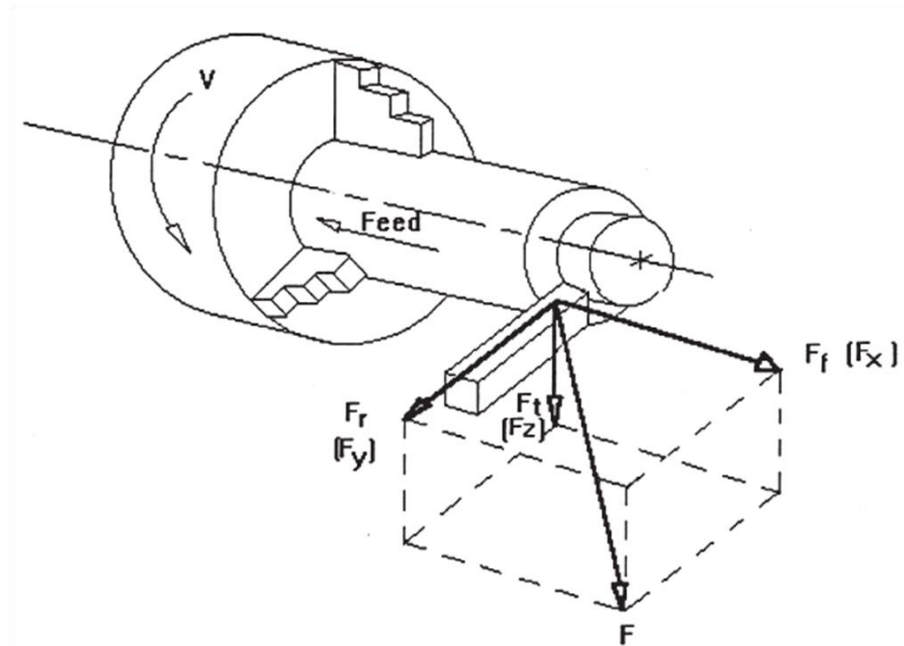


Figure 2.7: Cutting force components on a single point tool during turning [Dimla and Lister, 2000]

The cutting forces are also split into dynamic forces and static forces, but both static and dynamic forces are important in the TCM system. Dimla and Lister [2000] summarised that TCM systems are mostly-based on the static and dynamic forces. In conventional machining, static forces are more significant than the dynamic forces. But in micro-nano machining, the static forces are very small, only 0.1 N or less, and sometimes the dynamic forces are larger.

Direct force and indirect force measurements are used in cutting force monitoring. Direct force measurement is commonly undertaken by force transducers such as force-sensitive semiconductors or piezoelectric ceramic materials. Indirect force measurement normally points to strain-stress or distance measuring methods and is undertaken by strain transducers or force sensitive materials formed by strain structures either sticking or coating in/onto the cutting tool. Indirect force measuring methods are used on any force transmitting parts in machines and fixtures which have deformed elastically by the forces acting on them, such as housings, spindles, carriages, holders, rods etc. [Jemielniak, 1999].

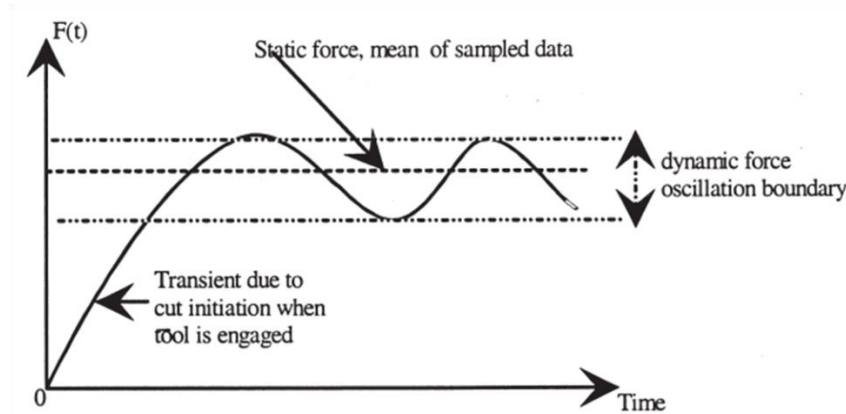


Figure 2.8: Force time diagram for static and dynamic force [Dimla and Lister, 2000]

2.2.4 Vibrations in the machining process

Vibrations are a physical phenomenon associated with cutting force, these two methods quite often appear together in research papers [Dimla and Lister, 2000]. Oscillations of cutting forces are the main reason for vibration of the machine structure. As shown in many publications the cutting forces would change because of tool wear, hence, the vibration would vary because different cutting forces appear in the machine system [Byrne et al., 1995]. These vibrations are detected by using accelerometers.

Different frequencies of vibration occur during the machining process because of the contact between the cutting tool and work-piece. There are two most commented on methods of monitoring the vibration: firstly, isolate the high amplitude and low amplitude of the vibration signal and analyse them; secondly, isolate and record the vibration in several independent bandwidths, and analyse them afterwards. The method used for evaluating the vibration signatures normally involves the transformation of signals from time to frequency domain by FFT.

The vibration method has been applied to condition monitoring for a long time,

however, there are few comments in tool condition monitoring. The reason is because intensive vibrations are significantly larger in machining; especially the noise levels are high during conventional machining processes. But, the advantage of the vibration measurement method is that it is very easy to operate, and adaptive to any machining environment [El-Wardany et al., 1996]. However, in the same paper, the disadvantages are stated including dependency of the vibration signals on different types of workpiece material, cutting parameters and machine structure. Barker et al. [1993] used accelerometers to measure the vibration signal and detect wear in a rotating machine. Both vibration and sound measurement are used to analyse the tool wear [Barker et al., 1993]. The cost of the vibration sensor is quite low; hence these types of condition monitoring methods were often in used in research papers ten years ago.

2.2.5 Other physical phenomena in the machining system

Besides the popular machine condition monitoring methods, there also other physical phenomena applied in the researches, such as ultrasonics, optical cameras, workpiece inspection, stress/strain analysis, spindle motor current monitoring etc.

These methods include:

- Spindle measurement/ torque measurement; and
- Optical measurement.

Many researchers would like to categorise the monitoring methods in tiny branches; however, the author would prefer to have two main categories where all other physical phenomenon approaches can be included. Spindle measurements include motor energy monitoring, power-based or current-based. Likewise, optical measurements include optical photo, laser, and surface roughness monitoring, all visualised and operated using lens-based equipment.

(1) Spindle measurement

Spindle measurement also means electrical motor or power measurement, the sensors are placed to measure the current or effective power from the main working spindle of

the manufacturing machine and also the feed drive motor current. It is quite similar when measuring torque, as the two methods are both measuring the power used during the machining process and also both advise about the dynamic of the cutting process. Jemielniak [1999] points out that torque measurements are more sensitive compared to spindle current measurements because normally torque sensors are positioned closer to the cutting area. However, measuring torque is more complex than measuring the spindle current and therefore the measurements are very popular choice of researchers [René de Jesús et al., 2003; Li et al., 2004; Rantatalo et al., 2007].

Spindle current is highly relevant to torque; the drive currents are actually reflecting of the thrust force. From Li's research, the feed drive current can be used to estimate the tool wear and tool failure by estimating the relevant thrust force using the measured spindle current [Li et al., 2000].

The shaft power, motor current, cutting force and torque are tightly related to each other and influence each other. According to Rangwala and Dornfeld [1990], measuring of each one of them during the machining process would suffice.

(2) Optical method

Optical measurement methods mean image capture and analysis of the captured image. Determining tool wear from processed images of the cutting tool has been pursued for over four decades now. Martin et al. [1986] have concluded in a review paper that the optical methods that have been in used in process monitoring can be summarised into the following categories: laser measurement aimed at surface finish, photodiodes aimed at reflected light measurements regards the cutting edge, and fibre optic photocell aimed at reflectance measurement of contact areas of the tool flank.

The laser monitoring method uses a special beam that has a longer wavelength than widely in used in the researches. Laser monitoring methods are targeting on monitoring the tool wear, chip formation and surface roughness. It is a very efficient method that analyses the tool wear and chip deformation along with different cutting parameters

[Madhava Reddy et al., 2012].

But because of technology development, a charge-coupled device (CCD) started to be widely used after the 1990s. The CCD is capable of monitoring the performance in real-time.

Pfeifer and Wieggers [2000] have reviewed the vision monitoring methods including illumination, image capture and data processing methods. One of their contributions is the discussion about the standard for the measurement result's quality, tool handling methods, and adaptive illumination for obtaining optimised camera images that could apply on different types of cutting tools. Also, a new approach of vision monitoring system was mentioned in the paper, claiming that they have successfully increased the accuracy to 70-90% of flank wear identifications for several cutting tools .

The laser and photo methods can be experimented at the same time to achieve a better result. Wong et al. [1997] have combined the laser sensor and CCD camera and used them to measure the surface roughness of the work-piece. The surface of the workpiece was measured by a special beam laser, and the camera was used to detect the reflected light. The research from Wong showed that after monitoring most workpieces, there is an obvious correlation found between the tool wear and intensity distribution of the scatted light pattern. However, the tool wear was not so obviously correlated with observing the surface roughness.

A new method was mentioned by Sortino of monitoring the cutting tool condition using optical measurement. The so-called 'WEARMON' method was designed by Soritino to proceed and analyse the CCD camera's flank wear image. This method verified an accuracy of 92% correct cases of calculating maximum wear land.

The optical monitoring method is actually a popular condition monitoring method only after temperature monitoring and cutting force monitoring. And it is worth mentioning that the optical monitoring method has an advantage of being easy to implement into an

experiment stage. However, clearly, none of these methods are applicable in a TCMS scenario as in-process tool wear measurement is more difficult to achieve.

2.3 Tool condition monitoring systems

The use of a sensor system of tool condition monitoring in machining is becoming common in industry [Byrne et al., 1995]. In fact, condition monitoring is majorly tool condition monitoring. The reason for this separate sector is to differentiate the tool monitoring and isolate the tool wear with its associated key factors in order to serve the reason for developing a sensor tool that can be claimed as a smart tool.

A reliable tool wear monitoring system is a quite essential target for a self-adjusting manufacturing system. Čuš and Župerl claim that they developed a monitoring system that can detect tool breakage in real-time by using a co-operation neural decision system and ANFIS tool wear estimator. Their tool wear estimate method is based on the correlation of flank wear and the resultant cutting forces [Čuš, 2010].

There are several physical phenomena that will affect the status of the cutting tool during the cutting process. There are events, some avoidable and some unavoidable, that are going to happen during machine process. Apart from tool breakage, the rest of the phenomena are normally due to the metal removal process.

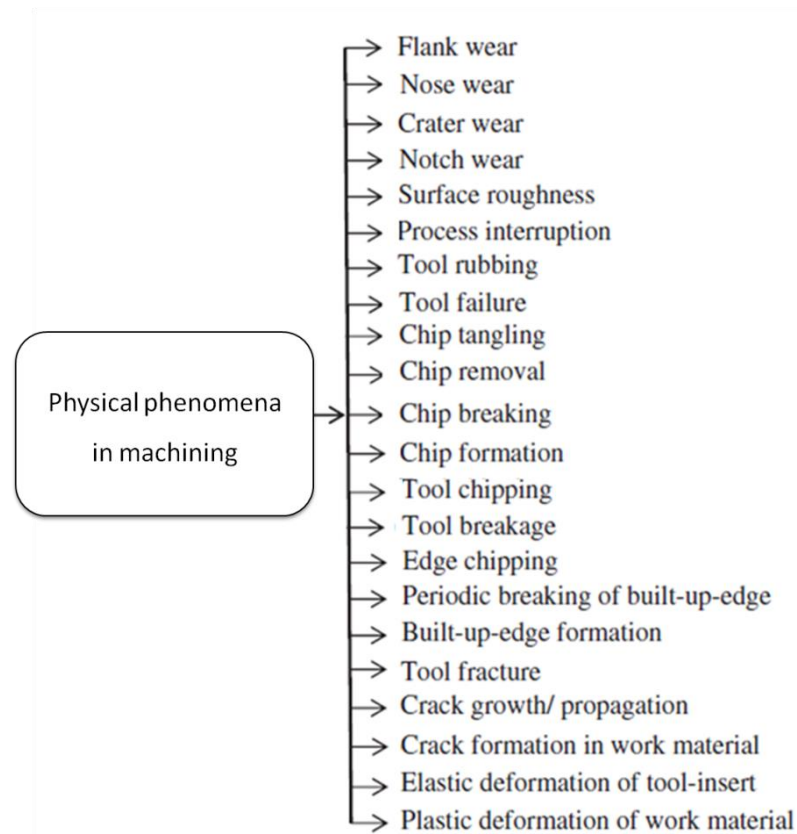


Figure 2.9: Physical phenomenon occurring in machining [Bhuiyan and Choudhury, 2014]

There are direct and indirect methods of monitoring the tool condition. Representative of the direct method are trigger probe, optical measurement, or any geometry measurement sensors for measuring the geometry and shape of the cutting edge. Indirect methods are cutting force measurement, torque measurement, AE sensor measurement, tool temperature measurement, vibration measurement, power and energy measurement, and spindle motor current measurement. According to Zhu et al. [2013], direct method and indirect methods have their unique advantages and disadvantages. Direct methods are reliable; however, they are unable to provide continuous measurement. On the other hand, indirect monitoring methods are able to be continuously monitoring, but are not as reliable as direct methods. The indirect monitoring methods are making the online monitoring of tool condition technology possible [Zhu et al., 2013].

2.3.1 Tool wear and the associated key factors

Tool wear is a very important effect in the machine process and will affect the surface finish quality of the work-piece. Tool wear in the metal cutting process is defined as the gradual loss of material from the surface of the tool as a result of the relative movement between the tool and the work piece [Astakhov and Davim, 2008].

Typically, multiple wear mechanisms may be present in metal cutting, in most cases simultaneously [Shaw, 1984], which makes a systematic study of tool wear very hard [Rabinowicz, 1995]. According to Groover [2010], there are five types of tool wear, which are abrasive, adhesive, diffusion, plastic deformation and chemical reaction. Groover claims that 50% of tool wear is abrasive, 20% is from adhesive, 10% is because of the chemical reaction and the remaining 20% are for other reasons.

Most tool wear occurs at high cutting speed and high temperature [Hidayah et al., 2014]. At slow cutting speeds, adhesive and abrasive wear tend to be dominant. However, diffusion, dissolution, chemical reaction and oxidation are more relevant at high cutting speeds.

All the condition monitoring methods are in fact serving the purpose of estimated tool wear. Tool wear is a much discussed issue in manufacturing industries. The types of tool wear are often named as flank wear, crater wear, built-up edge, glazing and edge wear. All types of tool wear can be concluded as four different classes; adhesive wear, abrasive wear, diffusion wear and fracture wear. Adhesive wear is caused by the deformation or fracture of the workpiece and cutting tool. Abrasive wear is describing the materials from the cutting tool being removed by the workpiece through mechanical moves. Diffusion wear happens normally because the atoms travel from the tool material to the work-piece. And diffusion wear in traditional conventional machining is highly related to temperature increase. Fractures are normally caused by the fatigue from the chipping [Dimla and Lister, 2000; Shaw, 1984].

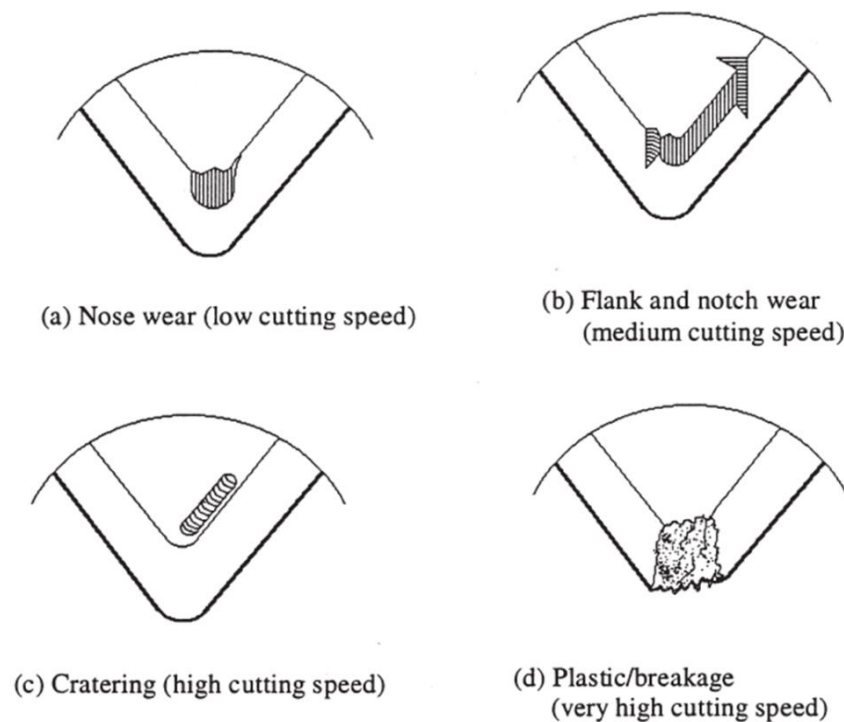


Figure 2.10: Tool wear forms in orthogonal metal cutting [Dimla and Lister, 2000]

From the above paragraph, several key factors were related to all kinds of tool wear, such as cutting force, tool material, workpiece material, cutting speed, depth of cut and feed rate. All these matters are known, or measurable. Examples of the effects on the workpiece are that it is damaged prematurely, unacceptable dimension tolerances of the workpiece and the quality of the workpiece surface is very severe [Zhou et al., 1995]. Many tool wear prediction models have been discovered by researchers. This thesis aims to discuss the development of a smart cutting tool for micro-diamond machining, Hence, the major topics of diamond cutting are cutting force and temperature in diamond turning and micro-cutting.

2.4 Sensored cutting tools and their development

Both industry and researchers have been interested in seeking a means of lowering cost and improving machine performance and maintainability continuously.

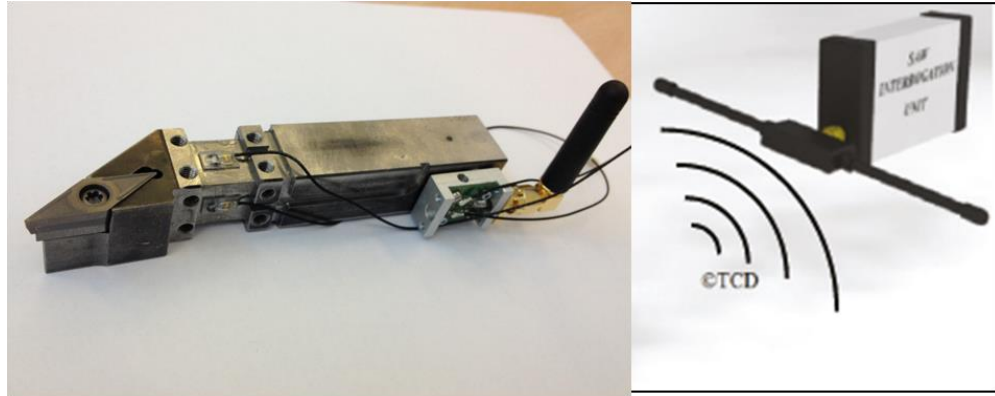


Figure 2.11: SAW-based smart cutting tool

The most representative sensed tools are MEMS tools, and the most representative are SAW tools (as shown in Figure 2.11). The author has decided to divide the sensors in machine monitoring into two groups: dynamometers and sensor-based cutting tools. The commercial dynamometers are dominated in the market by TCM industries; however, researchers also invented a number of sensed tools for TCM purposes. The sensed tool is a very economical method for TCM, if the sensed tool is guaranteed accuracy and reliability. However, there are no such standards for comparing the sensed tool. Hence, at chapter 6 the reference standard used for comparing the designed smart cutting tool is the Kistler Dynamometer.

2.4.1 Review of sensor tools in tool condition monitoring

Shinozuka et al. [008] have designed a sensor tool that is based on a thermocouple (TFTS). The three built-in three TFTS is a layer of nickel and nichrome films that are physically positioned at the tool insert. Werschmoeller et al. [2010] designed a thermo-sensor tool that used an array of nine micro thin film thermocouples embedded into polycrystalline cubic boron nitride (PCBN) cutting inserts. The sensor shows static and dynamic capabilities during experiments. Also in the following year Werschmoeller made some improvements in their designed tool and claimed that his temperature-based tool is more effective than a conventional force measurement dynamometer on the aspect of tool wear evaluation [Werschmoeller et al, 2012].

Yoshioka et al. [2004] designed a thermal sensor of size 520 x 250 x 5 mm to be used for ultraprecision machining process monitoring. The idea of this design was because the cutting force signals are comparatively much smaller. Hence, the major invention in sensor tools are thermometry-based sensor tools. Lüthje et al. [2004] presented their work on developing a novel thermo sensor focused on monitoring the machine process of turning machines. The thermo sensors are built by wear resistant hard layer system lithographic fabrication with a micro structuring method.

Besides the wired-based tools, wireless sensor tools have been attempted by researchers, such as the surface acoustic wave (SAW) technology-based sensor tools. Stoney et al. [2013] have proposed the feasibility of SAW-based sensor tools network that can become an approach for tool condition monitoring by providing the ability to monitor multiple sensors in one machine system. However, wireless sensors are still not popular in the condition monitoring field.

2.4.2 Smart machining and smart cutting tools

Smart machining, a subset of smart manufacturing, mainly focuses on the machining process in order to improve process reliability and optimise machining performance through the integration of sensor, tool and machine-tool technology. The potential advantages are [Wang et al., 2014]:

- Minimisation of the machining time;
- Improvement of surface roughness;
- Maximisation of tool life;
- Machining on special geometry workpieces with high precision and efficiency, such as slender shafts and thin-wall hollow cylinders;
- Self-monitoring and process optimisation;
- Self-learning and performance improvement over time;
- Awareness of the cutting process in dynamic real time, such as shear angle, chips formation, cutting forces and interaction within the cutting zone; and

- Plug-and-produce feature required for both the process and the machining system.

2.5 Piezoelectric material applications in sensors and actuators

The piezoelectric effect is the ability of piezoelectric materials to generate electric signals while being subjected to stress, pressure, or any other mechanical deformation. The piezoelectric effect originally occurred in quartz crystal, discovered by the brothers Pierre and Jacques Curie in 1880 [Jaffe et al., 1971]. Nowadays, after a century of technology evolution, people have successfully manufactured a certain type of ceramic material which has more sensitivity than quartz crystal and is widely used in industries and research facilities. A well-known original material for the piezoelectric ceramic is formulated by lead, zirconium and titanium (PZT).

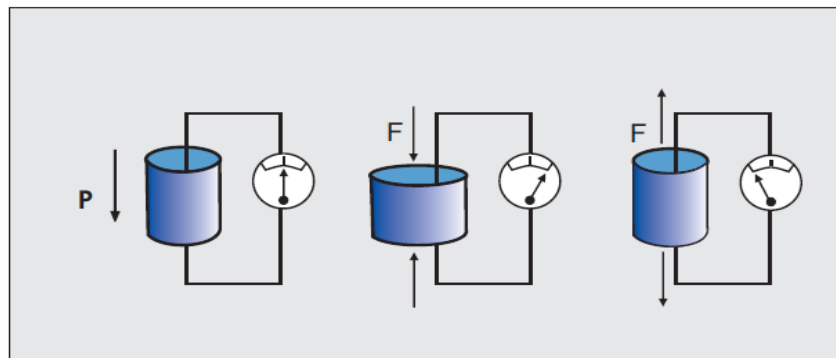


Figure 2.12: Piezoelectric effect on piezoelectric cylinder

The piezoelectric ceramic provides the feasibility of applying the ceramic to either sensor or actuator. In the last 35 years, the development of piezoelectric ceramic materials has been conceptualised, prototyped, fabricated, and implemented in varied applications, both research and industrial, but mainly used for medical purposes and military aspects. However, in recent decades, manufacturing industries were also applying piezoelectric ceramic material to two categories: sensing unit and actuator unit. Piezoelectric materials applied to machine process monitoring could be traced back to the late 1980s and the early 1990s [Rehorn et al., 2005]. Li and Li [1993] introduced a

thin film piezoelectric to replace the microphone AE sensor in TCM for turning.

2.5.1 Sensing unit and force measurement

The piezoelectric ceramic sensor is operated in three dimensions. It can transform the force or pressure into a voltage signal that provides a voltage potential between the two opposing faces of the ceramic. Alternatively, it transforms the strain into a voltage signal that acts on the other two opposing faces, vertical to where the voltage potential difference is located. The most common use for the piezoelectric ceramic sensor is for a pressure sensor to detect the vibration of sound waves, well known as the microphone.

The sensor's history for monitoring automatic machining can be traced back to the 1980s, where Tlusty and Andrews [1983] analysed the commercial sensors for manufacturing industries. Back to the 1980s, there was a Renishaw probe, K&G gauging station, Kistler Dynamometer, Sandvik thrust force sensor, Osaka Kiko CMM-1 and CMM-2 [Tlusty and Andrews, 1983]. Nowadays, piezoelectric ceramic-based sensors in the condition monitoring subject area can be divided into two groups as the division from the previous literature review: dynamometers and MEMS sensors.

2.5.2 Actuators

Piezoelectric materials can also be used as actuators because the piezoelectric ceramic material will create mechanical displacement while electrical voltage is applied to the actuator. The piezoelectric actuators applied in manufacturing are often categorised in vibration assist machining (VAM). The kinematic design of the VAM normally attaches a piezoelectric material on the tool shank of a specific customised tool holder in order to provide a small amplitude, high frequency tool displacement during the cutting motion [Brehl and Dow, 2008]. As regards the benefits of using the performance of the piezoelectric actuator vibration tools or tool holders during the machining process, the main achievements are, of course, to extend tool life and also to machine specific mechanical structures.

2.6 Smart system and smart cutting tool

In the year of information technology, machine tools' conditions can be monitored with numerous intelligent devices. Sensors can be implanted into factories for continuous mobility assistance and real-time accident prevention. Modern sensor-embedded machining, or smart machining, is not just assisting machining efficiency with reduced tool wear, but helping to resolve the other alternative matters.

In figure shown below, a smart system is distributed into 5 levels, where the final configuration should be self-configured, self-adjusting and self-optimising in all CPS.

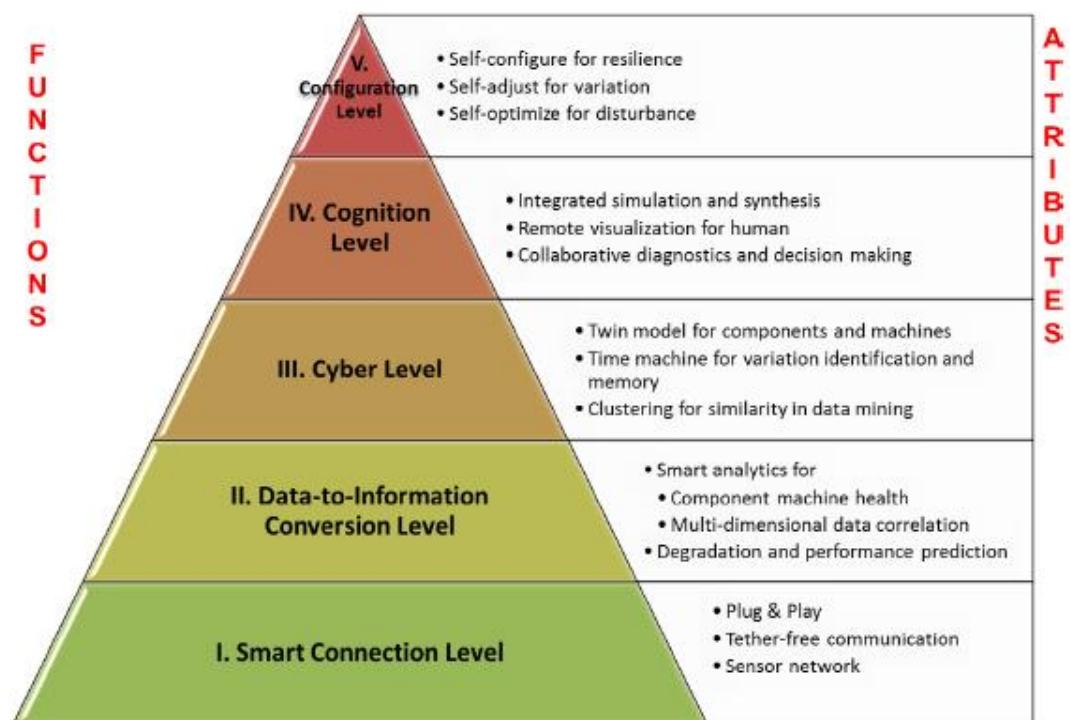


Figure 2.13: A pyramid of smart manufacturing system

A smart cutting tool belongs to this system where located at the base levels, for instance II and I from the figure, and concluded as operational level. The smart cutting tool should contain the features from operational level but also act as a rigid cutting tool. It should perform the following features:

- Plug-and-play;

- Stable and reliable communication;
- Multi-dimensionally data correlation;
- Degradation and performance prediction; and
- Robust in both sensor function and cutting function

2.7 Summary

Compared to the workpiece inspection and dynamometer methods, the advantages and disadvantages of the smart cutting tool are summarised below:

Limitations of using the workpiece inspection include:

- Slow response feedback;
- Size and form of the workpieces leads to a long time circle of the inspection;
- Limitation of the size of the work-piece;
- Damage already exists; and
- High costs.

Limitations of using dynamometers are as follows:

- Reliability of the sensors decreased in the harsh environment;
- Size and weight of the dynamometers leading to not being applicable for all layout constrained machines;
- Interfering with cutting performance because of stiffness reduction on the tooling system; and
- High costs.

Therefore, benefits of using smart cutting tools are:

- High dynamic response, reliability and cutting performance;
- Wireless data transmission;
- Simple and compact configuration;
- Self-learning;

- Low costs; and
- Plug-and-produce.

The limitations of using workpiece inspection are obviously a higher reflecting time period than the other two methods. If the workpiece is a giant structure, it could take several hours to identify the workpiece failure, and eventually the workpiece inspection is finished and certifies tool breakage – the workpiece is already damaged. The reliability of a dynamometer is not fixed while in a harsh environment, as well as the mechanical characteristic of the whole machining system is changed because a metal block is added to the machine. Also, the above two methods have the same problem in that the costs are relatively much higher than a plug-and-produce smart cutting tool [Ma et al., 2012].

2.7.1 The knowledge gaps identified

The literature review has shown us the big picture as in Figure 2.13. The reviews are focused at the machining monitoring subject area, especially in the aspect of sensor tool and tool condition monitoring. There are various sensor tools designed by researchers and engineers for the tool condition monitoring propose; however, the wireless sensor is not yet very popular in the subject area. Although the SAW tool was claimed as a wireless transmitting sensor tool, the effective ranges are very limited. In addition, at present there is no cutting force approach sensor tool designed for micro-machining. In a conclusion, the idea of designing the smart cutting tool-based on real-time cutting force monitoring for micro-cutting machines has not been researched before.

During the machining, in-process sensors play a significant role presently in assisting manufacturing systems in industry. In-process sensors are declared to generate control signals and improve both the control and productivity of manufacturing systems [Byrne et al., 1995].

But the literature survey had shown there is no evidence of real-time feedback on controlling the machining process. Most likely it was the in-process monitoring sensor

optimising the control of the machines after one machine circle.

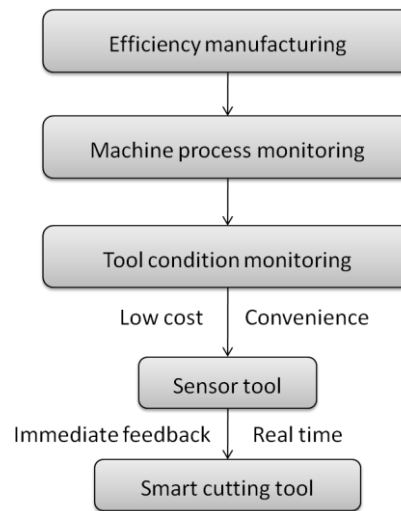


Figure 2.14: Literature review steps

Therefore, we summarise the non-researched subject area and literature for insufficient research achievements:

- Real-time: visible real-time cutting force signal during the machining process, delay less than 1 second.
- Wireless: feasible longer range wireless sensor tool, sensing distance up to at least 1 meter.
- Cutting force monitoring system in micromachining: this is quite an empty subject area of the micro machining force according to the literatures.

2.7.2 Research and development needs for smart cutting tools

All previous research has shown that, in order to achieve high performance manufacturing systems, machine process monitoring is a very important subject. The most reasonable machine process monitoring method is TCM. From the TCM monitoring literature researches it not hard to find out those sensor tools that are not precisely ‘real-time’ control although all authors claim ‘real-time’ monitoring. There is still more or less a data collection process after the cutting trial. The idea of designing a smart cutting tool is to bring up a novel approach with a prototype to prove the feasibility of:

- Real-time – Cutting force signal visualisation at the exact same time of the cutting process. The real-time cutting force signals are going to reference the cutting machine and then effectively responds on the machine controls to continue the cutting process with adjustment on cutting parameters or stop the machine if necessary.
- Plug-and-produce – Smart cutting tools are able to be disassembled and fitted in with another machine or tool tip within a very limited time period. And also the wireless control via Bluetooth technology gives the feasibility of communication at different platforms.
- Feasibility for real-time cutting parameter optimisation machine control via monitored data.

Plug and produce has been mentioned by Wu et al. [1995]. Each part of the figure is able to be physically plug-and-produce. However, the original document cannot be found [Byrne et al., 1995].

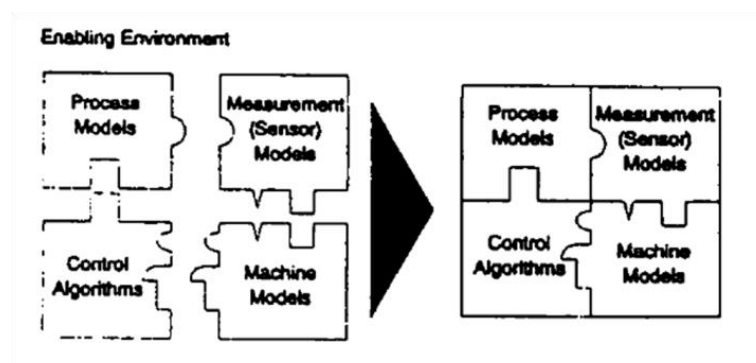


Figure 2.15: Plug-and-play software development environment [Byrne et al., 1995]

The term ‘plug-and-produce’ comes from the software and robotic design term ‘plug-and-play’. The IEEE 1415.5 Smart Transducer Interface Standard is the best standard supporting the multi-platform feasibility of plug-and-produce by enabling a full sensor network in industrial environments.

Chapter 3 Multi-physics-based approach to design and analysis of the smart cutting tool

This chapter presents the modelling and simulation studies in multi-physics environments of the smart cutting tool, explains the design process in the way of simulation and optimises the tool design by using the COMSOL multi-physics software. The simulation can be broken down into three main parts: mechanical, electrical and implementation. The modelling approach integrates cutting force, electron charges and radio wave models,-based on a novel mechanism and machining environment.

3.1. Introduction

Metal cutting is a process of removing material from a workpiece in the form of chips using single or multi-point cutting tools with a clearly defined geometry. To some extent the performance of a cutting tool determines the cutting behaviour and the process capability [Yan et al., 2009].

The design of this smart cutting tool required multi-physics analysis to synchronise the piezoelectric sensor and electronic amplifier and wireless communications. This chapter aims to explain the multi-physics-based approach to design and analysis of the smart turning tool. The multi-physics analysis of the smart turning tool is carried out in the light of its mechanical design, piezoelectric sensor and electronic amplification, and wireless communication. The smart turning tool could be seen as an MEMS device at some points, along with the circuitry board and the wireless sensing/transfer functions. The multi-physics approach is used to simulate the physics in cutting force, piezoelectric electrons amplification, and electromagnetic induction and data transfer. The simulation of the prototype tool design and the corresponding analysis are

undertaken using COMSOL environment, which aims to lead to the optimal design of the tool having the desired cutting force sensing resolution, accuracy and bandwidth. The design analysis is also carried out against the experimental data from the cutting trial with the smart turning tool.

This smart cutting tool is similar to a cascade design [Jones, 2011]; the mechanical input in this research would be the cutting forces. Cutting forces input act as a mechanical damping and react on the electron mechanical transducer, coupling these motions into electrical signals, which are going to be conditioned and amplified by a microchip.

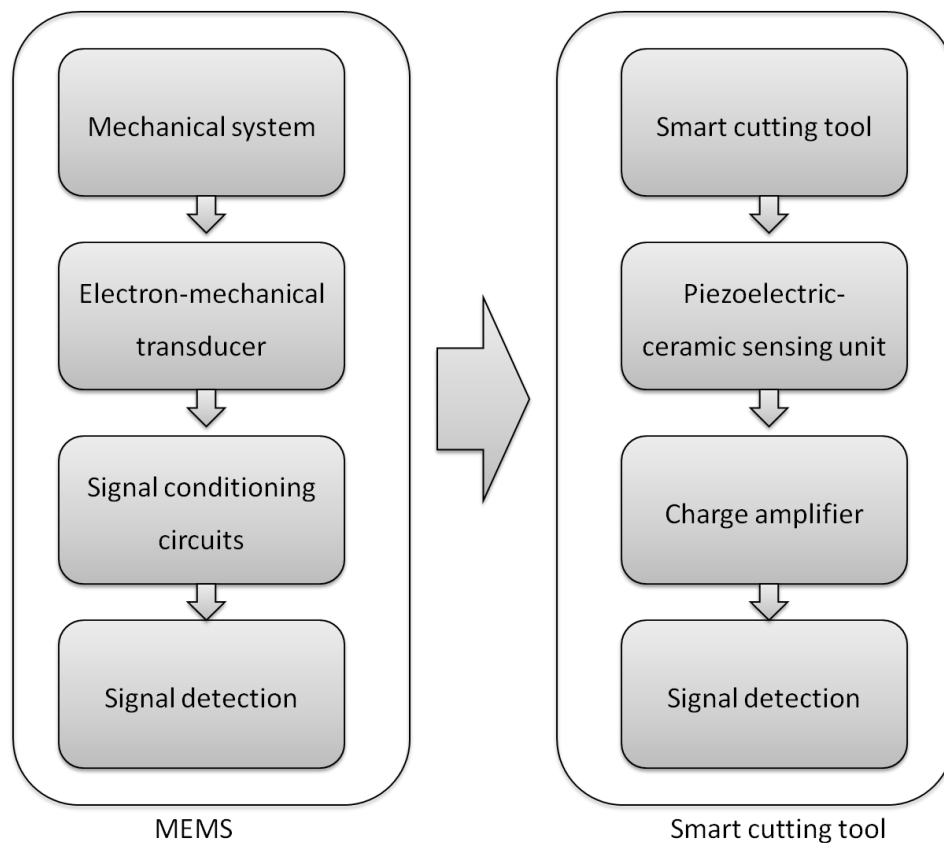


Figure 3.1: Comparison of the development of a smart cutting tool versus the MEMS

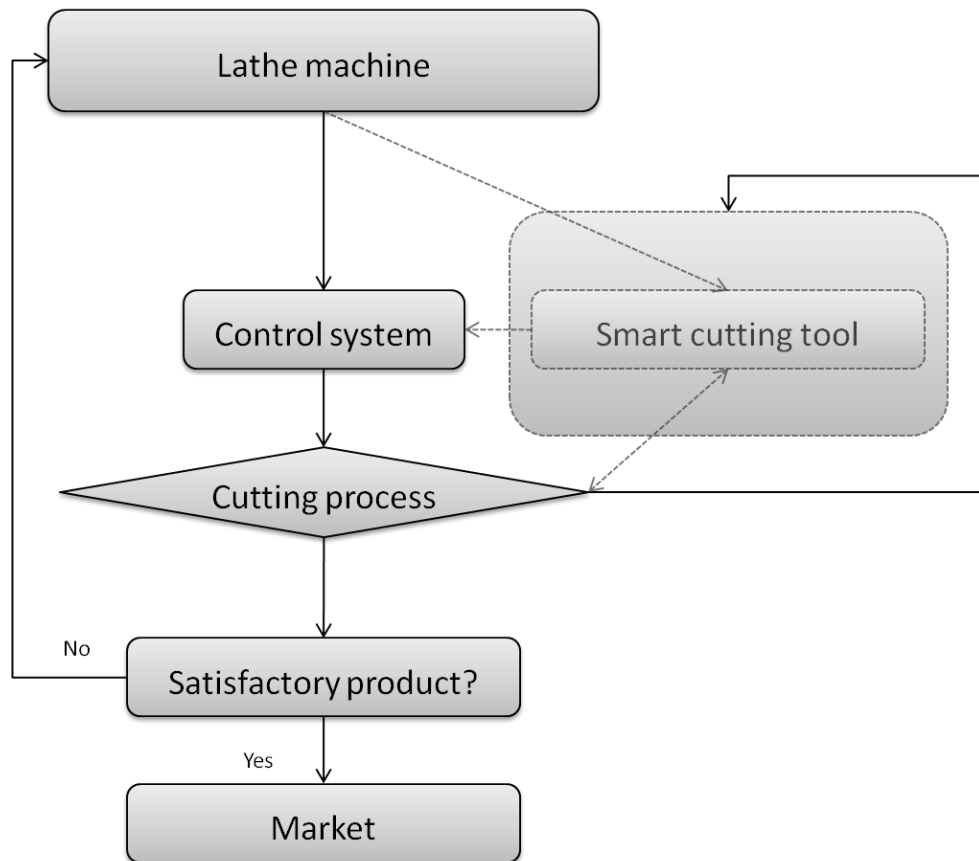


Figure 3.2: One scenario of applying the smart cutting tool in the machining system

This electrical-mechanical system is going to take a very important role in the manufacturing process. In Figure 3.2, the specific manufacturing process flow chart with the smart cutting tool is presented; rather than in a traditional manufacturing process, the smart cutting tool fits into the system. The advantage of the smart cutting tool embedded system is having a real-time feedback loop to the control system and it prevents the false product being produced before the manufacturing loop finishes.

3.2. Design methodology

The idea of the design of this smart cutting tool came from the limitations of previous smart cutting tools. Both RF and SAW smart cutting tools aimed at conventional turning, and involve very large forces compared to micro-cutting. In micro-machining, the forces are normally at the 0.1 to 1 N scale, and the variation of the forces during the

machining is even smaller.

This smart cutting tool was developed and planned systematically. In this chapter, the design process of the smart cutting tool is explained by the flowchart shown in Figure 3.3.

(1) Clarification of the smart tool design specifications

The tasks of this designed smart cutting tool are:

- 0.1 N resolution of force;
- Stiff structure capable of high speed turning, e.g. 10000 rpm;
- Bandwidth 2.5 kHz;
- Transmission range ≥ 2 meter; and
- Minimised cross talk.

By breaking down the tasks, 0.1 N resolutions are decided by the piezoelectric material characteristic and the amplifier circuit. The piezoelectric characteristics from the data sheet are fully capable of these resolutions; thus, the resolution can be adjustable by tuning the charge amplifier circuit. High sensitivities are decided by the smart cutting tool's eigen frequency and wireless data transmission frequency. The Kistler Minidyn was only a cabled dynamometer which depended on the eigen frequency from the tool, tool holder and itself. Stiff structures aimed for high speed turning are going to satisfied by at least 1500 rpm of spindle speed, which is the maximum speed used in this thesis. A stable single transmission is essential, particularly for real-time cutting condition monitoring. Bluetooth is the most reliable data transferring technology nowadays, with also a satisfactory distance for at least 10 metre radius. Bluetooth transmissions are not easily blocked by architectural structures and metal obstacles that stand between the two communication ports.

(2) Industrial-feasibility of smart cutting tool

Traditionally a strain gauge was used widely in machining condition monitoring, and has been used for many years. The idea of the smart cutting tool is to provide a plug-and-produce mobility tool with a smart monitoring approach, rather than traditional

strain gauge sensors. Researchers would need stop calibrating each time the strain gauge sensor was applied on each machine. And with the trend of IOT, Bluetooth wireless technology is convenient to be adapted by the cloud data network in real-time, hence to share the real-time cutting condition to each node of the industrial line.

(3) Conceptual design and embodiment design

- Size and dimension;
- Robust and stiffness; and
- Sensitivity of the smart cutting tool.

The conceptual design was included in the basic idea of the smart cutting tool. The size and dimension are designed to fit the micro-machine, thus the tool shank has to be similar to that of a normal micro-cutting tool. The initial size of the smart cutting tool was decided at 40 mm long, 10 mm wide and 1.5 mm high. The stiffness and sensitivity of the smart cutting tool is going to be presented via a multi-physics simulation approach in the following paragraphs.

The detail design of this smart cutting tool was divided into two main phases: mechanical part and electrical part, and a multi-physics simulation for the electro-mechanic integrated system.

In this case, the advantages of using a multi-physics test are:

- Reduction of the development cycle and time; and
- Optimising the design before the physical prototype build.

Finally, an evaluation of the smart cutting tool for testing the prototype design is essential, so as to optimise the design and planning a future research update.

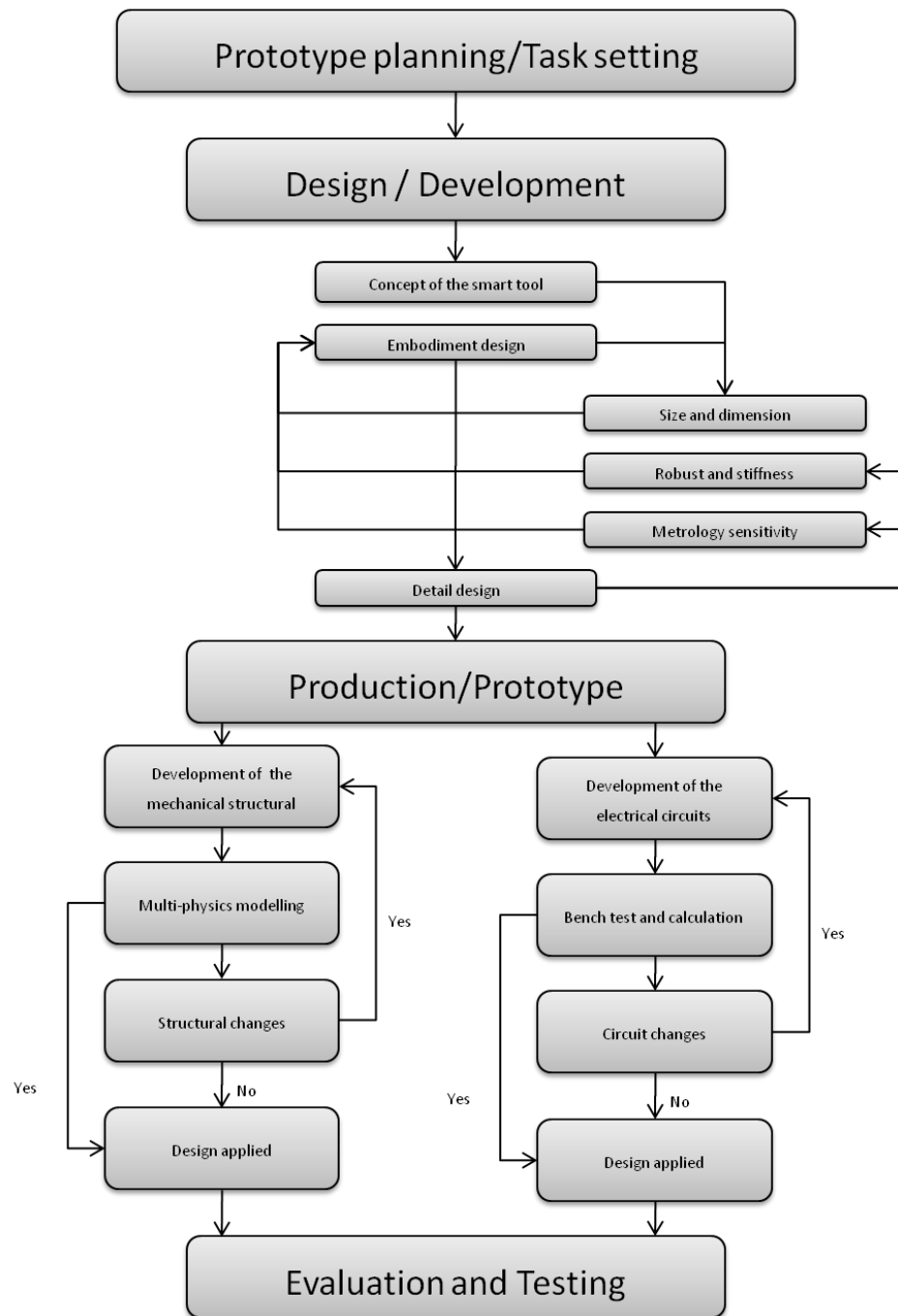


Figure 3.3: Flowchart of smart cutting tool mechanical design process

In Figure 3.3 above, the smart cutting tool design process is explained in detail. The main phases of the design process include [Phal and Beitz, 1995]:

- Design needs analysis;
- Feasibility study;

- Conceptual design;
- Detail design;
- Production; and
- Consumption and service.

3.3. Integrated multi-physics based approach to modelling and analysis

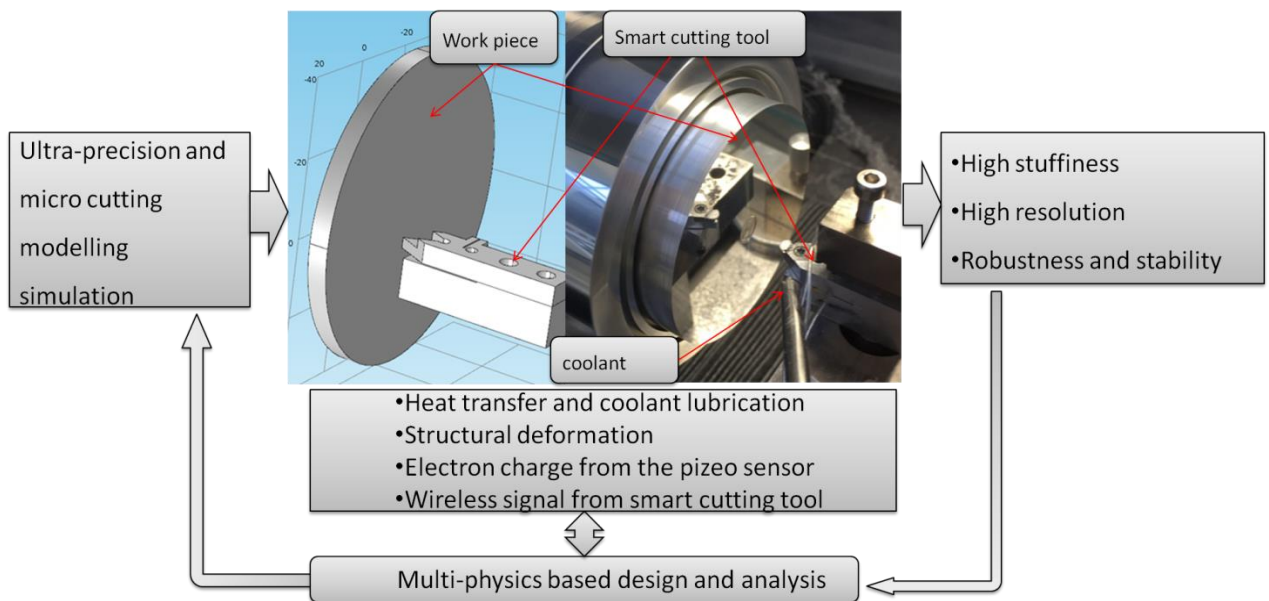


Figure 3.4: Multi-physics approach design specifications

The simulation was designed to explain the structural deformation and electron variation from piezoelectric transducers and signal transmission at the machining environment. The simulation is giving intuitive answers for the whole system-based on structural deformation, electron charges from piezoelectric transducers and the signals transmitted from the smart tool.

3.3.1. Evaluation of design constraints

The piezoelectric ceramic material is able to convert force and pressure signals into electric charges; the process was simulated in this chapter. The theory of the piezoelectric ceramic characteristic is determined by three matrices.

While the piezoelectric effect converting a force (N) into an electric voltage (V), the process can be simulated in terms of a stiffness matrix or compliance matrix, dielectric matrix and piezoelectric constant matrix. All these elements of the below three matrices can be derived from the known parameters supplied in the manufacturer's data as shown below in the following form of Eq (3. 1) and (3. 2), to calculate the voltage output. [Wang, 2012]:

$$[S^E] = [C^E]^{-1} = \begin{matrix} \text{Stiffness matrix:} \\ \begin{bmatrix} 11.8 & -3.42 & -4.12 & 0 & 0 & 0 \\ & 11.8 & -4.12 & 0 & 0 & 0 \\ & & 14.2 & 0 & 0 & 0 \\ & & & 30.4 & 0 & 0 \\ & & & & 53.5 & 0 \\ & & & & & 53.5 \end{bmatrix} \end{matrix} 10^{-12} \quad [\text{N/m}]$$

$$[\varepsilon^S] = \varepsilon_0 \begin{bmatrix} K_{11}^S & 0 & 0 \\ & K_{11}^S & 0 \\ & & K_{33}^S \end{bmatrix} = (8.85 \times 10^{-12}) \begin{bmatrix} 1023.7 & 0 & 0 \\ & 1023.7 & 0 \\ & & 571.35 \end{bmatrix} \quad [\text{farad/m}]$$

$$[d]^t = \begin{matrix} \text{Piezoelectric constant matrix:} \\ \begin{bmatrix} 0 & 0 & 0 & 0 & 0 & 4.75 \\ 0 & 0 & 0 & 0 & 4.75 & 0 \\ -1.20 & -1.20 & 2.65 & 0 & 0 & 0 \end{bmatrix} \end{matrix} \times 10^{-10} \quad [\text{C/N}]$$

Using Equations (3.1) and (3.2) to calculate the voltage output.

$$\{T\} = [C^E]\{S\} + [e]\{E\} \quad (3.1)$$

$$\{D\} = [e]^t + [\varepsilon^S]\{E\} \quad (3.2)$$

Where

$\{\mathbf{T}\}$ - stress vector;

$\{\mathbf{S}\}$ - strain vector;

$\{\mathbf{D}\}$ - electric displacement vector;

$\{\mathbf{E}\}$ - electric field vector;

$[\mathbf{C}^{\mathbf{E}}]$ - stiffness matrix evaluated at constant electric field, i.e. short circuit;

$[\mathbf{e}]$ - piezoelectric matrix relating stress/electric field;

$[\mathbf{e}]^t$ - piezoelectric matrix relating stress/electric field (transposed);

$[\boldsymbol{\varepsilon}^{\mathbf{S}}]$ - dielectric matrix evaluated at constant strain, i.e. mechanically clamped.

This multi-physics simulation was developed by using the on COMSOL multi-physics software. Static forces are in used in the simulation model in order to investigate the structural design's efficiency and stability. The simulations of the forces are mainly on the force shunt. From Figure 3.5, the blue point is the point of force load. And the bottom surface, rear surfaces and the screw slots were fixed. The piezoelectric ceramic sensors are located between the top part and bottom part and within the slot of the projection in the X direction.

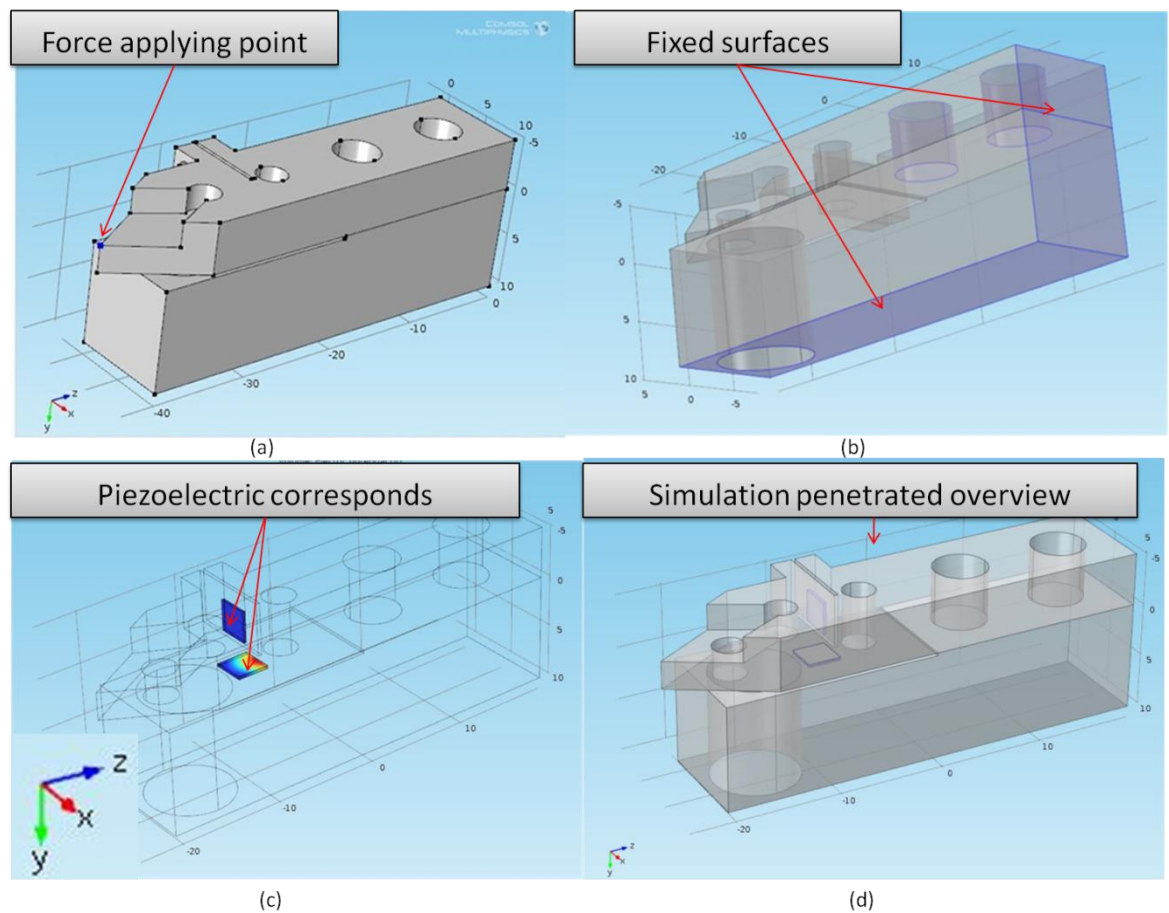


Figure 3.5: 3D illustration of the smart cutting tool mechanical design. (a) Force load point (b) Fixed surface; (c) Piezoelectric ceramic demonstration; (d) Overview of the tool

The tool shank was designed using Pro/ENGINEER, and is imported into the COMSOL multi-physics software as a means to calculate the following features: FEA analysis, modal analysis and piezoelectric device studies. In Figure 3.5(a), the simulated cutting force, feed force and radial force are all given at the specified point, the blue point. Figure 3.5(b) is the definition of the fixed constraint surface so that the simulated tool shank has a reference coordinate. Figure 3.5(c) has insulated the location of the two piezoelectric ceramic sensors for sensing the cutting forces. Figure 3.5(d) defines the corresponding boundary conditions.

Besides the two piezoelectric materials, the rest of the materials in this simulation are defined as linear elastic materials, which comprise the tool shank. The piezoelectric

sensors are in contact directly within the gaps of the tool shank. The vertical piezoelectric sensor fits tightly into the gap at the projection of the tool shank, where the projected two blocks are going to be pre-stressed during the whole process. Thus the vertical piezoelectric sensor is considered along Z directions. The horizontal piezoelectric sensor also fits tightly into the gap between the top and bottom part of the tool shank, and this horizontal piezoelectric is considered along Y directions. The holes are mainly made for pre-stressing the top and bottom part of the tool shank, thus making the structure one unified form. Figure 3.5 has pointed out the direction of X, Y and Z axes, where the force in the X direction is the radial force, Y direction is the cutting force, and Z direction is the feed force.

The material will be determined by collaboration with the workshop at the university, and the options are aluminium alloy or steel.

3.3.2. FEA analysis of the tool mechanical structure

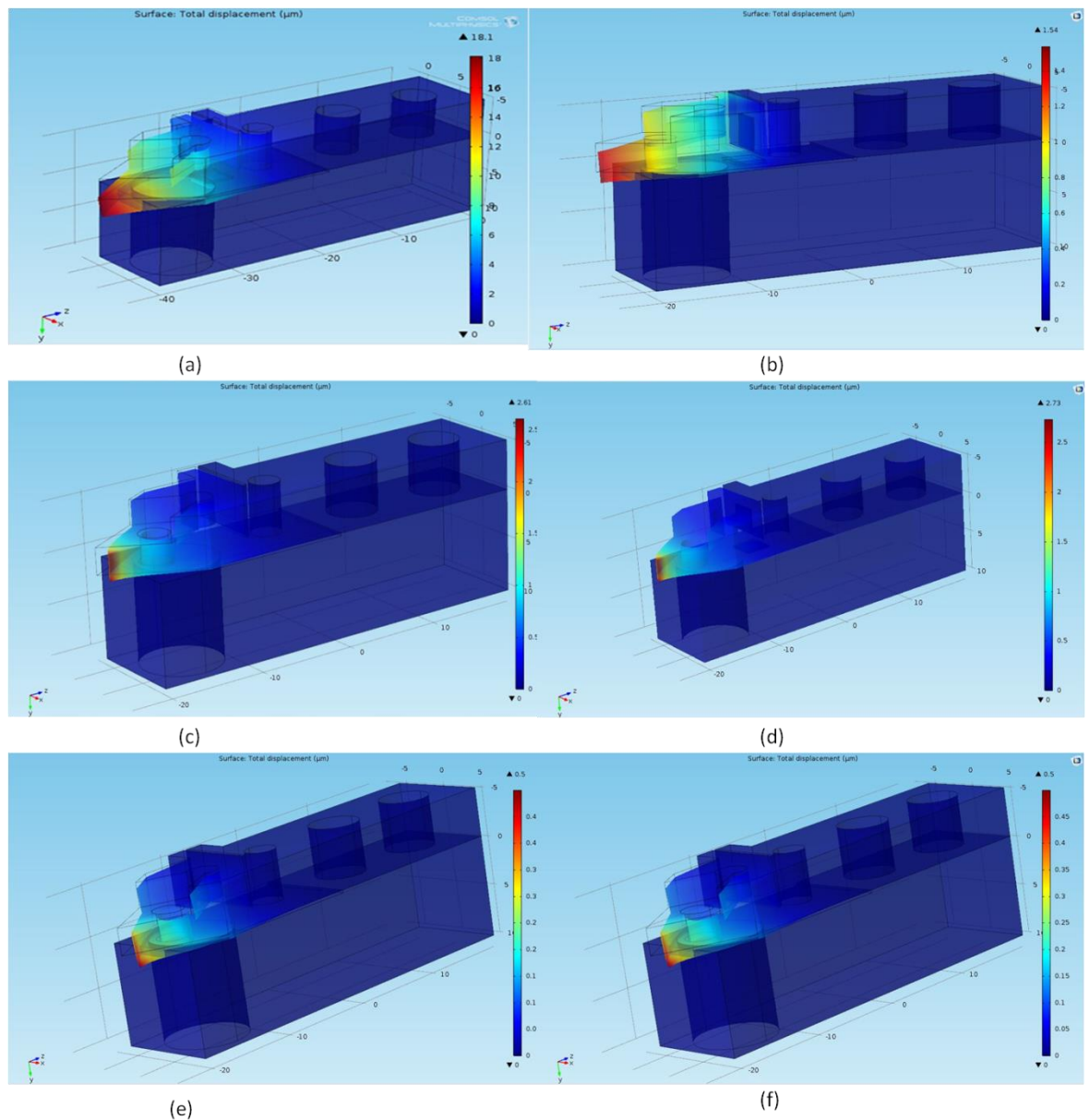


Figure 3.6: Surface displacement under 10 N, Y direction without piezoelectric ceramic (a); Y direction with piezoelectric ceramic (b); X direction without piezoelectric

The FEA analysis will show whether the designed tool structure will wear out or break using the following methods. The following simulations are based on aluminium alloy material for the tool shank.

The static analysis:

Figure 3.6 shows the deformation along the Y axis (horizontal) when a force of 10 N is applied horizontally on the cutting tip. So the stiffness of the structure is calculated as:

$$K = \frac{F}{X} \quad (3.3)$$

$$K = \frac{F}{X} = \frac{10\text{N}}{18.1\mu\text{m}} = 0.55 \text{ N}/\mu\text{m} \quad (\text{Without piezoelectric ceramic}) \quad (3.4)$$

$$K = \frac{F}{X} = \frac{10\text{N}}{1.54\mu\text{m}} = 6.49 \text{ N}/\mu\text{m} \quad (\text{With piezoelectric ceramic}) \quad (3.5)$$

Obviously, the stiffness is quite low due to the absence of the piezoelectric film between the top and the bottom; the optimum solution would be to insert the piezoelectric sensor into the slot, when the displacement has risen to 1.54 μm , by considering the piezoelectric film stiffness of 638 N/mm^3 -based on the elastic stiffness coefficient given from manufacturer data in the simulation. If we substitute the new X in to the equation (3.3), 6.49 $\text{N}/\mu\text{m}$ is attained (equation 3.5) which is much more acceptable.

Although normally the stiffer the structure the better, this tool has to insert a piezoelectric ceramic sensor to sense the force. Because in micro-cutting the cutting forces are very unlikely to go over 10 N, this stiffness is the best solution so far that can also provide an ideal environment for the piezoelectric ceramic sensor to do its job without wearing out the structure. The same boundary conditions and amount of force are applied for this simulation.

Figure 3.6 shows the deformation along the X axis (vertical) when a force of 10 N is applied vertically on the cutting tip. So the stiffness of the structure is calculated as below:

$$K = \frac{F}{X} = \frac{10\text{N}}{2.61\mu\text{m}} = 3.83 \text{ N}/\mu\text{m} \quad (\text{Without piezoelectric ceramic}) \quad (3.6)$$

$$K = \frac{F}{X} = \frac{10N}{2.73\mu m} = 3.66 N/\mu m \quad (\text{With piezoelectric ceramic}) \quad (3.7)$$

The stiffness on the X axis (vertical) is similar with or without the piezoelectric ceramic inserted in the gap, because the gap was pre-stressed paired.

The stiffness is similar on the Z axis (vertical):

$$K = \frac{F}{X} = \frac{10N}{0.5\mu m} = 20N/\mu m \quad (\text{Without piezoelectric ceramic}) \quad (3.8)$$

$$K = \frac{F}{X} = \frac{10N}{0.5\mu m} = 20N/\mu m \quad (\text{With piezoelectric ceramic}) \quad (3.9)$$

In conclusion, the stiffness is meeting the expectation and is ready to be implemented. Although at the cutting force direction the stiffness depends on the piezoelectric ceramic insert, 6.49 N can be considered as a relatively high cutting force during the micro-cutting process.

3.3.3. Modal analysis

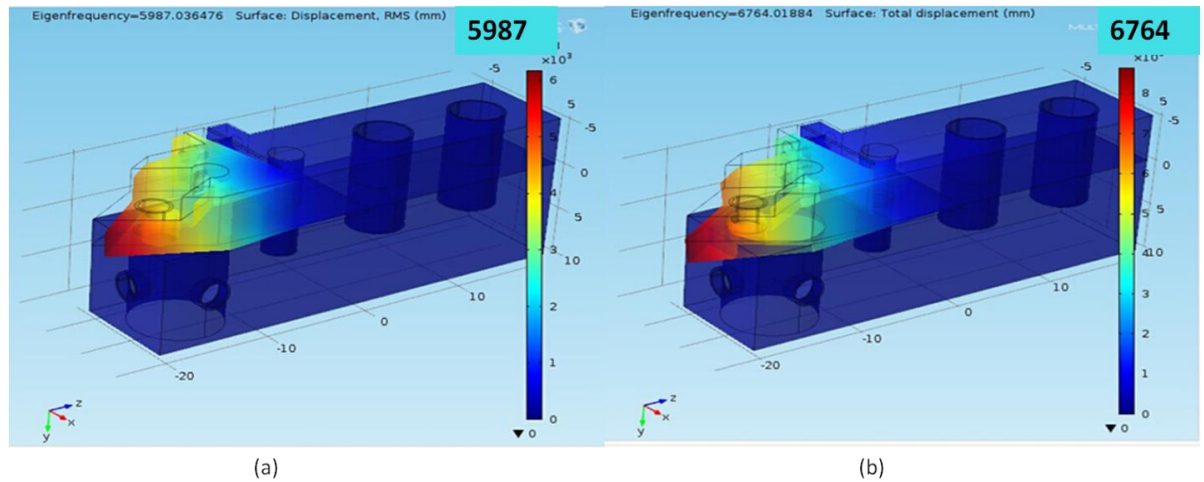


Figure 3.7: Fundamental natural frequency (a) and second step natural frequency (b)

Although the natural frequencies of the smart cutting tool with absence of the piezoelectric film are higher than the ones required in the diamond turning condition (less than 200 Hz), there is still a need to consider the natural frequencies with the piezoelectric film inserted at the top and the bottom. Figure 3.7(a) shows that the

fundamental natural frequency increases to be 5987 Hz in the cutting force direction. The following Figure 3.7(b) shows the first harmonic frequency at 6764 Hz. Moreover, the corresponding stress reduces to be only 3.4 MPa without considering the piezoelectric film due to the decreased deformation when subjected to a 10 N force.

3.4. Simulation development

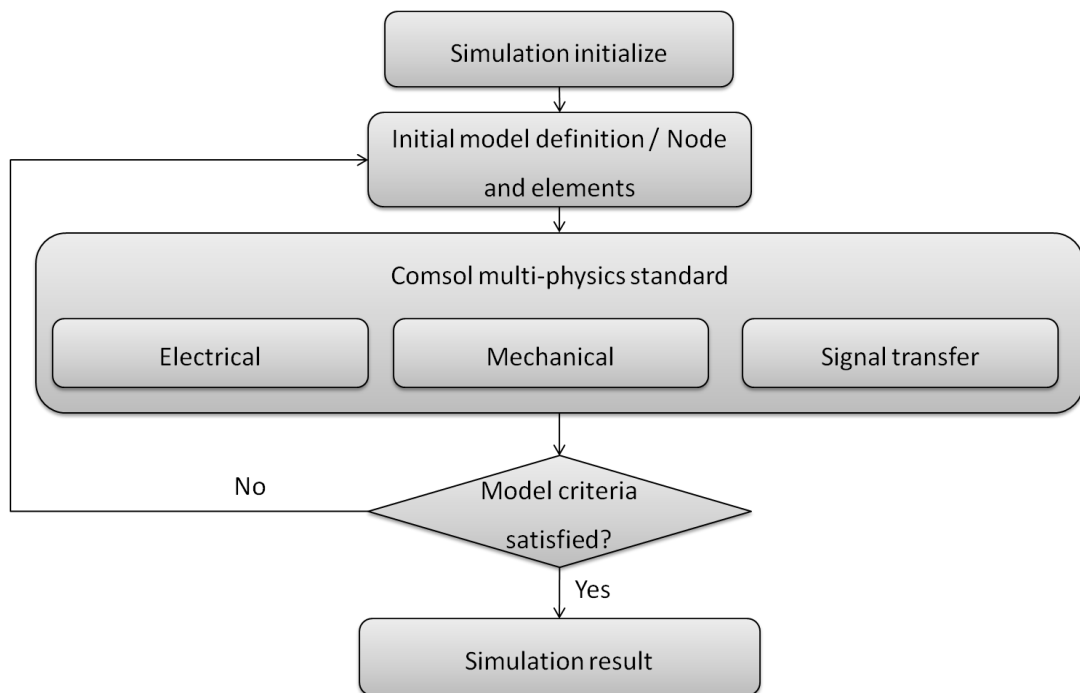


Figure 3.8: Flow chart of the simulation approach

The simulation process was separated into 3 steps; the flow chart, figure 3.8, summarises the simulation approaches. The simulation was aimed at 3 different physics philosophies: electrical, mechanical, and signal transfer.

Electrical physics is the piezoelectric physics that simulates the relation between cutting force and piezoelectric ceramic. Mechanical physics is the structural physics that simulates the structure of the tool, optimising the structure design until it fits the stiffness for the custom cutting trial required. Signal transfer physics is the radio

frequency physics that simulates the wireless signal transmission in a simulated environment designed under the consideration of a real machining environment.

3.4.1. Multi-physics process and the F-V-E algorithms

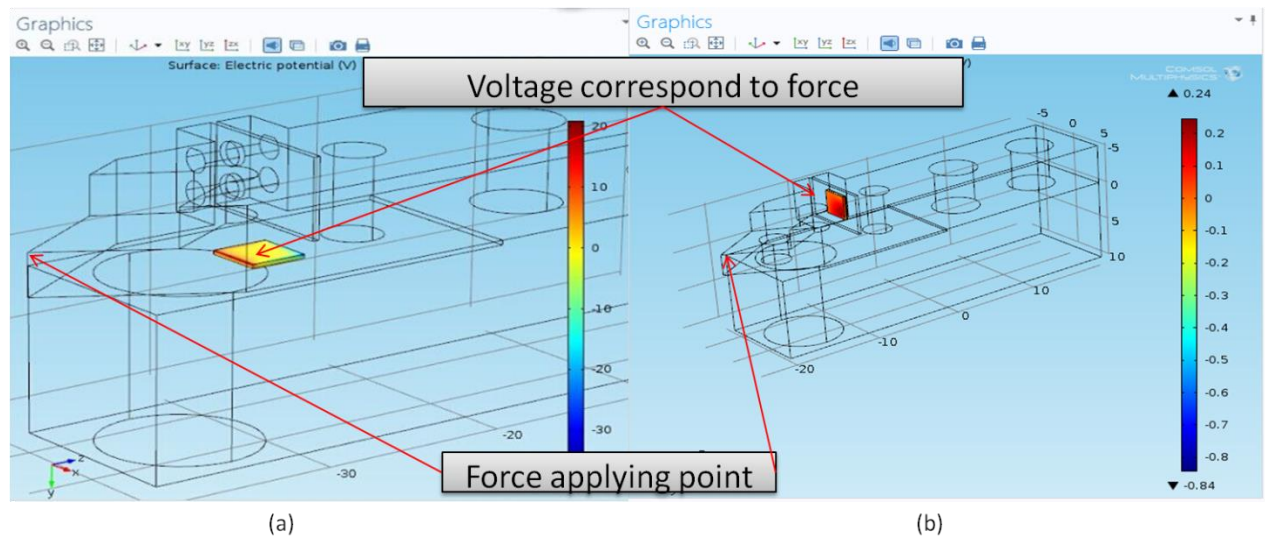


Figure 3.9: Force to voltage transformation cutting force direction (a). Feed force direction (b)

Figure 3.9 shows where the vertical and horizontal piezoelectric sensors are located; the relative voltage will be provided by forces applied on the structure. In the simulation, 10^{-1} N force is applied on the point of the cutting tool. COMSOL is used to study its voltage output corresponding to the mechanical deformation.

Through the whole simulation, known static forces from 1 to 10 N are applied on the blue point through X, Y and Z axes, in steps of 1 N. The voltage output is applied on the tool tip in order to produce an equivalent voltage output representing the force measurement by the proposed smart cutting tool.

Table 3.1: The simulated cutting force correlated to the piezoelectric sensor result

Cutting force (N)	Simulation results (V)	Simulation result while radial force is 1 N (N)
1	0.192	0.209
2	0.385	0.402
3	0.577	0.594
4	0.77	0.786
5	0.962	0.979
6	1.15	1.17
7	1.35	1.36
8	1.54	1.56
9	1.73	1.75
10	1.92	1.94

The known force loading is applied on the tool tip for a few seconds and then removed. This procedure produced a voltage output step due to the corresponding force loading. The force to voltage algorithm is given from the calculation of the table 3.1.

$$0.192 \times F = V \quad (3.10)$$

$$0.192 \times F + 0.016 = V \quad (3.11)$$

$$0.117 \times F = V \quad (3.12)$$

$$0.106 \times F + 0.202 = V \quad (3.13)$$

Equation (3.10) is the linear relationship between cutting forces correlated voltage output. Equation (3.11) is the linear correlation between cutting force, coupling radial force with the voltage output. Equation (3.12) is the linear relationship between feed force correlated voltage output, and equation (3.13) is the feed force coupling radial force correlated voltage output.

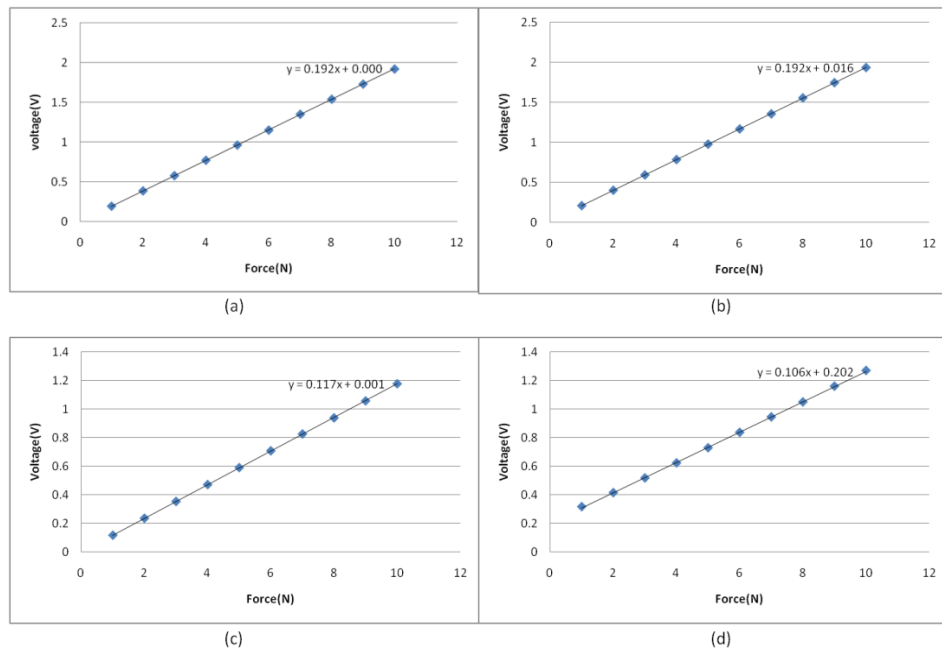


Figure 3.10: Linear relationship between the simulated cutting force and the sensor voltage output (a) and with radial force 1 N simultaneously (b) Linear relationship between the simulated feed force and the sensor voltage output (c) with radial force 1 N associated (d)

Figures 3.9 and 3.10 show a 10 N force applied on the point the cutting tool. COMSOL studies its voltage output corresponded to the mechanical deformation.

From Figure 3.10 the force applied in the simulation resulted in a piezoelectric voltage of 1.92 V. Because the position of the piezoelectric ceramic sensor was not directly under the forces load point, there is a momentum required to be calculated.

Table 3.2: The simulated feed force correlated to the piezoelectric sensor result

Feed Force (N)	Simulation Result (V)	Simulation Result with Radial Force 1 N (V)
1	0.118	0.317
2	0.237	0.415
3	0.355	0.518
4	0.473	0.623
5	0.592	0.729
6	0.71	0.837
7	0.828	0.945
8	0.941	1.05
9	1.06	1.16
10	1.18	1.27

Table 3.3: The simulated result of the coupling forces on vertical piezoelectric sensor

Force (N)	Feed force [1-10], Radial force [0] (Simulation Result) (V)	Radial force [1-10], Feed force [0] (Simulation Result) (V)	Radial force [1-10], Feed force [1-10] (Simulation Result) (V)
1	0.118	0.228	0.3172
2	0.237	0.449	0.63439
3	0.355	0.673	0.95159
4	0.473	0.897	1.2688
5	0.592	1.122	1.585995
6	0.71	1.346	1.903195
7	0.828	1.57	2.220395
8	0.941	1.795	2.537595
9	1.06	2.019	2.854795
10	1.18	2.243	3.171995

From Table 3.3, the relation between feed force direction and radial force direction can be assumed as:

$$V_{F_{vp}} = aV_{F_f} + bV_{F_r} \quad (3.14)$$

Where, substituting the data from the table we get:

$$a=2.39, b= 0.1536.$$

Therefore, the correlation of the feed force and the radial forces is resolved. According to the real cutting trials, the Kistler Dynamometer is used to associate the calibrations, and from the actual measurement data we have found that radial forces are normally 0.01-0.2 N in ultra-precision machining processes, which gives:

$$V_{F_{vp}} = aV_{F_f} + b(0) \quad (3.15)$$

$$V_{F_{vp}} = aV_{F_f} + b(0.1) \quad (3.16)$$

$$V_{F_{vp}} = aV_{F_f} + b(0.2) \quad (3.17)$$

Analysing the equations by substituting the voltage of the possible radial force, the correlation equation for the vertical piezoelectric ceramic can be seen as:

$$V_{F_{vp}} = aV_{F_f} \quad (3.18)$$

3.5. Machining environment and its effect

The simulation of the smart cutting tool performance under a machining environment and its effects are aimed to investigate the wireless signal strength, and hence to ensure the Bluetooth transmission signals are reliable during the machining environment.

The simulation of the machining environment was set up using three components: antenna, air and a one sided free metal block. The antenna was drawn to match the 2.4 GHz Bluetooth signal that was applied on the smart cutting tool; the dimension of the metal block was 1.5 m long x 0.5 m wide x 0.5 m high to simulate the cutting machine (the metal block is an obstruction for the wireless signal transmission). This simulation is aimed to give a peek at the advantages of the electron mechanic smart cutting tool system at stability and range aspects.

3.6. Simulation of the antenna transmitted efficiency using analogue signal (factory) environment

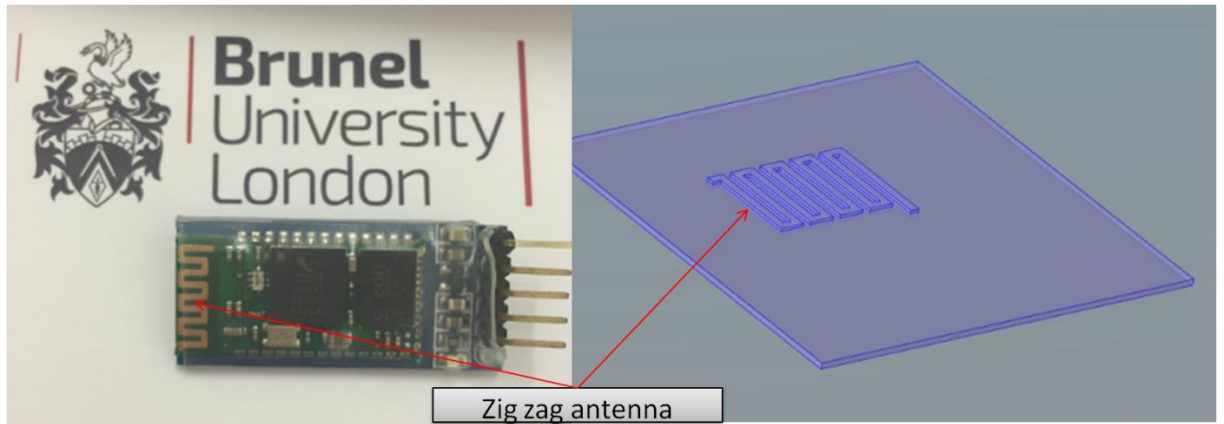


Figure 3.11: Real Bluetooth module and 3D model antenna under COMSOL

The S structural metal shim is the zig-zag antenna of the Bluetooth chip. Because the wireless signal operates at 2.4 GHz, hence the wavelength of the signal is 125 mm. This antenna has 1/4 of the wavelength, where the simulated antenna is length 31.25 mm in total. Copper was chosen as the material of the antenna.

The simulation of the wireless signal of the machining environment is constructed in three parts: machine body, antenna and air. The metal hollows insulate the cutting machine and with one face boundary defined as glass. The Bluetooth signals applied in the smart cutting tool used the meander line antenna. In Figure 3.12, the meander line antenna is shown, the frequency in the simulation was customised to 2.4 GHz, and the circles of the air were unable to be enlarged due to the computer's memory tolerance while the COMSOL software is running.

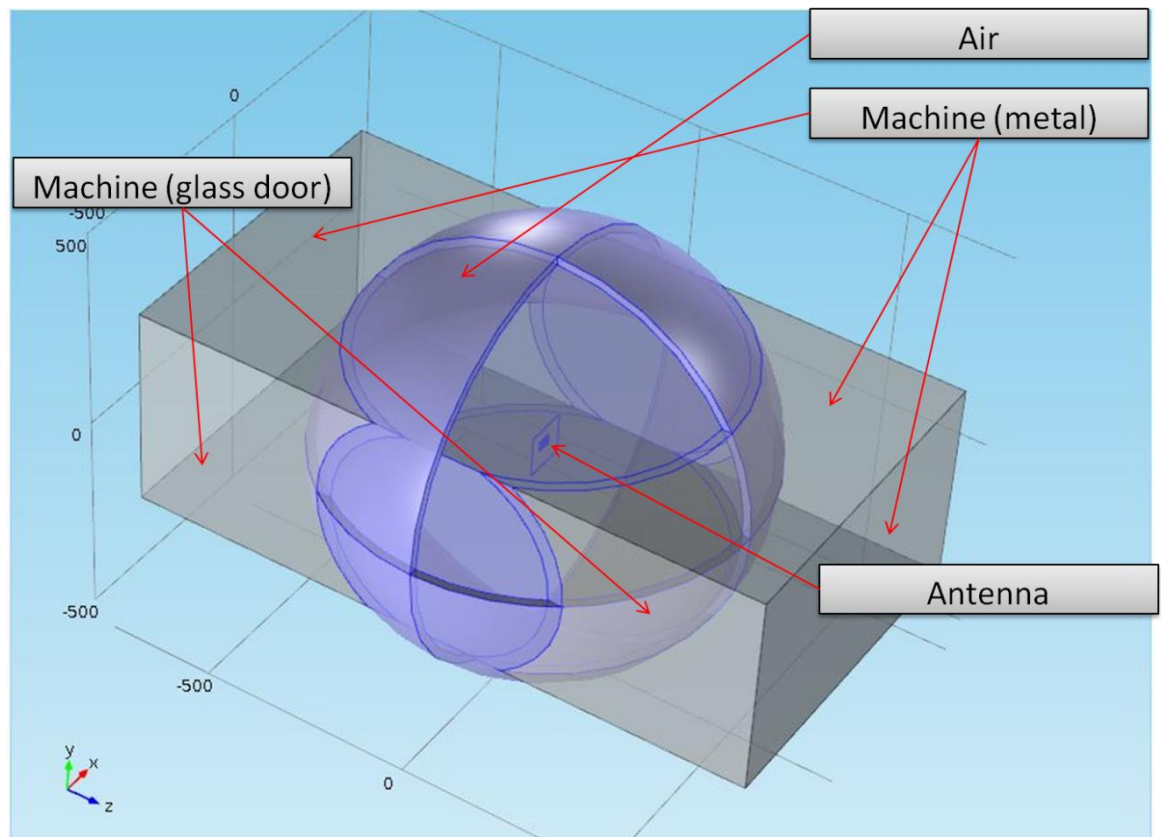


Figure 3.12: Machine environment simulation for dipole antenna transmission efficiency

Because the antenna's structure is comparatively much smaller than the 'machine', the air ball distance is in reality unlikely to be expanded due to the meshing problem since it is enough that part of the 'air' out of the machine body. The meshing problem means that while the 'air' ball expands in COMSOL multiphysics, the requirement of computer hardware becomes unreasonably large. Hence the diameter of the 'air' was decided as 1.5 m.

The wireless signals from 1.5 m away are shown in the following Figure 3.13, the far field gain was less than 15 dB, thus there was a very clear signal for a professional Bluetooth device to pick up and then analyse.

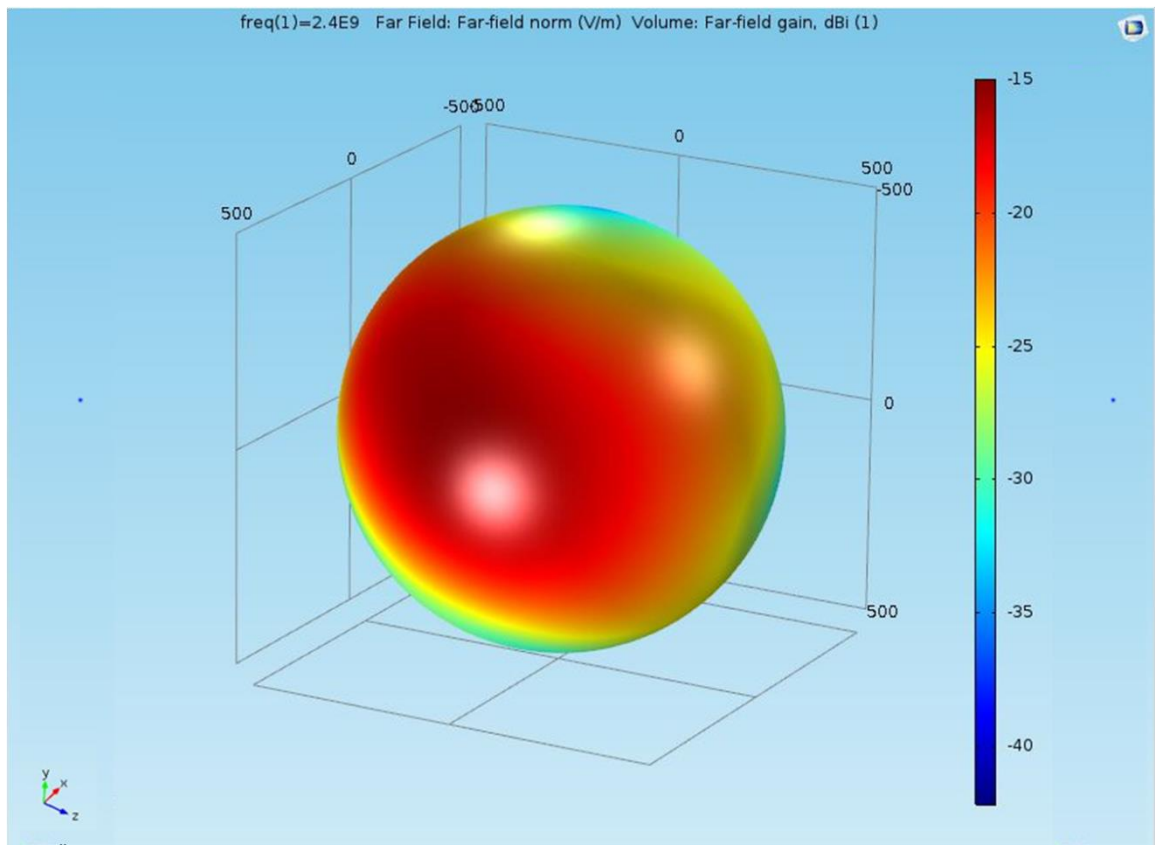


Figure 3.13: Electric field result in machining environment

3.7. Summary

Smart tooling has to be a subset of smart manufacturing. The main targets were to improve the process reliability and optimise the machine performance in order to obtain a better prototype.

As illustrated in the Figure 3.14, the simulation is developed based on the integration of three main physics involved, i.e. electrical, mechanical, and electronic signal transfer. However, there is normally another physical phenomenon, i.e. cutting temperature along with a cutting process, which is not included in the simulations. It is because the cutting temperature changes in micro cutting are extremely small compared with the conventional cutting process. Additionally, the piezoelectric material in the smart cutting tool is modified to resist cutting temperature up to 80-160°C. Therefore the heat

transfer is not taken account in this specific study.

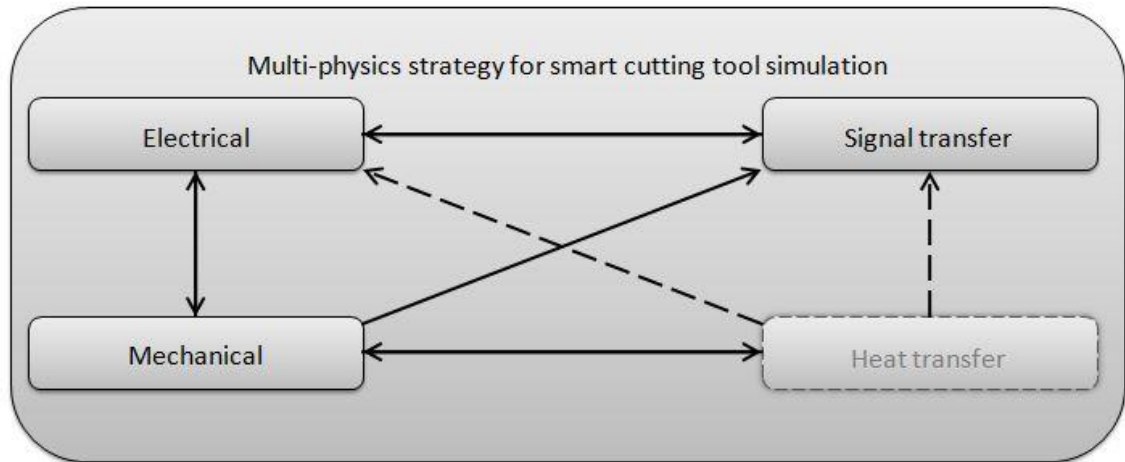


Figure 3.14: Physical couplings in smart cutting tool

The smart cutting tool to be designed aims to have a better sampling rate and longer remote sensing distance. This tool is operational in plug-and-produce manner, where not only being used for micro-cutting purposes. This smart cutting tool is automatically operated autonomously interfacing with machine tools. All data are transmitted under the standard Bluetooth transmission protocols, which can ensure the data has being proofread and checked.

All data captured are stored and analysed in order to determine the best cutting condition and extend the tool life. In further research, this is going to feed back and control the cutting tool in order to maintain the best positions or motions.

From previous researches, the proposed smart cutting tool configuration with wire connection to the piezoelectric ceramic and a BNC cable connected to the charge amplifier needs to be fully protected because it could be damaged by swarf or struck by flying chips, which could affect the accuracy of the force measurement.

Therefore, wireless technology could be a better solution for the above issue. We have designed several different types of wireless smart cutting tools. The Bluetooth transmitted piezoelectric ceramic smart cutting tool showed good performance and the

ability to show clear results on cutting force and hence to monitor the cutting condition. This designed wireless smart cutting tool was fully performance tested and awaits to be proven in cutting trials and be compared with commercialised tools as regards their accuracy, capabilities and stabilities.

Chapter 4 Development of the prototype smart cutting tool

In this chapter, the main goal is to present the prototype design process from conceptual design into detail design. The design processes are presented with structural design then followed by calibration steps and the accuracy and reliability test at the same time. Finally, a designed prototype of the smart cutting tool is shown and ready for cutting trial tests.

4.1 Introduction and the design process

A smart cutting tool takes an important role in a precision machine. It is a sub-system of a typical precision machine. The design of the smart cutting tool is used to develop a smart cutting tool that is not only a sensing/measuring item but also a part of the machine tools. Hence, the mechanical design of the smart cutting tool has to adhere to high stiffness and natural frequency.

A force can generally be measured by three methods: using force shunt, direct and indirect force measurement. The proposed smart cutting tool has employed the force shunt for cutting force measurement by taking account of the tool design and refitted tool configuration. For the direct force measurement, it is difficult to mount a sensor fully in line with the force path, which may result in fracture of the piezoelectric film element. With the indirect method, the measured strain may only represent a small proportion of the cutting force and the measurement sensitivity may well be limited [Stein, 2002]. To achieve a high resolution in measuring the cutting forces in process, the piezoelectric ceramic films are applied with the direct force measurement method.

The film sensor is secured onto a metal shim between the slots on the tool shank and being pre-stressed enhances its measurement sensitivity.

This proposed smart cutting tool has been tested before the wireless module is implemented on it. There is a slot reserved for a capacitive sensor; a calibrated smart cutting tool will allow removal of this. The capacitive sensor is for ensuring the calibration of the mechanical structure instead of the piezoelectric sensor because the piezoelectric sensor has to be calibrated in the meantime to ensure the result's accuracy.

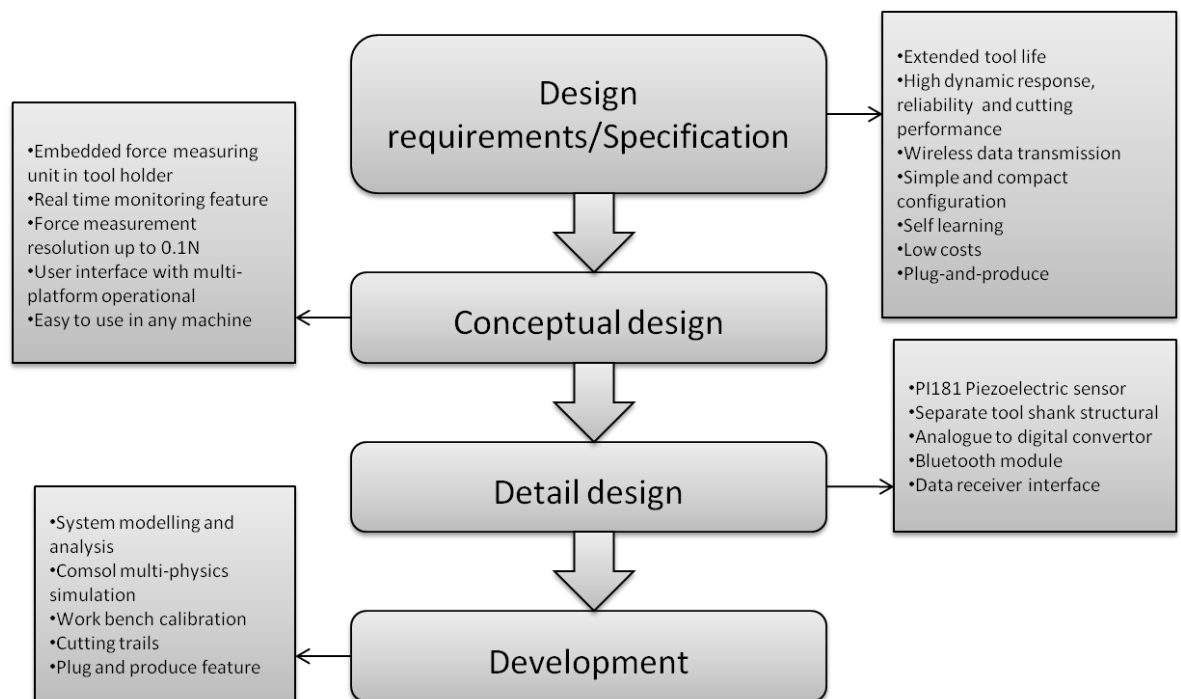


Figure 4.1: Design process for the smart cutting tool

Figure 4.1 shows the design process from design specification to development of the smart cutting tool. This design process was adopted from the total design method proposed by Stuart Pugh [Pugh, 1991].

4.2 Conceptual design process

As regards the idea of a smart cutting tool being ‘Smart’, the major differences compared with the reviewed sensed tools are that a smart cutting tool should have the ability to communicate with a control platform with machining process in real-time and also have plug-and-produce characteristics. These features require the smart cutting tool to be able to adapt to most of the machine tools, different industrial environments, and also various control platforms. Besides these features not possessed by the reviewed sensed tool, of course the smart cutting tool will have high dynamic response, high reliability, high cutting performance as well as all the sensors, cutting tools and sensed tools.

It should be mentioned that this idea of the ‘smart cutting tool’ is a new novel approach initially proposed by Professor Kai Cheng [Cheng et al., 2015]. However, the version of the smart cutting tool was not uniformed. Hence a novel model was built, presented by the author in chapter 2.

4.2.1 Design requirements

The smart cutting tool is aimed to help design a smart unit that not only has a role as a cutting tool, but also as a sensor, a real-time sensor that has the ability to adapt into any machining environment. Hence, this prototype design is to test first the stability of the structure as a reliable cutting tool, then test the system and its correspondence as a sensor. The design was required to provide:

- Dynamic response of the physical structure;
- Stress concentration of the smart cutting tool; and
- Sensitivity of the tool.

The tool tip and tool holder were not essential to consider in the design, because the tool tips were replaceable as were the tool holders. 0.1 N resolution of the force’s variation was decided by both electronic and mechanical parts. Dynamic response and stress

concentration had detailed simulations in the previous chapter. The dynamic behaviour of the smart cutting tool structure results from the multi-physics simulation. During the process of real-world machining, the dynamic response should be anticipated by the simulated results.

Although the static stiffness is relatively easy to be predicted before the prototype is produced, the dynamic stiffness is difficult to be predicted at the design stage. Hence, in this chapter the optimisation and calibration is also presented before the actual prototype structure is fully packaged.

4.2.2 Tool conceptual design and configuration

Brain storming is the initial method to think out the conceptual design. In this stage, the selections of key components in this smart cutting tool are explained in the following paragraph. These key components include: tool shank material, tool shank structural design, piezoelectric ceramic sensor dimension, piezoelectric ceramic sensor position in the smart cutting tool, and the fixtures.

The mechanical design process included the structural design and size identification, conceptual design and its feasibility study. The previous chapter has discussed the modal and FEA analysis in view of the multi-physics simulation.

4.3 Detailed design

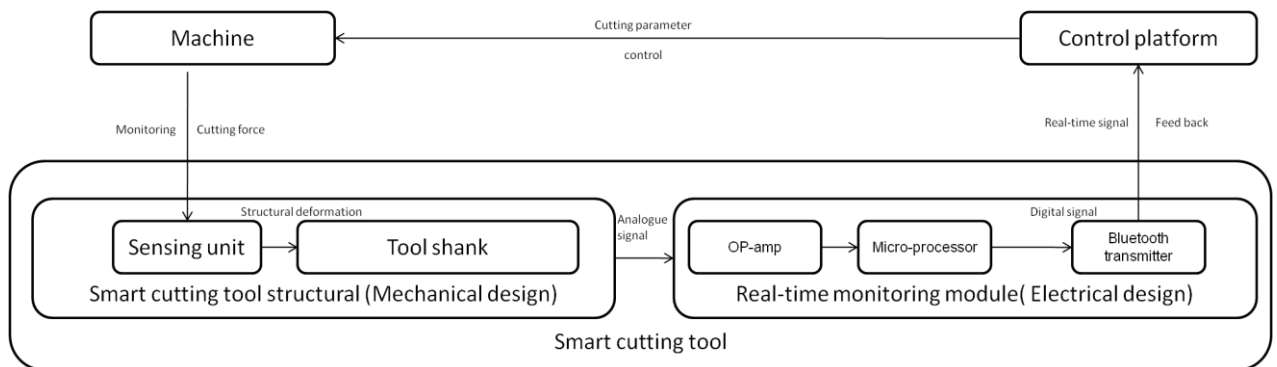


Figure 4.2: Detail design of the smart cutting tool

The detailed design of the smart cutting tool should be broken-down into two main parts, mechanical and electrical. This chapter is mainly focused on the mechanical structural design of the smart cutting tool and its calibration. The mechanical design of the smart cutting tool basically incorporated two elements, the sensing unit, which is piezoelectric ceramic, and the tool shank. The whole mechanical design is aimed to be sensitive for force measurement; the force led structural deformation will be detected by the mechanical design of the smart cutting tool and the deformation signal will be passed to the real-time monitoring module, hence a complete smart cutting tool. The smart cutting tool will feedback the real-time signal to the control platform of the cutting machine, then the cutting parameter can be adjusted according to the force monitoring signal. The real-time force signal is fully visualised when the cutting process is in operation.

4.3.1 Material selection

Material selection for this smart cutting tool is one very important factor in determining final smart cutting tool performance, as was already explained in chapter 3. Before the prototype was built there were two options available at the laboratory at Brunel for the

materials of the smart cutting tool, namely aluminium alloy and steel alloy. Considering the two materials' characteristics for dynamic structure response and stiffness, steel alloy seems to be better choice. However, the smart cutting tool also required sensitivity, and from this view when considering the selection of material, aluminium had the advantage. After FEA analysis and modal analysis, aluminium material met the stiffness requirement for the experimental cutting condition. The smart cutting tool was designed to measure the feed force and cutting force, and direct force measurement would be a better and intuitive way. Hence, the piezoelectric sensors are located vertically and horizontally around the tool shank as shown in Figure 4.3. The capacitive sensor was in used in the prototype to verify the design and awaits calibration.

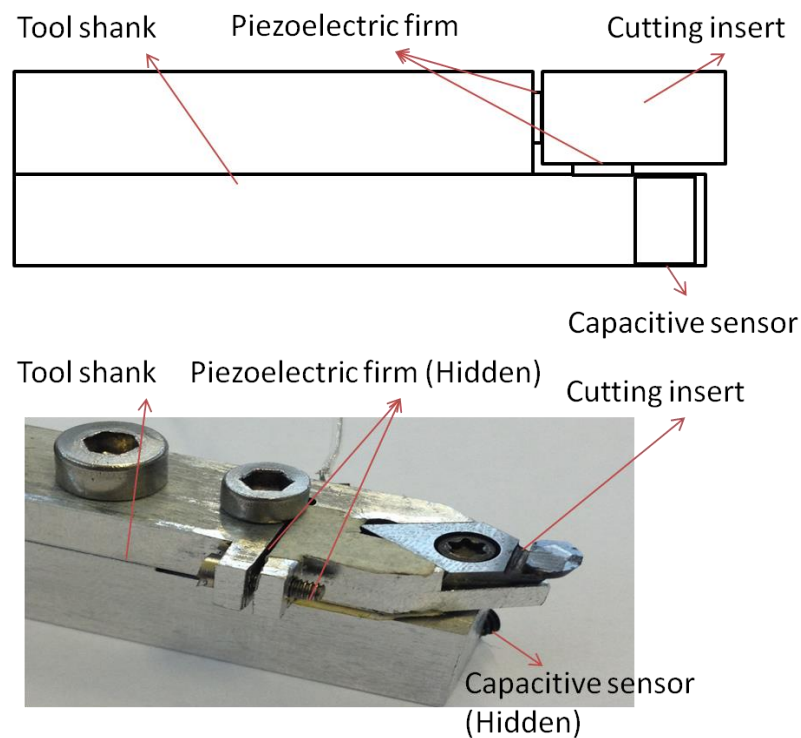


Figure 4.3: Tool design and configurations mechanical

4.3.2 Structural design

A mechanical structure is comprised of stationary and/or moving mechanical objects. The stationary object in this thesis is the smart cutting tool shank, where the moving

objects are the cutting force variations and the machining vibration during the machining process. The structural design is essential since the structure of the tool shank not only provides the static support of the diamond tool tip but also contributes to the dynamic performance required in the machining process [Slocum, 1992]. The major design issues of a mechanical system are:

- Stiffness;
- Structural configuration;
- Structural connectivity; and
- Structure dynamic performance.

A two-part assembly structure of the smart cutting tool was used rather than a unified structure. The stiffness and dynamic responses are rigid enough for most micro-turning machining processes, and, of course, expected experiment cutting conditions for cutting trials were fully covered. The upper part and base part of the tool shank are firmly bolted together with two screws (M3).

The proposed design configuration for the smart cutting tool is shown in Figure 4.4, and comprises a diamond cutting insert, a refitted tool holder and two single layer piezoelectric film sensors. The piezoelectric film sensors have dimensions of $3 \times 3 \times 0.26$ mm. One piezoelectric film, namely sensor 1, is embedded between the upper part and base part and placed 15 mm away from the cutting tip in order to measure the cutting force. A slot of thickness of 0.35 mm was machined on the upper part to embed the other piezoelectric film, named as sensor 2, in order to measure the feed force. Two pieces of insulation tape, placed on top of the piezoelectric film sensor and the bottom of the metal shim respectively, are applied to insulate and fix the piezoelectric film into a position. A connection wire is soldered onto the metal shim that functions as the electrode extension of the piezoelectric film sensor and makes available the voltage output generated from the sensor.

The pre-stress imposed by pre-stress screws can reduce the unwanted hysteresis effect, which can then provide a better linear relationship between an applied force and the sensor voltage output, as it enhances the piezoelectric film sensor performance through a much improved surface contact. For this smart cutting tool, two screws (M5) are applied for pre-stressing the piezoelectric film in the cutting force direction, and one screw (M3) is used for pre-stressing the piezoelectric film in the feed force direction.

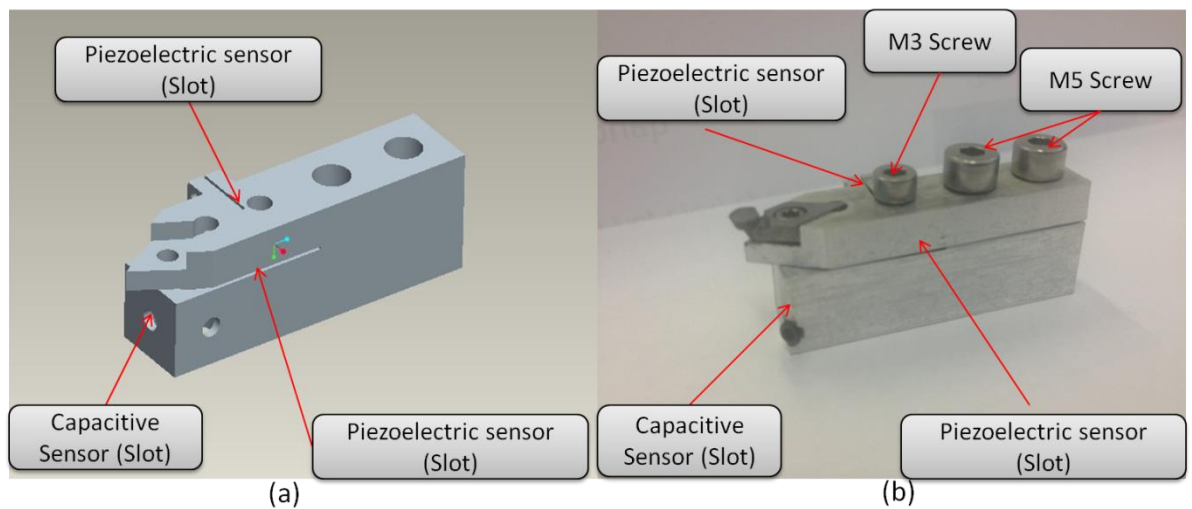


Figure 4.4: The design configuration of the smart cutting tool 3D model (a) and the design configuration of the smart cutting tool prototype (b)

Two slots on the tool shank were reserved to insert the piezoelectric ceramic sensor unit. The upper part and base part are shown in Figure 4.5. The slot on the upper part on the left hand side is where the feed force sensor was going to locate. This slice opening ended at the middle, just before the pre-stress screw slot; the reason for this was to secure the stress concentration of the smart cutting tool to make sure the piezoelectric sensor received as much pressure as possible, and the tool shank deformed as little as possible at the same time. The cutting force direction sensor is located on the identified step of the base part. The smart cutting tool is still after all going to be used in the real

machining. The base part and upper part will be combining as a unit through these pre-screw holes.

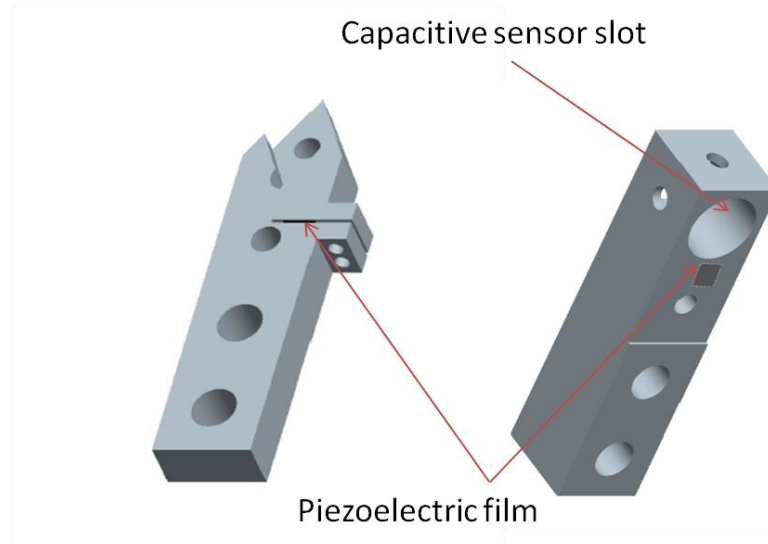


Figure 4.5: The design of upper part (left) and base part (right) of the smart cutting tool

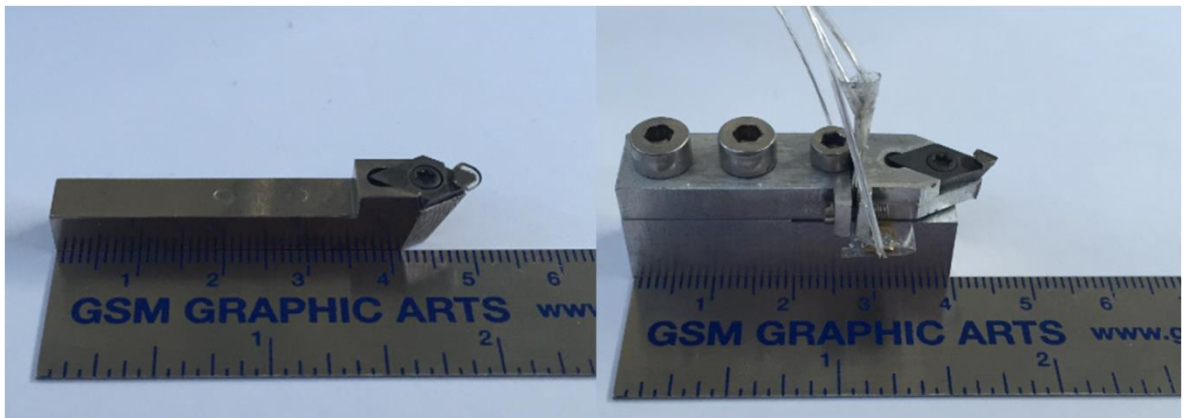


Figure 4.6: Diamond micro-cutting tool and diamond smart cutting tool comparison

Figure 4.5 has shown the virtual structural of the prototype smart cutting tool in detail pointing out where the sensor unit is to be attached. Figure 4.6 has shown the comparison in size and dimensions of the normal diamond micro-cutting tool and the prototype smart cutting tool.

The study was focused on determining the force variation during the micro-cutting

process. Cutting tools normally have dimensions of 45 mm × 10 mm × 10 mm. Hence, the smart cutting tool has to have a similar size in order to fit in to the same tool holder, otherwise it is unable to acquire the feature of plug-and-produce ability.

Since the multi-physics modelling has approved that the natural frequency of this combination of parts has more than enough stiffness to be used at the test cutting machine under any reasonable cutting conditions, the smart cutting tool prototype was built.

4.3.3 The piezoelectric film sensors and integration

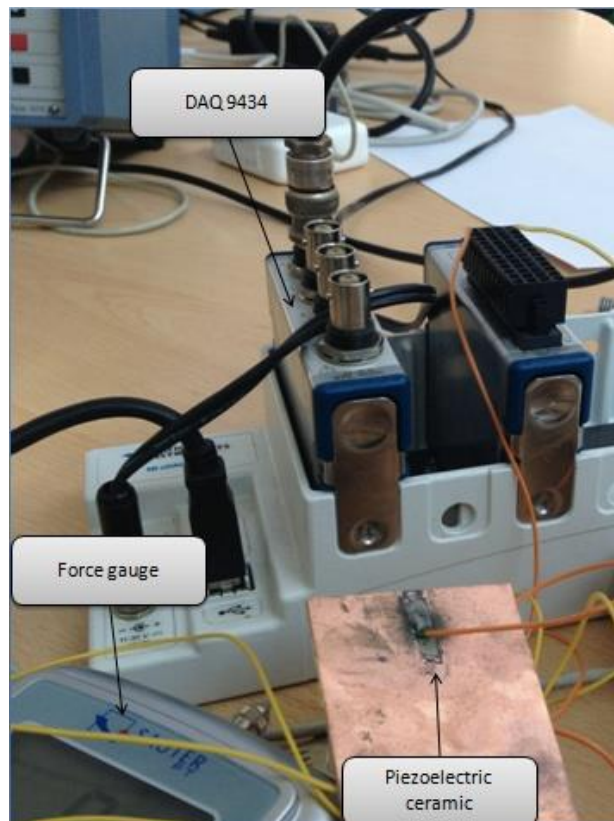


Figure 4.7: The bench test of the piezoelectric ceramic response

Piezoelectricity is popular in applications such as the production and detection of vibrations; hence, the formulated ceramic material is a very good transducer for force sensing. Piezoelectric ceramics are multi-functional devices with many applications.

They can work to convert electrical energy into vibration mechanical energy; they can also work as sensors and transducers to convert various physical parameters into electrical signals. In this article the piezoelectric ceramics are being using as force sensors. The reason for applying piezoelectric ceramics in the smart cutting tool for the force shunt force measurement in this design is because the piezoelectric ceramics applied in this experiment are very tiny, but generate obvious voltage differences while the force is applied directly.

The piezoelectric sensor dimension was decided at $3 \times 3 \times 0.26$ mm because it was the minimum size we could order to do modification of the smart cutting tool under the laboratory conditions. A relatively small piezoelectric sensor can be considered as a point rather than a phase. Hence the voltage output was computed directly and converted in to forces for further studies. This sensor was being tested before packaging into the tool shank and the operation was shown in Figure 4.7, where the force gauge were using to measure the provided force to be known,DAQ acquisition card are used to collect the correspondence signals from the pizeo and compared with a capacitive sensor. and the result is shown in Figure 4.8 on self programmed LABveiw software graphic interface.

The shown signal were quite representative that the signal are generated by a single press of 0.25N because this is the limitation of stationary force manually applied on the pizeo by author holding the force gauge in the experiment.

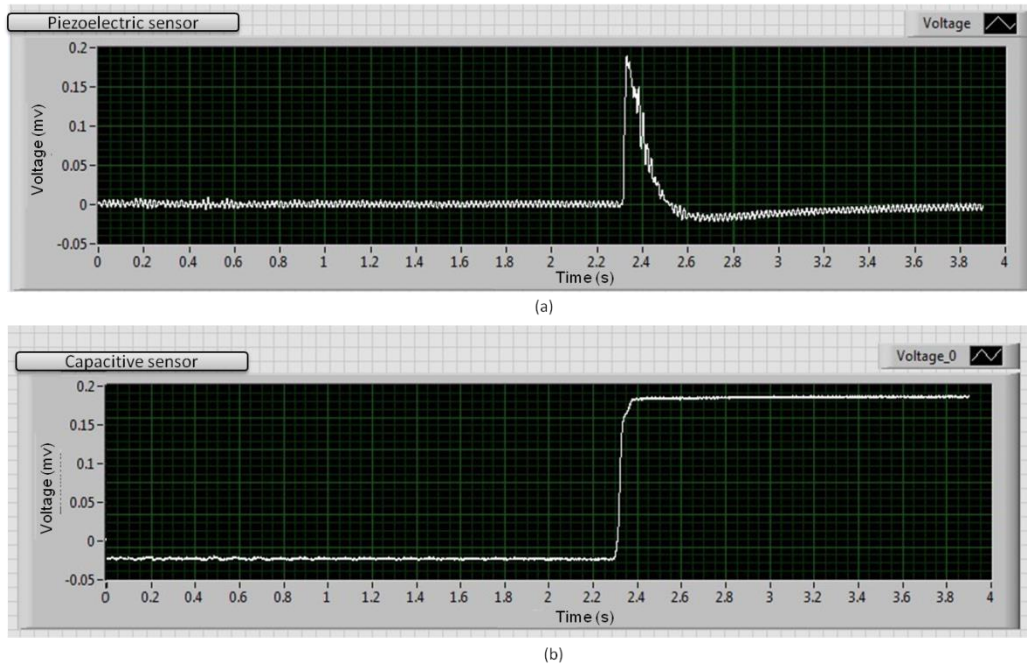


Figure 4.8: Force response result of the piezoelectric sensor (a) demonstration compared with capacitive sensor (b)

In the project, PI181 and PI255 were purchased from Physik Instrumente (PI) the piezoelectric technology company. Piezoelectric ceramics are elastic materials that will build an electric charge because of the pressure, temperature, vibration and light changes. The polarized piezoelectric was able to progressively increase the output of electron charges according to the stimulation.

PI181 is a modified lead zirconate – lead titanate material with extremely high mechanical quality factor and also very high Curie temperature. The good temperature and time stability of its dielectric and elastic constant make it fully cover the requirement of being a sensing unit for the cutting forces. PI255 also has a high Curie temperature, very similar to PI181; however, its mechanical quality factors are very low and hence it was purchased for actuator tasks, which is the project following after the smart cutting tool.

Material Data

Material type		PIC 181	PIC 255
Parameter			
Physical and dielectric properties			
Density	ρ (g/cm ³)	7.80	7.80
Curie temperature	T_c (°C)	330	350
Permittivity	In the polarization direction $\epsilon_{33}^T/\epsilon_0$	1200	1750
	perpendicular to the polarity ϵ_{\perp}	1500	1650
Dielectric loss factor	$\tan\delta$	3	20
Electromechanical properties			
Coupling factors	k_D	0.56	0.62
	k_t	0.46	0.47
	k_{31}	0.32	0.35
	k_{33}	0.66	0.69
	k_{15}	0.63	0.66
Piezoelectric charge constants	d_{31}	-120	-180
	d_{33} (10 ⁻¹² C/N)	265	400
	d_{15}	475	550
Piezoelectric voltage constants	g_{31} (10 ⁶ V/m/N)	-11.2	-11.3
	g_{33}	25	25
Acousto-mechanical properties			
Frequency constants	N_o	2270	2000
	N_1	1640	1420
	N_3	2010	
	N_t	2110	2000
Elastic constants (compliance)	S_{11}^T (10 ⁻¹² m ² /N)	11.8	16.1
	S_{33}^T	14.2	20.7
Elastic constants (stiffness)	C_{33}^D (10 ¹⁰ N/m ²)	16.6	
Mechanical quality factor	Q_m	2000	80
Temperature stability			
Temperature coefficient of g_{33} (in the range -20°C up to +125°C)	TK g_{33} (x10 ⁻³ /K)	3	4
Aging stability (relative change of the parameter per decade in %)			
Relative dielectric constant	C (%)		-1.0
Coupling factor	C_K (%)		-1.0

Figure 4.9: The material data of piezoelectric ceramic

The coefficient of sensing location and tool tip are calculated as follows:

$$V = g_{33} \times T \times h \quad (4.1)$$

Where V is the voltage output,

g_{33} is the piezoelectric voltage constant and can be found from figure below;

T is the mechanical pressure applied onto the piezoelectric ceramic; and

h is the height of the piezoelectric sensor, in this application, 0.26 mm.

By substituting 1 N force in to this algorithm:

$$V = 25 \times 10^{-3} \times \frac{1}{3 \times 3 \times 10^{-6}} \times 0.26 \times 10^{-3} \quad (4.2)$$

$$V = 0.722v \quad (4.3)$$

From equation (4.3), the voltage reading from a 1 N force pressing directly on the piezoelectric ceramic should be 0.722 V. From the previous chapter, neither of the simulation results on the vertical and horizontal piezoelectric sensor inserts were 0.722 V. And also, from the geometry aspect, there is a moment of force in between the force loading point and piezoelectric stress concentration.

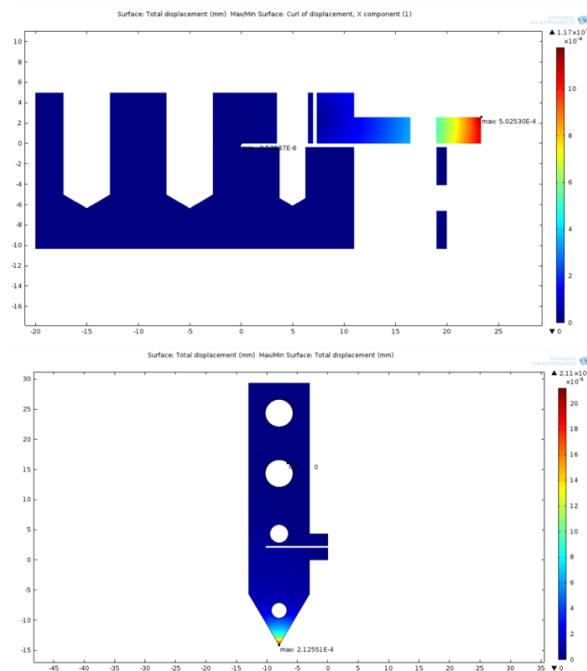


Figure 4.10: 2D plot of stress deformation, 1 N force on cutting force direction (top), and 1 N force on feed force direction (bottom)

Because the relation between the sensor voltage and smart cutting tool voltage output is actually linear, a ratio is calculated by the table below. Also, the force to voltage steps were linear mathematically; hence, the force is represented by voltage in the following calculation.

Table 4.1: Smart cutting tool sensor voltage output with regulated piezoelectric ceramic reference voltage output

Piezoelectric on its own	Voltage (V)	Cutting force (N)	Voltage (V)	Feed force (N)	Voltage (V)
1	0.722	1	0.192	1	0.118
2	1.444	2	0.385	2	0.237
3	2.166	3	0.577	3	0.355
4	2.888	4	0.77	4	0.473
5	3.61	5	0.962	5	0.592
6	4.332	6	1.15	6	0.71
7	5.054	7	1.35	7	0.828
8	5.776	8	1.54	8	0.941
9	6.498	9	1.73	9	1.06
10	7.22	10	1.92	10	1.18

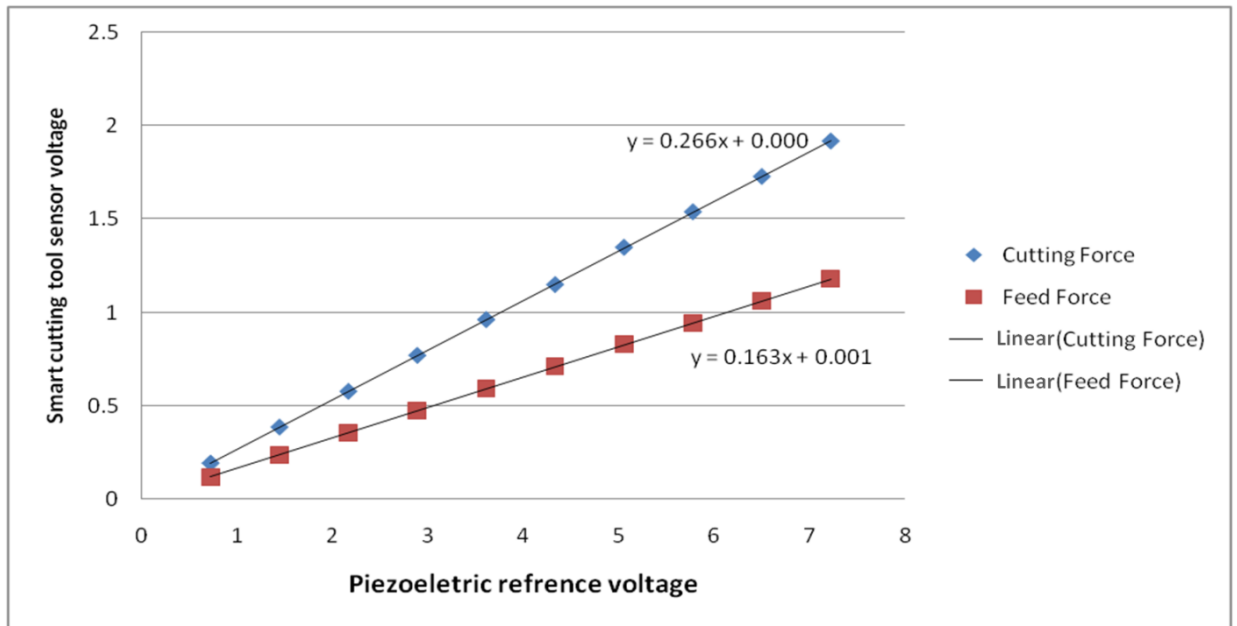


Figure 4.11: The linear ratio relationship between force sensors and piezoelectric reference voltage

Figure 4.11 shows the ratio relationship between cutting force sensor voltage output and the piezoelectric ceramic reference voltage output (red), and also the linear ratio between feed force sensor voltage output and piezoelectric ceramic reference voltage output (blue).

$$V_{cf} = 0.266 \times V_p \quad (4.4)$$

$$V_{ff} = 0.163 \times V_p + 0.001 \quad (4.5)$$

Hence, the correlation equations of the force related to smart cutting tool sensor results are:

$$V_{cf} = g_{33} \times T_c \times h \times 0.266 \quad (4.6)$$

$$V_{cf} = g_{33} \times T_c \times h \times 0.163 \quad (4.7)$$

$$V_{cf} = 0.722 \times 0.266 \times F_c \approx 0.192F_c \quad (4.8)$$

$$V_{cf} = 0.722 \times 0.163 \times F_c \approx 0.118F_c \quad (4.9)$$

Where, V_{cf} is the voltage of cutting force sensor and V_{ff} is the voltage of the feed force sensor. The constant coefficients in these linear equations are considered as 0.

4.4 The sensors calibration on integrated prototype

A piezoelectric ceramic is a multi-functional material having many applications. It can convert electrical energy into vibration mechanical energy, and it can also work as a sensor and a transducer to convert various physical variables into electric charge signals. As the piezoelectric film is used as the sensor in this applied research, it is capable of generating electric charge signals only when it experiences a change in the force applied. Under a static force load condition, the charges generated by the piezoelectric film migrate towards the dipoles, neutralizing the charges on the dipoles [Jun et al., 2002].

However, the calibration of this research has a difficulty, the smart cutting was targeting a force resolution of 0.1 N. There is no precision force generating method for 0.1 N to 1 N force. Gravity solves this issue in practice; weight blocks were in use and by using Newtown's laws of universal gravitation (equation 4.10):

$$F = Mg \quad (4.10)$$

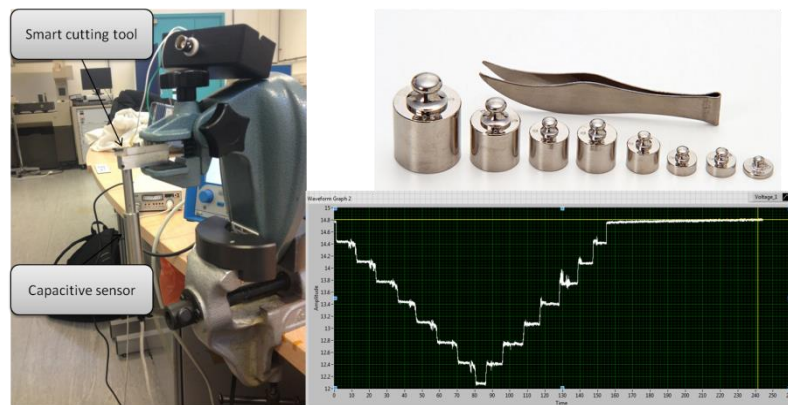


Figure 4.12: Preliminary dynamic response calibration set up

The preliminary calibration bench was set up as shown in Figure 4.11. The capacitive sensor is used since the calibration required a reliable reference guide to the piezoelectric ceramic insert.

4.4.1 Data acquisition and calibration platform build up

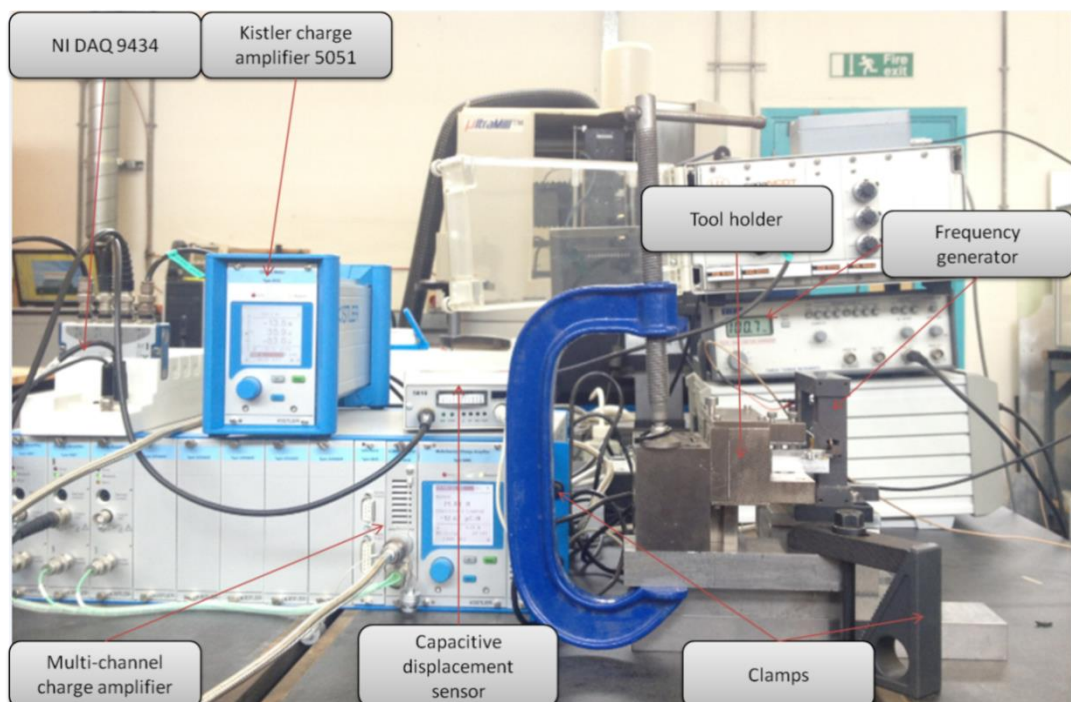


Figure 4.13: Smart cutting tool calibration platform

The data acquisition for the mechanical design of the smart cutting tool was collected through a Kistler charge amplifier 5051 and NI DAQ 9434 data acquisition card. The Kistler charge amplifier provides the amplified voltage signal from the piezoelectric sensor in order to be picked up by the data acquisition card, otherwise the voltage signal was comparatively too small to be picked up. The detailed experimental steps are explained in the following paragraphs.

The calibration platform was set up as shown in Figure 4.13. The large blue clamp associated with the two grey clamps are to fix and constrain the big metal tool holder.

Cutting forces generated in the turning process include static and dynamic components. The static force component can be used to investigate the cutting process performance and cutting tool condition to some extent. In order to use the smart cutting tool as a device for cutting force measurement in process, the tool calibration is carried out to discover the correlation factor between the sensor output voltage and cutting force. A known static force loading from 0 to 8 N, in steps of 1 N, is applied on the tool tip in order to produce an equivalent voltage output representing the force measurement by the proposed smart cutting tool. The known force loading is applied on the tool tip for a few seconds and then removed. This procedure produced a voltage output step due to the corresponding force loading. Figures 4.14 (a) and 4.14 (b) show a linear relationship between the force loading and the voltage output within the range of 0 to 8 N for sensor 1 and sensor 2, respectively, which confirms that the tool holder is deforming in the elastic region [Wang et al., 2013]. Curve fitting has shown the exact equation for describing the relationship between the loading force and the voltage output for each sensor, with a considerably high R-squared value of 0.993 and 0.994, respectively.

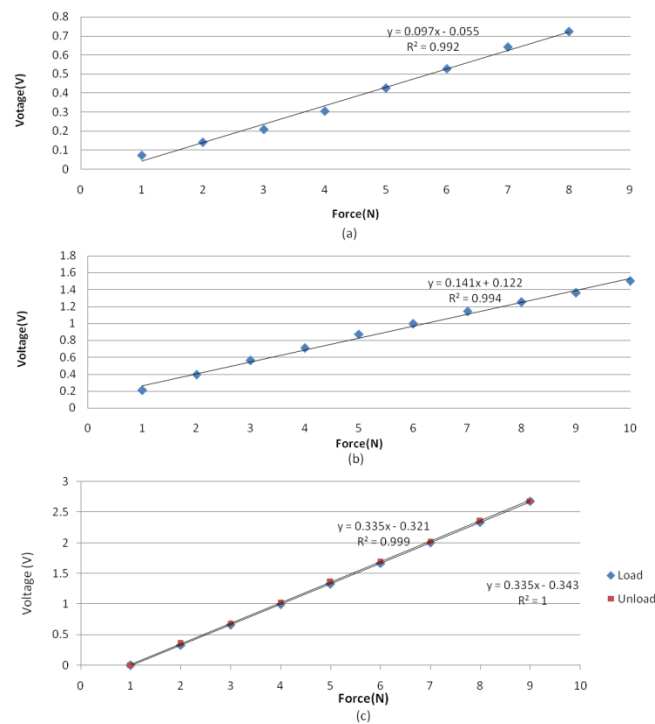


Figure 4.14: (a) Linear relationship between the emulated cutting force and the sensor 1 voltage output; (b) Linear relationship between the emulated feed force and the sensor 2 voltage output; (c) Hysteresis at the sensor 1 with loading and unloading test

The capacitive displacement sensor is integrated onto the tool holder to measure the hysteresis at the smart cutting tool. The hysteresis is 1.6% as calculated-based on the two displayed equations as shown in Figure 4.14 (c), which is in light of the loading and unloading tests on the tool shank over the full range of up to 10 N.

4.5 Conclusion

We have an innovative development of a refitted smart cutting tool, using piezoelectric film sensors as sensing elements integrated within the tool shank, to measure cutting force and feed force in process with a high resolution and accuracy. The experimental calibration is performed to assess the structure design of the smart cutting tool. The smart cutting tool has great potential for ultraprecision and micro-cutting purposes, particularly in machining high value difficult-to-machine materials. Currently, the tool

is awaiting the electrical wireless system to be integrated with the structural prototype and will be presented in the next few chapters.

Chapter 5 Electrical system design for smart cutting tools

This chapter will breakdown the electrical system design process. The design process of the electrical circuitry of the smart cutting tool is also a combination of conceptual design and detail design. The first part of this chapter is going to identify the critical components of the electrical system and then expand in detail on the development process. The methods and development procedure are aimed to deliver the features of wireless and real-time monitoring for the smart cutting tool.

5.1 Introduction

The electrical system of the smart cutting tool is generally divided into three parts:

- Power supply;
- Charge amplifier; and
- Data processing and transmission.

The main circuitry was operated by the designed voltage stabiliser power supply unit where the cutting force measurements are dependent on the design of the charge amplifier for the piezoelectric ceramic sensing unit. Finally data processing and transmission are responsible for the ADC converted digital signal for microchip to package and sent.

5.2 Design overview

Following the previous researches, this project is to bring online cutting condition

monitoring communication with a plug-and-play possibility. This smart device is theoretically able to be run on multiple platforms and feeds back data to control the machine.

Previous research has refined the mechanical structure for the smart tool design and mechanical structure with tested wired sensor. The task for this chapter is focusing on adaption of the wireless feature. Hence this smart cutting tool now has been modified to be wireless controlled using the Bluetooth transmitting method. The system had a transmitting part and a receiving part. There are three main parts in the transmitting side: charge amplifier, microprocessor, and Bluetooth transmitter.

The forces are detectable with 0.1 N force resolution and adjustable by changing the detecting range of the cutting forces. The input signal has been split in to 1024 units because of the resolution of the electronic ADC. The inputs in this experiment are applied into 10 N range where the forces have $1/1024=0.0098$ N resolution. In the micro-cutting process, the cutting forces normally range between 0.1 to 10 N depending on the different cutting materials.

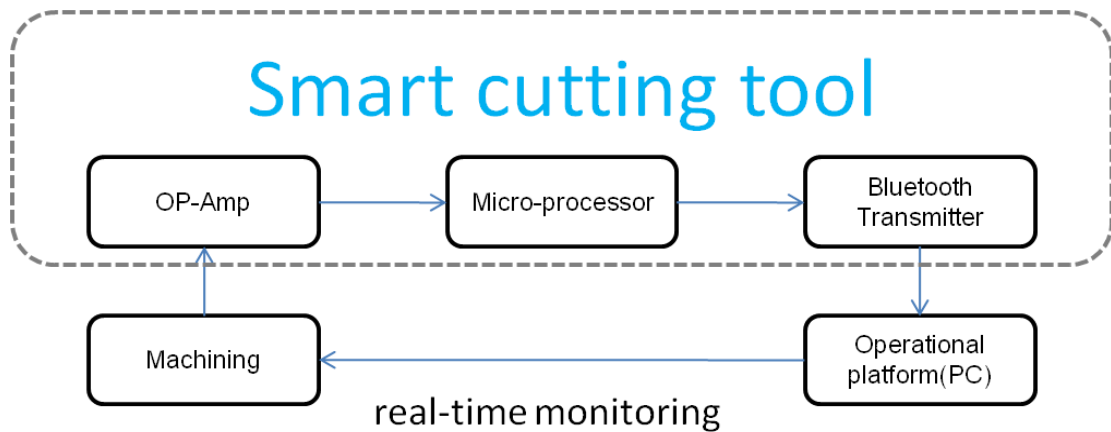


Figure 5.1: Electrical design of the smart cutting tool for real-time monitoring

5.2.1 Design requirements and aim of the design related to simulation

This electrical system is designed to fit the mechanical prototype of the smart cutting

tool that was introduced in previous chapters. There are a few criteria to be taken into account before the actual design begins. This electrical system is designed to be integrated with the prototype mechanical structure to form a unified mechatronic system.

From the previous chapter, the mechanical structural of the smart cutting tool was explained. The main specifications of the wireless smart cutting tool includes:

- N resolution to satisfy micro cutting;
- Meter at least 1 read/revolution during high speed cutting process;
- Stable real-time cutting condition monitoring;
- Cutting condition data saved after machining process; and
- Plug-and-produce.

The sensor's resolution is decided by both the mechanical structure and the electrical system. From the previous chapter, the force

5.3 Design of the charge amplifier and Bluetooth adaption

The idea of adding a wireless module onto this smart cutting tool follows from two critical thoughts. Firstly, embedding the tool with a wireless module allows greater flexibility with mounting and monitoring on various machines without the need for complex wiring. Secondly, the force signals are very small, which will affect the electrical signals after the piezoelectric effect that appear also to be very small. Hence, even a very minor disturbance of the wire's structure and shape would affect the voltage signal, i.e. shifted or distorted. In this case, this problem will be solved by minimising the connection wire length or through an exclusive noise removal technique.

5.3.1 Component selection and justification

The main circuitry design includes three main components: microcontroller, operational amplifier (Op-amp), Bluetooth module and piezoelectric ceramic sensing units. The components are Microchip PIC16F1828, operational amplifier (Op-amp) microchip

MPC 6023, and HC-06 Bluetooth module and PII81 sensing unit.

The circuit needed to consist of three areas; signal collection and amplification signal digitising and signal transmission. The collection and amplification needed an operational amplifier and supporting components. The signal digitising needed an Analog to Digital converter (ADC) which can be found as a hardware module block in most microcontrollers. A microcontroller was also needed to control the sample rate of the ADC and the processing, packaging and transmission of the digitised signals to the Bluetooth module. The Bluetooth transmission is handled by an off-the-shelf integrated module. As well as these, some auxiliary components were needed for power management on the circuit board for the different components.

The components chosen for the development of the signal sensing, conditioning recording and wireless transmission had to fulfil certain criteria. To reduce circuit complexity, the chosen components had to use the same voltage levels. This was dictated by the microcontroller and the Bluetooth module chosen. The digitising by the microcontroller also influences the operational amplifier used in regards to its operating voltages.

The operational amplifier chosen was the Microchip MPC6023. This amplifier is ideal for use in digital circuits as it was designed for amplifying between logic levels for easy interfacing with a microcontroller. Some of its features include rail to rail operation, which means that the amplified output voltage can swing between the lower voltage level, usually ground (V_{ss}), and the supply voltage level (V_{dd}). This then allows the full resolution of ADC on the microcontroller to be utilised as that is also usually between the same V_{ss} and V_{dd} voltage levels. Other features which make this amplifier suitable for use in the desired type of digital circuit is the regulated voltage output pin which outputs a voltage that is half of the supplied potential difference. This facilitates the easy design of an amplifier circuit where the input piezoelectric signal swings around this mid voltage level, which allows both positive and negative voltages produced by

the piezoelectric element to be successfully amplified and then recorded by the supporting microcontroller through the ADC module. This amplifier also has a chip select pin which allows the microcontroller to select if the amplifier is active. This can then be used as a power saving feature by turning off the amplifier if it is not needed.

The MPC6023 also well suited when it comes to the amplification of the piezoelectric signal itself. It has a wide bandwidth of 10 MHz, giving it a fast response and the ability to handle the vibration of the piezoelectric element used, which should not exceed 2000 Hz. As well as being fast the chip also has good noise characteristics with only 8.7 nV/ $\sqrt{\text{Hz}}$ and low harmonic distortion of 0.00053%. The noise and harmonic distortion can never be removed as the chip itself will never be ideal. There will always be small flaws in materials used or a design that will cause noise. However, the low values mean that the input piezoelectric signal will be amplified and reproduced as faithfully as possible. Furthermore, noise and harmonic distortion should not be an issue with the circuit since the gain used is relatively low and, as previously described, the frequency is low when compared to the bandwidth at which the operational amplifier can work.

The chosen microcontroller was the Microchip 8-bit PIC16f1827. It was chosen as it is easy to program and has a relatively fast clock speed of 32 MHz. It also has multiple ADC inputs with a 10-bit resolution allowing for accurate digitising of the amplified piezoelectric signal. It also has a dedicated Universal Synchronous Asynchronous Receiver Transmitter (USART) hardware module which allows easy and fast communication to be established between the microcontroller and the Bluetooth module and the well-established RS232 communication protocol to be used. As well as this there are many other Input/output (I/O) digital pins that can be used as needed as well as pulse width modulation modules and multiple hardware timers, making it a powerful solution and very suitable for the project.

The Bluetooth module chosen was an inexpensive off the shelf module (JY-MCU-HC-06) which is a fully integrated circuit consisting of an on-circuit antenna, Bluetooth chipset and supporting electronic components. It has a serial data input and expects by default RS232

communication and data from a host microcontroller at 9600 Baud, where baud is the number of bits transmitted per second. This is relatively slow; however, the settings on the Bluetooth chip can be increased for faster data transmission to the module, therefore reducing the time required by the microcontrollers ADC to be taken between samples.

V_m refers to the peak voltage while the sensor units are applied by any force in the horizontal direction to the piezoelectric surface. The chosen operating voltage of the circuit was 5 V, which is necessary for the Bluetooth module and is within the recommended operating range of the microcontroller and operational amplifier. This means that the piezoelectric signal is amplified to be between 0 V (V_{ss}) and 5 V (V_{dd}) with the signal swinging around $V_{dd}/2$, which is 2.5 V. This means that a negative piezoelectric response will be between 0 V and 2.5 V while a positive piezoelectric response will be between 2.5 V and 5 V, which allows the full piezoelectric response to be recorded. The resolution and the frequency at which this data can be recorded is determined by the ADC module of the microcontroller. The resolution of the ADC for the microcontroller PIC16F1827 is 10-bit, which gives 1024 steps between V_{ss} and V_{ref} , which are 0 V and 5 V, respectively. This gives a voltage resolution for the amplified input voltage signal of 4.88 mV per step.

The maximum frequency or maximum sample rate that can be achieved using the ADC is 76.9 kHz, given in the PIC16F1827 data sheet by using the information provided. With a 32 MHz main clock speed the time it takes to read each bit is 1 μ S. As the resolution is 10 bits, to record the input signal voltage takes 10 μ S; however, as shown in the datasheet there are also other time delays necessary before the start of the ADC read cycle of at least 3 μ S. This gives a minimum time between each ADC sample of 13 μ S and therefore a maximum frequency or sample rate of 76923 Hz (~76.9 kHz). This is the minimum time to read a single ADC channel and the project needs three piezoelectric elements and therefore the use of three separate ADC channels. The microcontroller data sheet specifies that when the ADC channel to be read is changed, a wait time must be observed to ensure an accurate voltage reading. This further reduces the maximum sample rate. Having a high sample rate is very important since without an

adequate sample rate parts of the signal response from the piezoelectric element will be missed causing aliasing and so the microcontroller will not record an accurate representation of the piezoelectric element's output voltage.

The necessary sampling frequency for faithful digital representation of any analog signal is given by the Nyquist theorem, which states that the sampling frequency should be at least twice the expected maximum frequency of the analog signal ($2f_{\max}$). For this application the expected maximum frequency is around 2 kHz; therefore, a sampling frequency of at least 4 kHz needs to be achieved for this application to work correctly.

In this project, the sensing unit was PI181 that bought from Physik Instrumente (PI). Piezoelectric ceramics are elastic materials that will bounce the electric charge because of the pressure, temperature, vibration and light changes. The polarized piezoelectric was able to progressively increase the output electron charges according to the stimulation. The sizes of the piezoelectric units were the minimum option to choose to modify in the laboratory considering the author's ability at the time. PI181 is a modulated piezo ceramic material that has a formulated output under a physically applied linear force.

5.3.2 Charge amplifier design overview

The electric charge will return to zero by itself in a very short time period, or in other words the DC signal is unable to be held. Piezoelectric sensors are mostly used when analysing the AC signal. The charge amplifier hereby designed was aimed to keep the peak value of the charge pulse for a longer period for the microchip to collect. It is placed in parallel with a capacitor C_g and resistor R_g .

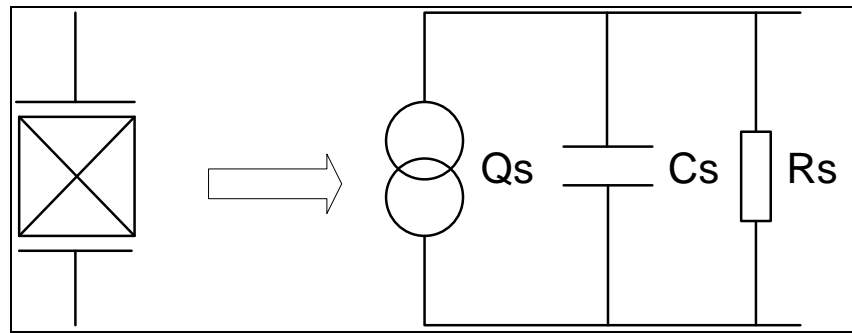


Figure 5.2: The theoretical equivalent circuit model for a piezoelectric material

5.3.3 Amplifier design

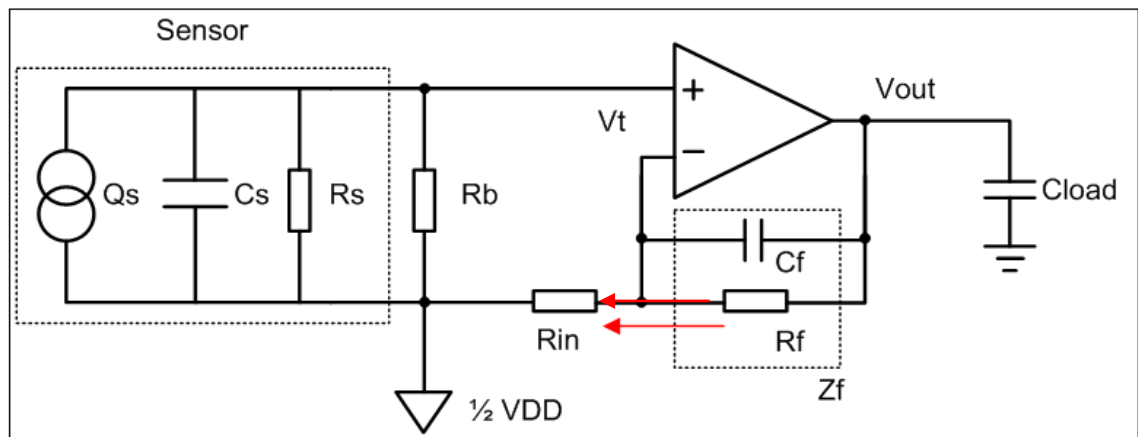


Figure 5.3: The charge amplifier design sketch

This charge amplifier design is shown in Figure 5.3. For the project a non-inverting amplifier design will be used where the gain is positive and so the input signal just undergoes amplification without inversion. $V_{dd}/2$ is used rather than ground (0 V), so that the signal produced by the piezoelectric sensor will swing around this voltage level so that both the positive and negative voltages produced by the piezoelectric sensor can be measured. In order to simplify the designed circuitry, the capacitor C_f and resistor R_f can be seen as impedance Z_f .

$$V_{\text{ref}} = \frac{1}{2} V_{\text{dd}} \quad (5.1)$$

In this model, V_{ref} is playing the role of ground. The datasheet of MCP6023 has announced DC gains of at least 90 dB. Assume the input voltages at positive and negative end, V_t , are equivalent. From the figure, inside the dashed box and with currents flowing from left to right.

$$\frac{V_t}{R_{\text{in}}} = \frac{V_{\text{out}} - V_t}{Z_f} \quad (5.2)$$

$$\Rightarrow V_{\text{out}} = \frac{Z_f + R_{\text{in}}}{R_{\text{in}}} \cdot V_t \quad (5.3)$$

$$\delta V_t = \frac{\delta Q}{C_s} \quad (5.4)$$

From the equation, the V_{out} are related and decided by impedance Z_f ;

the relationship with input voltage V_t and electron charges Q are decided by the capacitor C_s ; and

from the same figure, resistor R_b should be as large as possible because it is used for referencing the positive voltage input. Resistor R_s should also be as large as possible.

Hence the gain:

$$\delta V_{\text{out}} = \frac{Z_f + R_{\text{in}}}{R_{\text{in}}} \cdot \delta V_t = \frac{Z_f + R_{\text{in}}}{R_{\text{in}}} \cdot \frac{\delta Q}{C_s} \quad (5.5)$$

By solving Z_f :

$$\delta V_{\text{out}} = \left(1 + \frac{R_f}{R_{\text{in}}} \cdot \frac{1}{1 + s R_f C_f}\right) \cdot \delta V_t = \left(1 + \frac{R_f}{R_{\text{in}}} \cdot \frac{1}{1 + s R_f C_f}\right) \cdot \frac{\delta Q}{C_s} \quad (5.6)$$

From the equation, V_{out} has been given. The values for R_f and R_{in} are what give the effective gain (amplification factor) of the amplifier design. The gain desired is found by measuring the maximum or calculating the maximum voltage output from the piezoelectric sensor. This value needs to be multiplied to around 5 V (Vdd). This multiplication factor is then used as the needed gain (gain = R_f/R_{in}). The resistor values used are shown in Figure 5.4 below and the actual gain is 10,000.

5.3.4 Circuitry sketch and preliminary board design

The schematic diagram shown in Figure 5.4 is for part of the initial circuit developed. It is, as explained in the previous section, a non-inverting amplifier which is biased to $V_{dd}/2$ so that the piezoelectric signal will swing around that voltage. This part of the circuit is connected to the microcontroller from V_{out} on the operational amplifier to one of the ADC inputs on the microcontroller.

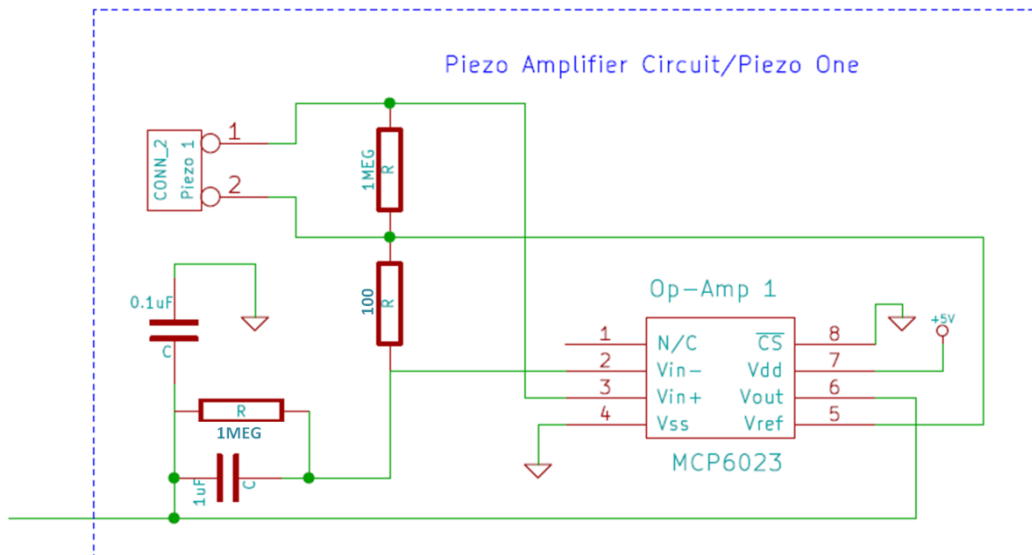


Figure 5.4: Charge amplifier design circuit diagram

From the figure above, two extra features other than a normal amplifier are applied by

using MPC6023, which are CS (chip select) and V_{ref} . The CS function was used to switch the chip on and off and V_{ref} is an $\frac{1}{2}V_{dd}$ input as the reference voltage to calibrate the DC point of the designed circuit.

The microcontroller circuit consists of the microcontroller itself and some supporting components, including a male header to allow in Circuit Serial Programming (ICSP) of the microcontroller when the circuit board is completed. This means that the microcontroller's code can be changed quickly and easily to optimise and ensure full functionality. A female header is also needed to connect the Bluetooth module to the power rails and also to the microcontroller.

A bi-colour Light Emitting Diode (LED) was included to give visual indication of the operational state of the microcontroller. This is utilised to visually indicate correct operation or any errors that may be occurring. Including a visual indicator makes initial testing, development and integration with the rest of the designed system easier as it allows the user to see immediately where any problems may lie and at what point they occur. A momentary push to make button was also included with the circuit so that the recording and transmission of data from the piezoelectric element could be quickly and easily turned on and off as needed during testing and experimentation. Figure 5.5 below shows the schematic for the microcontroller part of the circuit including all the elements explained above and the supporting components needed for them.

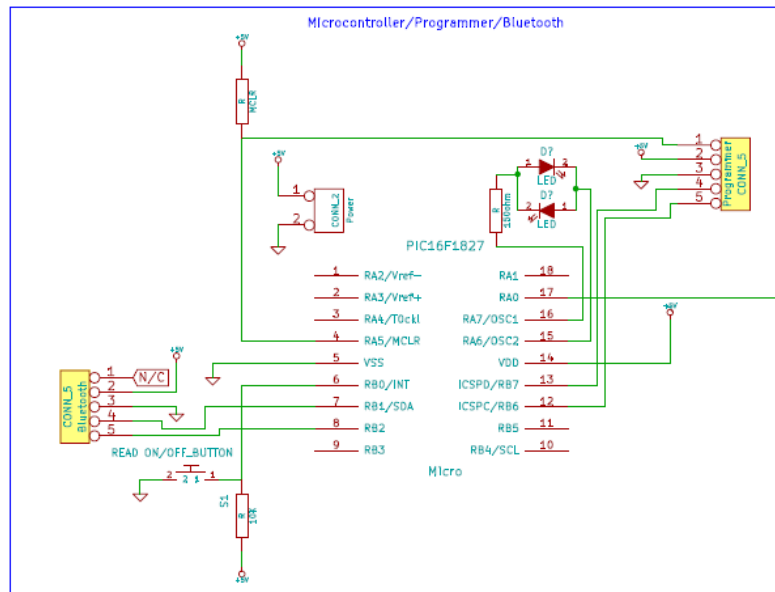


Figure 5.5: Circuit diagram of the microcontroller and Bluetooth

The only other components present on the developed circuit board were for power management and which regulated and smoothed the input voltage to 5 V for use by all components on the circuit board. This was done using a low drop out (LDO) voltage regulator that could take any voltage between 7 V and 12 V and produce a regulated 5 V. This allowed a battery pack to be used to power the circuit board without any issues occurring from the change in voltage that occurs with batteries as they discharge.

The circuit was initially developed using a breadboard which allows components and different component values to be tested efficiently to ensure that the circuit operates as desired. From the initial prototype breadboard circuit a schematic is then developed using a CAD package (KiCAD) designed specifically for development of printed circuit boards (PCB). The program contains part diagrams for a large number of common electronic components that then can be positioned and wired together to create a schematic diagram.

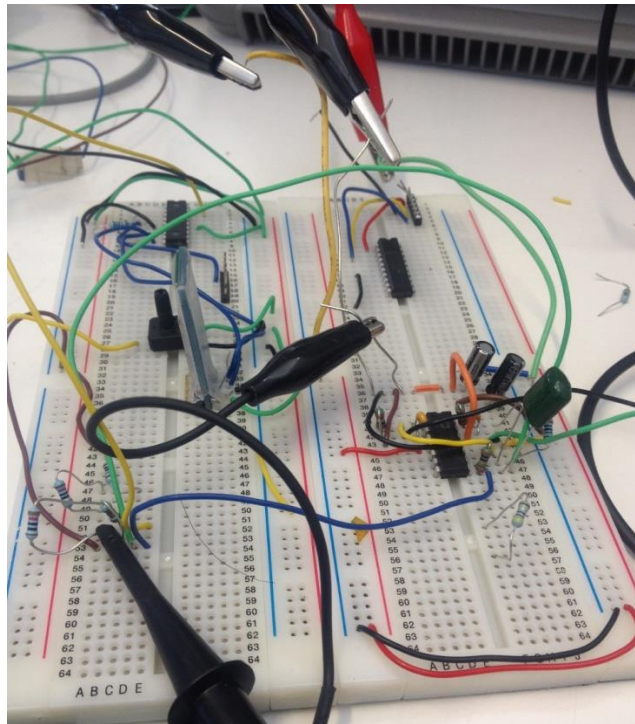


Figure 5.6: Preliminary circuitry on a breadboard

Once the schematic has been completed then the program allows the creation from the schematic of a PCB layout; this is the image of what and where the electrical component pads and tracks will be when the PCB is made. Once the layout is complete then the circuit design can be exported using a Gerber file standard and the circuit board can be created.

The circuits created were routed using a PCB CAD router (LPKF ProtoMat S103). This uses a computer controlled router system to selectively remove copper from the FR-4 standard circuit board sheet. The board is made up of a glass reinforced fibre sheet with a thin layer (35 μm) of copper laminated onto it. The machine only removes the copper leaving the glass reinforced fibre sheet below, isolating areas of copper, which become the component pads and tracks. The machine can also cut through the entire thickness of the board to cut the final circuit board to the desired size.

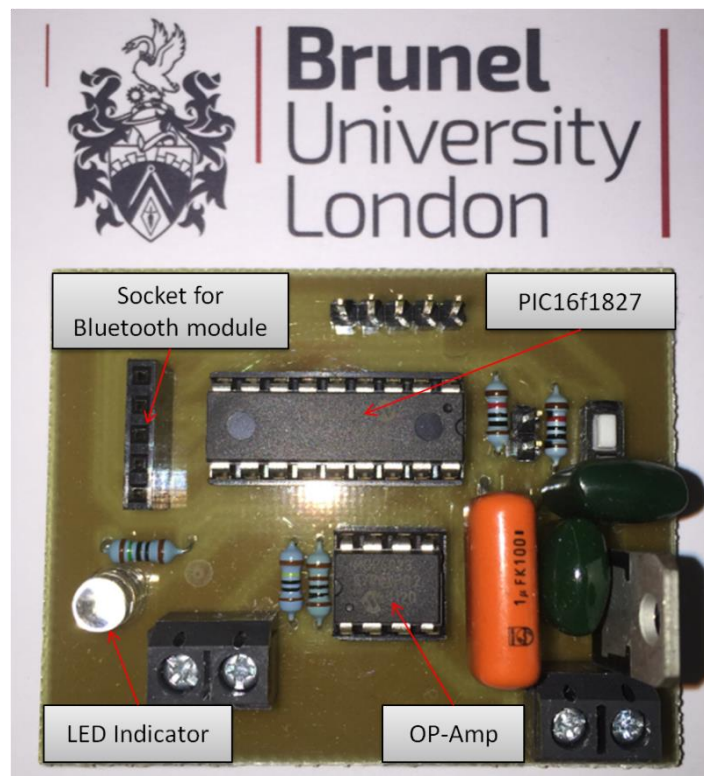


Figure 5.7: 1st attempt single sensor input circuit board

The code for this initial prototype by necessity had to be very simple since it was essential to ensure the smallest possible delay between ADC reads which maximises the sample rate. The code was built up and tested incrementally to ensure everything worked as expected. The code was written in C programming language and compiled using the CCS C platform. The integrated development environment (IDE) used was Microchips MPLAB program which allowed easy programming and in-circuit debugging of the microcontroller.

The final code used for this prototype can be split into three parts:

- The initialisation of the microcontroller and communication setup;
- The interrupt function that manages the push button; and
- The ADC read and data transmission.

In the initialisation phase the microcontroller is set up so that the microcontroller operates at 32 MHz; however; the crystal within the microcontroller itself oscillates at

500 kHz. A method of increasing the effective clock speed through circuitry called phase locked loop (PLL) is used. This happens in two stages: first increasing the frequency to 8 MHz and then multiplying the frequency by four to 32 MHz using a second PLL circuit.

The initialisation code also specifies which ADC channel is to be used, in this case pin A0 (first I/O on port A) and also what resolution the ADC is to be read at, in this case 10 bits. The initialisation also sets up the correct registers for using the external interrupt that is attached to pin B0 (first pin on port B), which sets this I/O as an interrupt which is triggered when a logic level change is detected on the pin. As shown in Figure 5.5, the button is connected to this pin.

The interrupt works by constantly monitoring this pin for a change in voltage level. When a change is detected normal operation stops and the running code is interrupted while a piece of code known as an interrupt function is executed instead. So when the button is pressed the microcontroller responds virtually instantly, stopping ADC reads and communication to the Bluetooth module.

Finally, the RS232 communication protocol and the UART hardware block is initialised to allow communication data to be sent to the Bluetooth module and which can then be understood by the host computer program that is used for recording and graphing the sent data. The data from the ADC is 10 bits long; therefore, it is transmitted using a long data type variable. This type of variable is 16 bits so 6 bits are unused but still transmitted, which is inefficient, however the RS232 protocol works in blocks of 8 bits (1 byte) and so while using this communication protocol it is unavoidable. The data transmission also contains more than just the ADC data as there are stop bits and a termination byte that contains a bit sequence that is recognised by the receiver program.

These aspects of the data transmission limit the speed of the data transfer to the Bluetooth module as a minimum of three bytes are being transmitted per ADC read. The

baud rate is set in the initialisation code to 115200 bits per second giving an approximate maximum data rate of 4800 transmissions per second as we are sending 3 bytes (24 bits) per transmission. This was then tested by timing how many transmissions were sent in a minute. This came to an equivalent of around 2800 samples per second. The difference in transmission speeds is accounted for by when the delay that occurs during the ADC read is also taken into account. This is the fastest transmission speed that can be achieved using this approach with the chosen hardware and the data package expected by the receiver computer program.

5.3.5 Final circuit board design

As three piezoelectric sensing elements are needed for investigating the tool cutting force in all axes, then the circuit needed changing to accommodate all the sensors. To achieve this, three operational amplifiers all using the same gain and supporting circuitry were included in the design of a new circuit board. As before the circuit board was developed on breadboard and then once the hardware had been shown to be working it was developed using the CAD package to a schematic diagram. The schematic for each of the three operational amplifiers is the same as for the initial circuit design as shown in Figure 5.4.

Figure 5.8 shows the schematic developed for the microcontroller aspect as this is now more complicated due to having the three operational amplifiers. The main point to note is that the amplifiers are connected to the first three pins of port A – pins RA0, RA1 and RA2 as designated on the PIC16F1827 datasheet [datasheet]. These are all ADC channels so that the amplified signal outputs from the operational amplifiers can be digitised and then transmitted. Additionally, on this schematic three LEDs have been included; these are used as indicators to show which of the operational amplifiers are being read via the ADC. This was primarily used during the testing and development stages. In the final code iteration these LEDs became indicators to show any errors that may have occurred during the running of the code and reading of ADC.

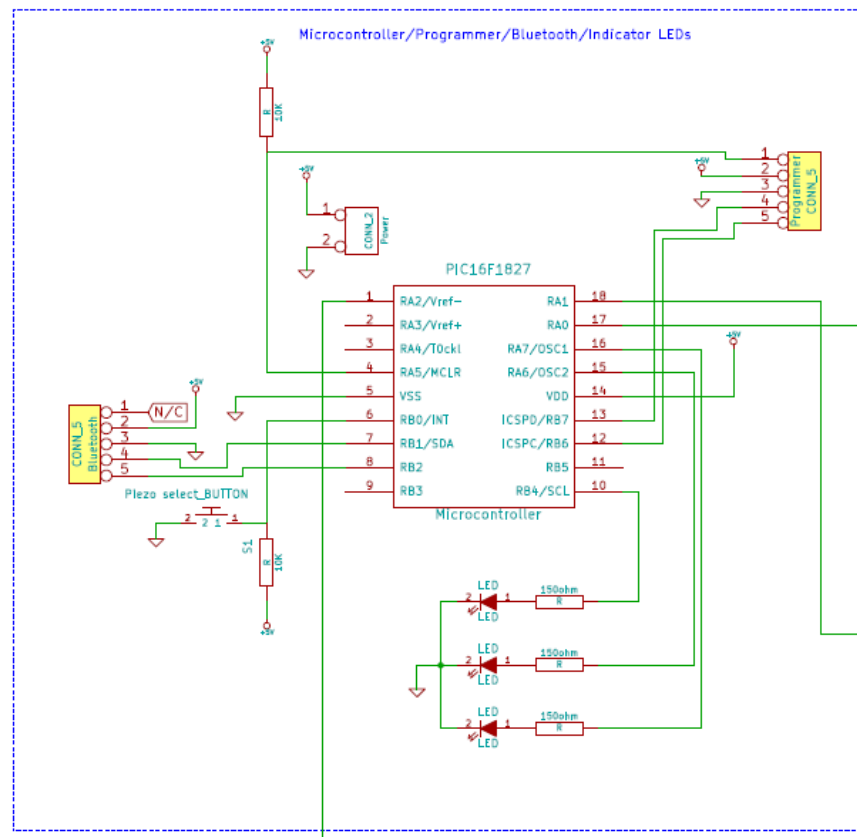


Figure 5.8: 2nd attempted circuit diagram of the microcontroller and Bluetooth

As with the previous developed circuit, headers were needed for ICSP connection and also the Bluetooth module. A button was again included so that during testing the ADC channels used could be selectively turned on and off so that the communication and functionality could be tested more easily. This functionality is kept in the final iteration of code to allow the user to select which ADC inputs are to be read, or to turn off all ADC inputs and stop data transmission. Additionally, the same power management circuitry incorporating a LDO voltage regulator is included in this circuit. Figure 5.9 shows the circuit layout that was developed from the schematic and then produced as a PCB using the CAD PCB router.

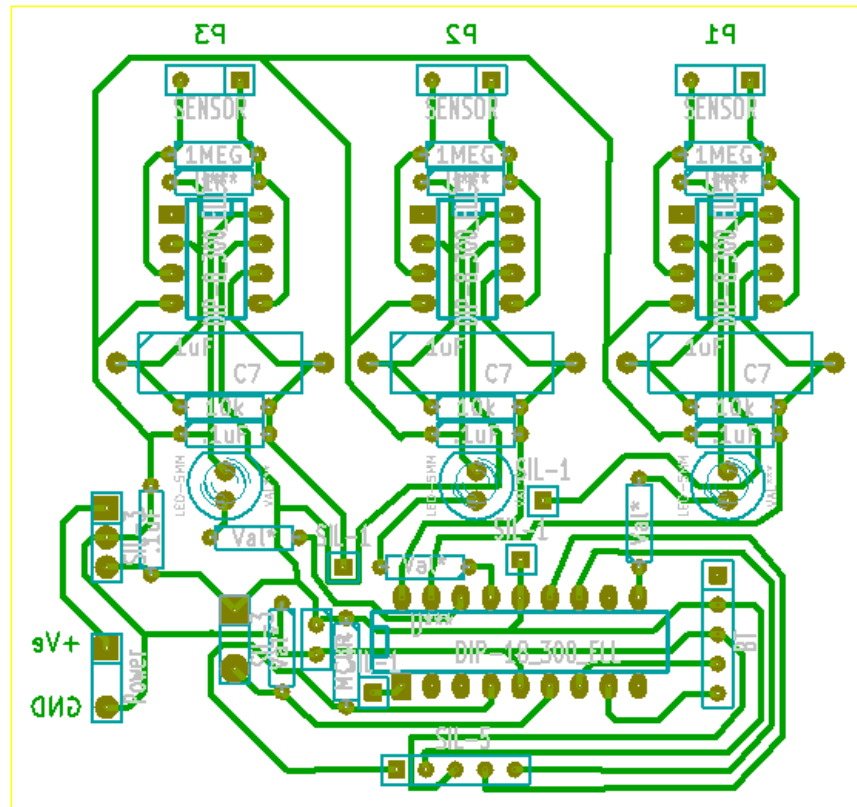


Figure 5.9: CAD sketch of the PCB routing

Finally, the circuit was populated and the final board could then be tested with the components mounted as shown in Figure 5.10. The code that was implemented for the final circuit was similar in structure to the original code. The setup for the microcontroller clock frequency, ADC and RS232 communication is the same as for the initial prototype. The interrupt function has been extended so that on each press of the button it cycles to those ADC channels that are active or all the ADC channels if all are active. If only one ADC channel is active, then the code is the same as before with the same sample rate as for the initial prototype. However, if all three ADC channels are being used sequentially to record data from each piezoelectric element, then the sample rate is reduced by a factor of three between each read of the same sensor. This reduction in sample rate is further reduced as a delay has to be observed after the ADC channel is changed between each ADC read. The delay needed as specified in the microcontroller datasheet is of 1 μ S and is needed to allow the settling of the new voltage to be read.

The data transmission is handled differently as there are now three pieces of data being sent and the receiving computer program needs to know which data belongs to which piezoelectric sensor. This is achieved by transmitting different termination characters after data is sent depending on which ADC channel has been read. The receiving computer program then sorts the data depending on the termination character it receives after the data.

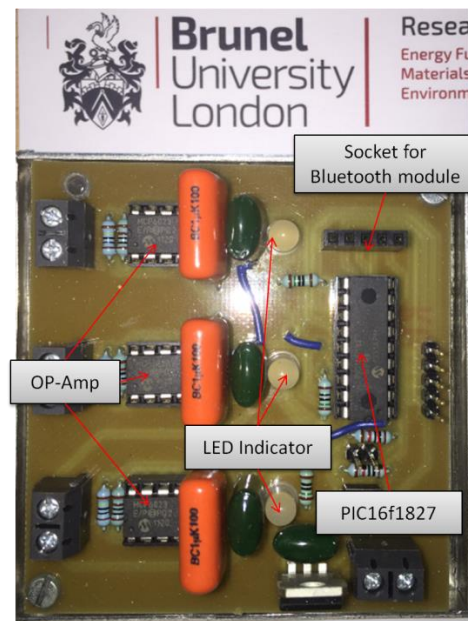


Figure 5.10: 2nd attempt on the circuit board with three sensor input in used

5.3.6 Force measuring resolution scale

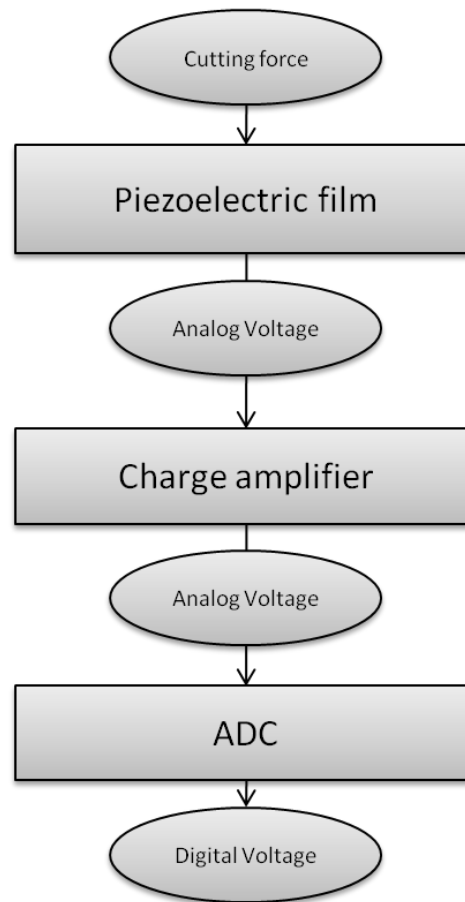


Figure 5.11: Flow chart of the cutting force converted to digital signal process

This figure demonstrates the footprint of the force input converting to a digital signal. The piezoelectric ceramic provides the piezoelectric effect of F to V transformation, where the ADC has 2^{10} resolution and the charge amplifier gain was designed as 10,000. Hence, the force resolution scale is calculated:

$$V_p = F_p \times g_{33} \quad (5.7)$$

$$V_{amp} = V_p \times Gain \quad (5.8)$$

$$V_{\text{amp}} \approx V_{\text{res}} \quad (5.9)$$

By simplifying the equations above,

$$V_{\text{res}} \approx F_{\text{res}} \times g_{33} \times \text{Gain} \quad (5.10)$$

$$4.88 \times 10^{-3} V \approx 0.1 \times 22 \times 10^{-3} \times 0.26 \times 10^{-3} \times 10000 = 5.72 \times 10^{-3} V \quad (5.11)$$

$$\frac{V_{\text{res}}}{V_{\text{amp}}} = 0.85 < 1 \quad (5.12)$$

In the equations above:

F_{res} stands for force resolution and its 0.1 N by requirements,

V_{res} stands for voltage resolution,

V_p is the piezoelectric voltage,

F_p is the applied force on the piezoelectric sensor,

V_{amp} refers to the voltage that amplified by 10k times after the charge amplifier, and

g_{33} is the piezoelectric voltage constant ($22 \times 10^{-3} Vm/N$) that could be found at

Figure 4.9.

From equation (5.7), F_p stands for the cutting force from the sensor system and V_p refers the piezoelectric effect voltage output from the mechanical deformation caused by F_p . The voltage resolution V_{res} was defined according to the operational voltage range and the resolution of the ADC, which was 4.88 mV. From equations (5.10) to 5.12, as long as the minimum quantisation voltage of the ADC V_{res} is smaller than the

amplified voltage V_{amp} while the cutting force is applied in 0.1 N steps, we can claim that the designed circuit has a 0.1 N force resolution and the maximum range of the force scale is:

$$V_{max} \approx F_{max} \times g_{33} \times Gain \quad (5.13)$$

By substituting the maximum voltage of 2.5 V into equation (5.6) the maximum operational force is 44 N, where V_{max} represent the maximum operational voltage of the ADC and F_{max} represents the maximum operational force for the piezoelectric sensor circuit.

5.4 Testing and calibrations

There are a few simple steps go through this circuitry's calibration. The whole electric system is integrated with the mechanical part and mounted on a giant metal tool holder with all the screws pre-stressed. A test force was set as a 150 g weight scale and used the same method as in the preliminary calibration presented in chapter 4. A fast response to a force pulse should be detected by this smart cutting tool.

The testing of the circuitry are taking place in an order of 1, circuitry testing, making sure all the pins in the smart cutting tool's circuitry is fully functional with an oscilloscope. And then 2, run the smart cutting tool system with applying a peak testing force to check the wireless responds on receiver end.

5.4.1 Circuitry testing

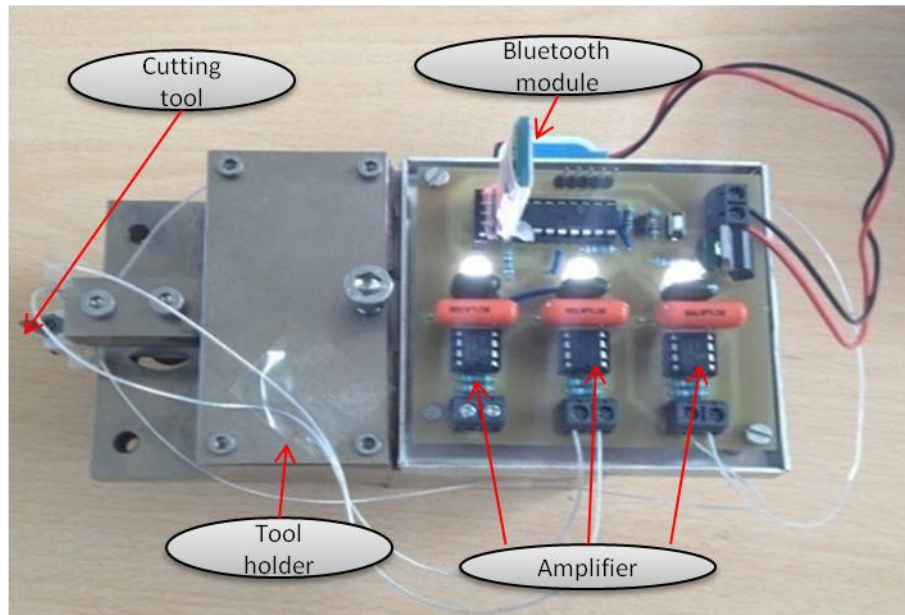


Figure 5.12: The prototype cutting tool with the wireless system embedded

Figure 5.12 shows the prototype of the smart cutting tool integrated with the electrical system and mechanical structure. The circuitry with three lights on indicates that each of the three channels of the op-amp is in operation; the Bluetooth module indicating red lights means it is also in operational status at the same time. The cutting force is going to applied at the tool tip edge for response testing and using the gravity method again that appeared in chapter 4.

The circuitry were powered by a 9V battery where under the circuit in the picture, when the indicator lights are refers to functioning terminals for inputs ready to be amplified, the metal tool holder were the stand of the cutting tool made form steel and it is replaceable.

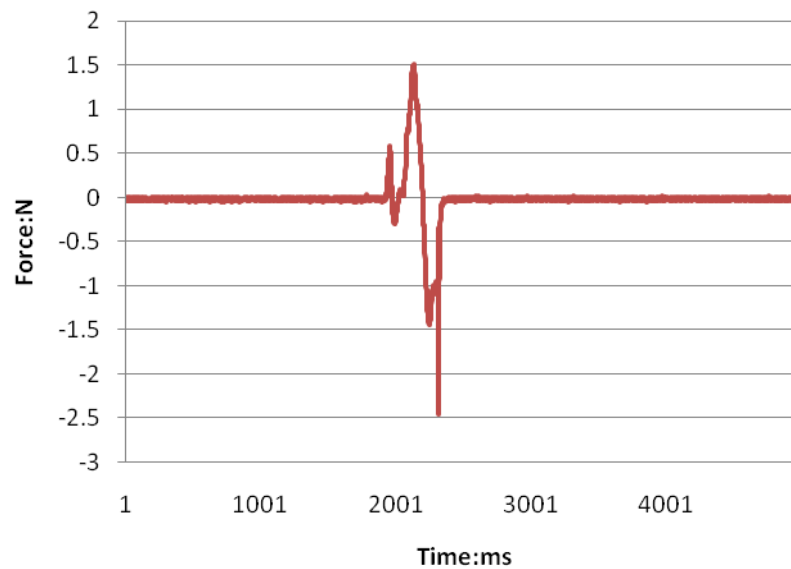


Figure 5.13: A test example sensor response for 1.5 N

Figure 5.13 above shows the test example for the wireless force sensor reaction while a 1.5 N force was applied in the cutting force direction on the cutting tool. The raw signal appears to rebound in half a second because of the characteristics of the piezoelectric sensor, where the piezoelectric effect does not generate energy, but only creates a temporary voltage difference. The voltage signal was generated but was unable to last for a long time. In this case, it is important to capture and record these moments accurately for the force analysis.

As mentioned above, the voltage signal disappears very fast, where the signal analysis is going to be signal processing in the receiver end, thus the computer in this specific topic. The calibration process uses MATLAB and will be well briefed in chapter 6.

5.4.2 Test with PC communication and receiver program design



Figure 5.14: The receiver program interface

From Figure 5.14, the interface of the receiver program is designed to receive and monitor the real-time signals of the cutting forces during machining. However, in chapter 4 it has been explained that radio forces affect the cutting condition less importantly and have been removed from the smart cutting tool. But still, the receiver program and the circuitry design of the smart cutting tool has three input ports that can be freely used to choose any sensor unit at the analog input stage.

This program has two main functions, which are real-time force signal plotting and signal saving after each measurement. The main part of the program is shown in the appendix after the main thesis.

5.5 Conclusion

The charge amplifier is here to stabilise the peak signal and ensure the leakage of the potential difference for the microprocessor to pick up the analog signal. The

microprocessor contains a built in ADC analog to digital converter which transfers the digital signal to the Bluetooth transmitter, which transfers the digital signal to the final receiver – the computer.

The advantage of using Bluetooth technology in this application is fast, stable reaction. A 10-bit resolution ADC was applied in this experiment. The ADC is embedded inside the micro-controller PIC16F1827. In this case 10-bit resolution is $2^{10} = 1024$. Therefore, the force range divided by 1024 is the evaluation of the resolution. In micro-cutting the forces are normally under 10 N. In this prototype 0.1 N was the target resolution. Therefore, the force range is 0.1 multiplied by 1024. In this design case, 102 N are the maximum range of the smart cutting tool.

Theoretically the piezoelectric ceramic's frequency is 2,000 Hz. However, the sampling frequency of this smart cutting tool was not decided by one factor alone. The microprocessor has a sampling frequency of 31 kHz ~32 MHz.-based on the program designed into the microprocessor, excluding the data bit used on the wireless transmitting protocol, the actual frequency is 2.5 sample/ms = 2,500 Hz. Hence this wireless circuitry's sampling frequency is 2,000 Hz.

The previous chapter has studied the mechanical aspect of the natural frequency of the smart cutting tool, which was 6158 Hz. Hence the sampling sensitivity of the smart cutting tool is decided by the electrical system, which is 2,000 Hz.

Chapter 6 Performance testing of the smart cutting tools

In this chapter, the smart cutting tool will be tested in both offline and online environments. The offline test is the experimental method for packaging the smart cutting tool and the resolution test. The online test uses the smart cutting tool in a real machining environment, monitoring and analysing the cutting forces at the same time with the Kistler Dynamometer.

6.1 Smart cutting tool calibration supplementary

The previous chapter has explained the development of the smart cutting tool in mechanical and electrical criteria. The basic calibration has been tested to ensure the design accuracy. However, there are still some calibration details that need to be mentioned. The dynamic responses are unable to be perfectly calibrated unless both electrical design and mechanical design are integrated.

The smart cutting tool calibration procedure was designed in two parts: bench calibration at static calibration platform and cutting trial at turning machine environments. In chapter 4, the mechanical design for the smart cutting tool has isolated the calibration of the static force response of the designed smart cutting tool. However, the dynamic response is as important as the static response, and the static calibration was tested under a force gauge and alternative methods.

Because the electrical system has been fully developed, the method of calibration of the tool reliability was to put the whole integrated smart cutting tool into the field test. This chapter demonstrates the experiment design step by step.

6.1.1 Experiment process design

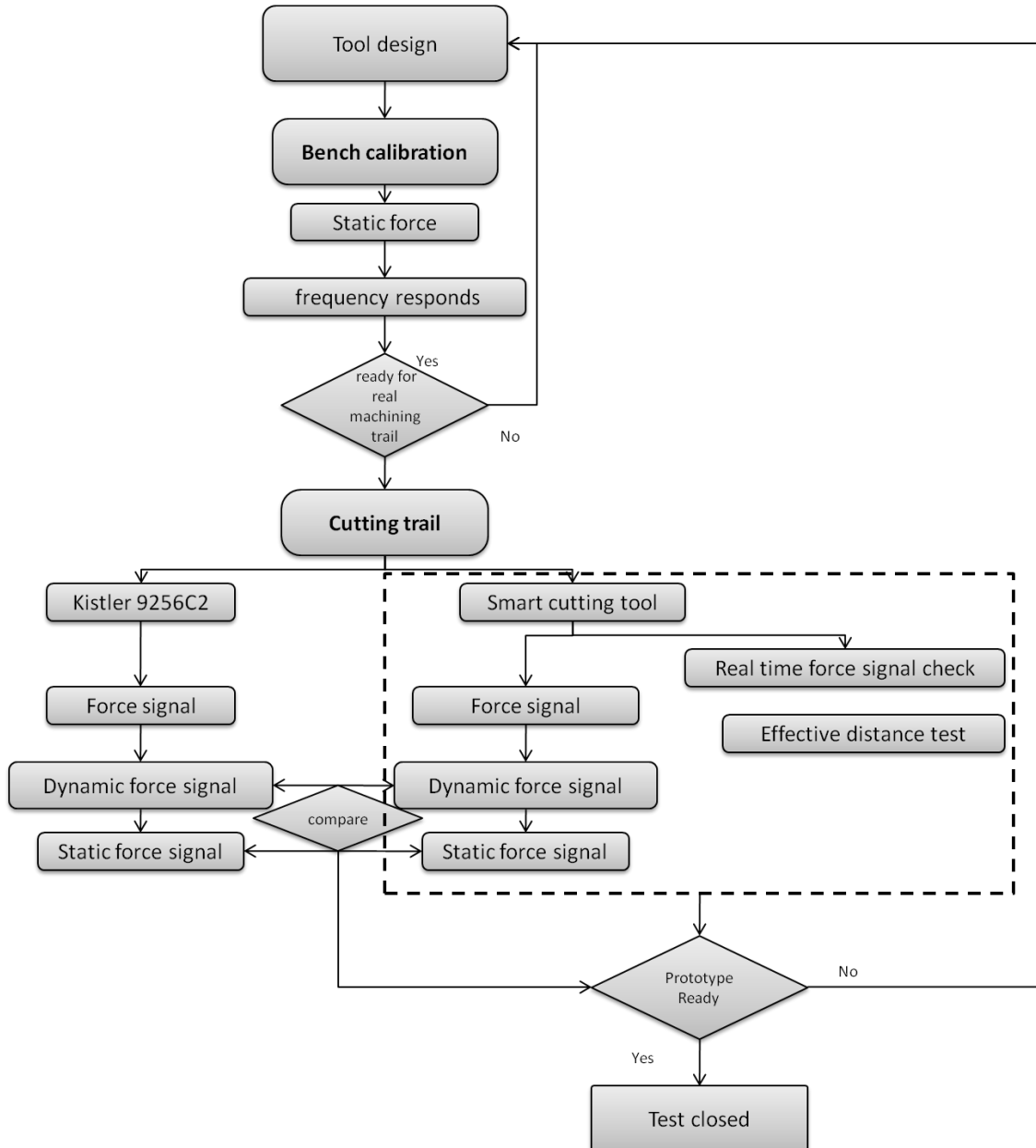


Figure 6.1: The smart cutting tool calibration process flow-chart

The design of the smart cutting tool is explained in detail in chapter 3, Figure 3.2. In Figure 6.1 we present the calibration flow-chart for testing the reliability of the smart

cutting tool. From the figure, the test was separated in to two parts, bench calibration and cutting trial. The bench calibration gave the specify outputs corresponding to the applied force of the smart cutting tool. The cutting trial is the key step to verify the reliability of the smart cutting tool system in a systematic view. In the cutting trial section there are also separated sections, Kistler 9256C2 and smart cutting tool. The intention of using Kistler 9256C2 is as a guide to reference the correct cutting force signal. Within the dotted line in Figure 6.11 the calibration of the smart cutting tool is again divided into two parts, data collection and real-time data monitoring. The cutting force signal as a source of data detected by the smart cutting tool will go directly to be stored in the memory at the receiver end. But since the smart cutting tool is so different from the literature reviewed sensed tools, the real-time monitoring feature should also be tested by the aspect of environments and distance.

6.1.2 Bench calibration set up

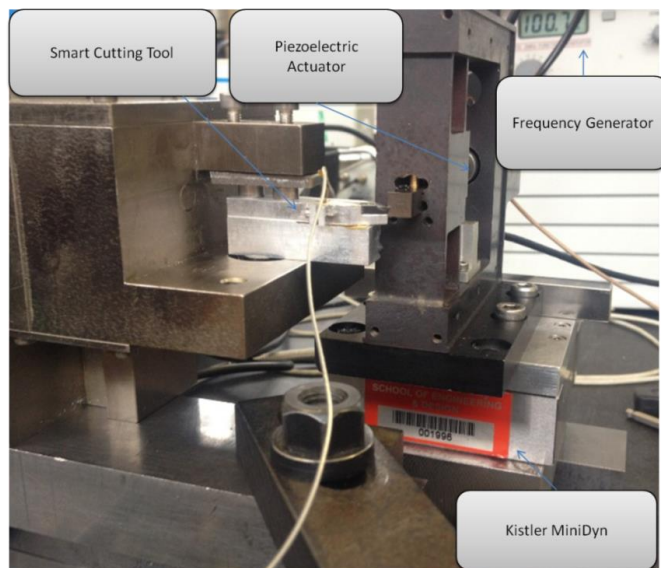


Figure 6.2: Dynamic force sensing test

This dynamic test should be only done after the smart cutting tool is completely integrated with its mechanical structure and electrical system. Hence the test bench was

set up as in Figure 6.2; the smart cutting tool contacts the fast tool servo, which is controlled by the frequency generator. The previous chapter has calculated the dynamic response for the smart cutting tool. However, bench tests are still required to verify it. The frequency generator is set to be at low and high frequencies of 4 Hz and 100 Hz, respectively. As always, the Kistler dynamometer was in used as a reference of the dynamic response.

6.1.3 Dynamic responses test

Figure 6.3 shows the dynamic response of the smart cutting tool at the low and high frequencies of 4 Hz and 100 Hz respectively. The comparisons have been made between the outputs from the smart cutting tool and the Kistler MiniDyn. The results are in good correlation with dynamic response at the low and high frequencies for both the square and sinusoidal force modes, which are particularly used to examine the dynamic response of the developed smart cutting tool.

The main spectrum characteristics show high similarity, although the Kistler dynamometer shows a higher possibility of suffering at higher frequencies. However, the smart cutting tool was calculated to have a response frequency of up to 2.5 kHz. The test is still necessary as a routine procedure.

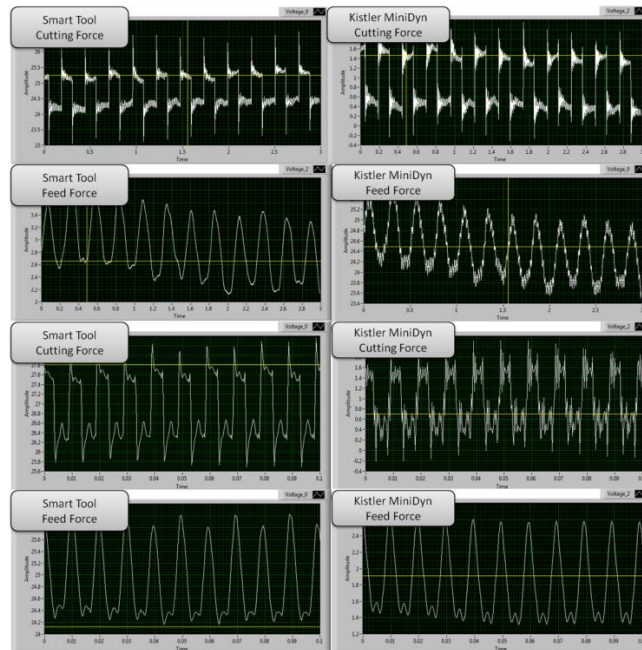


Figure 6.3: Dynamic response to the square and sinusoidal force modes by the smart cutting tool and Kistler MiniDyn dynamometer respectively: (a) at the low frequency of 4 Hz; and (b) at the high frequency of 100 Hz

6.2 Experiment set up on 1st attempt of cutting trial

The capacitive sensor has been removed as it was a reference cutting force for the prototype mechanical design, and additionally because the radio force was not strongly related to the tool wear. Hence, the smart cutting tool system only measured cutting force and feed force in this chapter.

The experiment was designed-based on the flow-chart shown in Figure 6.1. Considering the bottom part of the figure, machine trials are the ultimate goal of the smart cutting tool since it is designed to monitor the cutting forces during metal cutting in real-time.

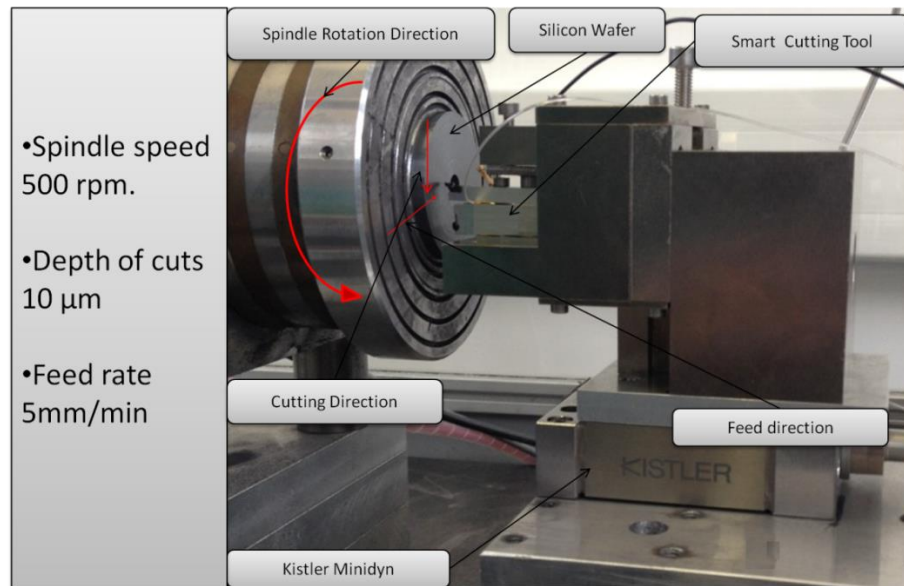


Figure 6.4: Cutting trials setup with the smart cutting tool on a self-developed customised cutting machine

The cutting trials with the smart cutting tool are carried out on a 3 axis diamond turning machine in dry cut conditions. The smart cutting tool is placed on top of the Kistler MiniDYN and the workpiece material is a single-crystal silicon wafer, 50 mm in diameter and 10 mm in thickness, firmly vacuum chucked on the air bearing spindle, as shown in Figure 6.4. The rake angle of the diamond tool is 0 degree. In order to avoid cutting the centre of the workpiece where the cutting speed approaches to zero, the centre area of the wafer has a pre-drilled hole of diameter of $\phi 7$ mm. The machining parameters selected in cutting trials are: depth of cut (a_p) = 10 μm , feed (f) = 5 mm/min, and cutting speed (V_c) = 100 m/min.

Figure 6.3 illustrates the comparison of the cutting force and feed force measured by the smart cutting tool and the Kistler Minidyn respectively. The cutting force signal patterns captured by the smart cutting tool show good agreement with those simultaneously captured by the Kistler Minidyn dynamometer.

6.2.1 Work-piece material and cutting parameter

The work piece was attempted in 3 different materials along with an associated colleague. The three materials are aluminium, silicon and titanium. The main task for the test is to see whether the smart cutting tool is reliable on force signal detection; hence, optimising of the cutting parameters is not discussed in the thesis.

Aluminium alloys typically have an elastic modulus of about 70 GPa. This is 1/3 of the elastic modulus of most of steels and steel alloys. Therefore, aluminium alloy would show more mechanical shape deformation than steels. Aluminium alloys are used in many applications in our life that require less elastic strength. Hence, aluminium alloy is very common material in everyday life, and importantly has been very important in manufacturing.

Silicon is a natural semi-conductor material and also very common type of metal used in manufacturing, as is aluminium alloy. In recent decades, alternative sustainable energy has become a very popular topic, where single crystal silicon is the main material of the solar panels, and also the alternative parts.

Table 6.1: Material characteristics of the workpiece in cutting trial

Work piece material	Aluminium T 6082	Single crystal Silicon	Titanium 6Al-4V
Diameter (mm)	40	25	50
Density (g/cm ³)	2.7	2.3	4.43
Shear strength	250	100	550
Poisson's Ratio	0.33	0.17	0.342
Tensile Strength (MPa)	295	125	950
Modulus of Elasticity (GPa)	70	150	113.8

Titanium alloy was developed in the last century. It has the properties of high elastic strength, less corrosion and is resistant to heat; hence, it has today become very popular in manufacturing. Titanium6Al4V is the most representative alloy in the titanium alloy family.

These materials were chosen to be representative in machining trials, all of them having different characteristics. The cutting forces for each material should be very different, even with the same cutting parameters. The characteristics of each material used in the experiment stage are explained in the Table 6.1.

The cutting parameter for the 1st cutting trial is set to be uniform at 10 μm with a constant spindle speed of 600 rpm. The feed rate is 5mm/min.

6.2.2 Dynamometer

The dynamometer used in the experimental design is Kistler 9256C2, which is well known as Kistler Minidyn. The Kistler dynamometers are widely used for force measurement in machine process monitoring. This Kistler Minidyn uses three layers of piezoelectric transducers fitted under high preload between the top and bottom plates. The transducers contain three quartz plates in a row with four different alignment measurement points at each corner of the rectangular face as shown in Figure 6.5.

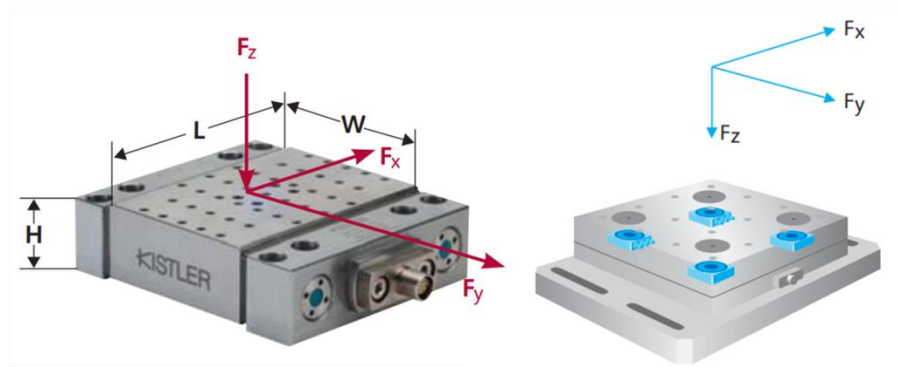


Figure 6.5: Construction of Kistler 9256C dynamometer

The three layers of each sensor (blue) are aimed to measure multi-components of forces and moments. The signal outputs are available from the flange socket. This dynamometer has a large force sensitive scale and a comparatively smaller force range

than other Kistler dynamometers, which makes it suitable for the micro-turning process where the cutting forces are normally below 10 N and vary in between 0.1 N scale. The details are present in the appendix of the thesis.

6.2.3 Data acquisition

The cutting force data collected from the machining process actually proceed in two ways; as Figure 6.1 shows the cutting trial experiments are divided into two parts, dynamometer and smart cutting tool. The previous chapter has explained the development process and the preliminary calibration of the smart cutting tool. These cutting trial experiments are the final calibration test for the reliability of the smart cutting tool.

In chapter 4, all the offline workbenches are tested after the mechanical structure design of the smart cutting tool using LabVIEW along with the Kistler charge amplifier 5015. The Kistler charge amplifier is employed to convert the piezoelectric charge into an equivalent voltage by taking account of the transducer sensitivity and transducer scale. The LabVIEW program was developed to collect voltage outputs through the NI DAQ 9434 data acquisition card.

In chapter 5, a customised GUI for the smart cutting tool is developed, and hence in the experiments the smart cutting tool will be real-time monitoring and also will be recording the cutting force signal on the data receiver interface in .txt file after each cut. Hence, the top right trace of Figure 6.10 shows the real-time signal and Figure 6.8 shows the analysis signal compared with the collected data from Kistler Minidyn.

6.2.4 Dynamic performance of the smart cutting tool

Figure 6.6 shows the dynamic force responses of the smart cutting tool and Kistler dynamometer. The results are satisfactory because they show all the identified peaks of each vibration. However, they are still not as sensitive as the commercial dynamometer

but are fully covered the experiment cutting condition.

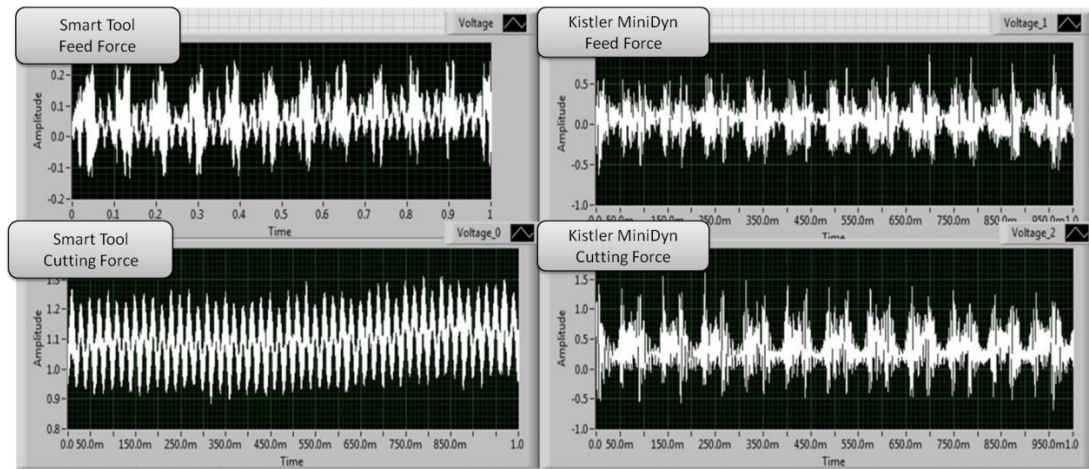


Figure 6.6: Dynamic force response in 1st cutting trial attempt

6.2.5 Static force response

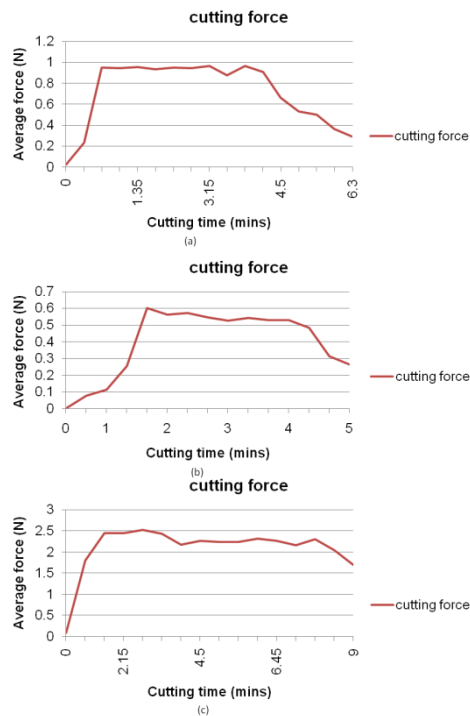


Figure 6.7: The smart cutting tool’s reading of cutting force respectively for (a) - Aluminium T 6082, (b) - Single crystal Silicon, (c) - Titanium 6Al-4V

Figure 6.7 shows the representative cutting force result from all the cuts, one for each material. The figure shows clearly that the lower elastic modulus materials are receiving lower cutting forces; however, the cutting forces are below 5 N at all times.

Figure 6.8 below is the comparison diagram combining the data collected from the Kistler dynamometer and smart cutting tool. The analysis data from the smart cutting tool and the data from the Kistler dynamometer are plotted. The figure shows that the smart cutting tool responds to the cutting forces in the correct way, just as a commercial dynamometer would do.

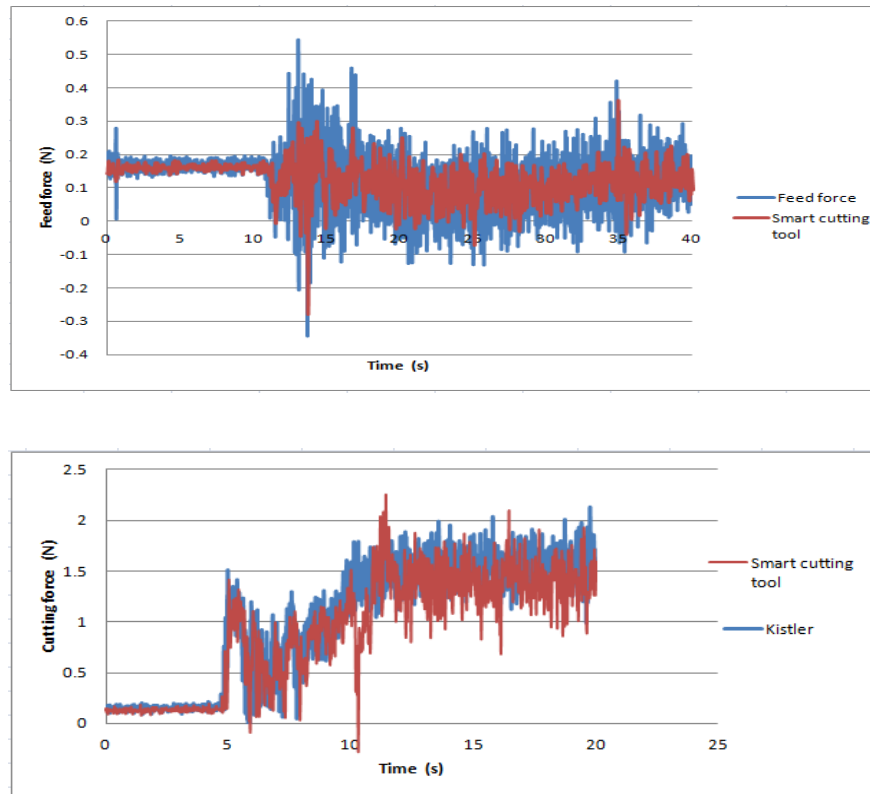


Figure 6.8: Comparison of cutting forces and feed force measured by the smart turning tool and Kistler MiniDyn dynamometer

6.3 Experiment on Moore 250UPL ultraprecision turning machine

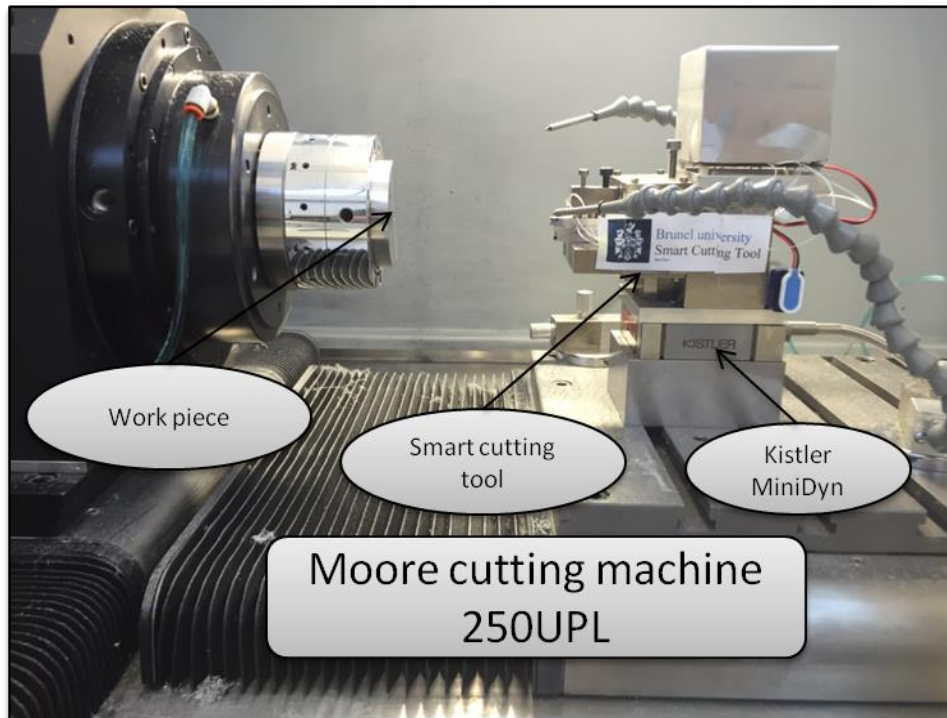


Figure 6.9: Cutting trials setup with the smart turning tool

The smart cutting tool's reliability has been verified from the first real machine trial. However, the author feels that this is not sufficient because the smart cutting tool can be adapted into more complex environments, and also where the plug-and-produce feature would be performed when installed on a different lathe machine. Hence, another machine trial on a different diamond turning machine is very necessary. Under these circumstances, Moore 250UPL has been chosen to be the second cutting trial machine.

Moore 250UPL is an ultraprecision lathe. The linear motor drives the spindle speed at up to 10000 rpm with a 64-bit motion controller on a Windows operation system. However, during the experiment the maximum spindle speed used was 1500 rpm. The

higher spindle speed, and more precision compared to the 3 direction turning machine, were the idea of choosing it to testify the reliability of the smart cutting tool.

The 2nd experiment was set up as shown in Figure 6.9. As with the first time, the Kistler dynamometer is set to the bottom of the feed drive. The workpiece is Aluminium T 6082 wafer only. Since the tests using different material have been satisfied, one type of workpiece for the 2nd cutting trial should be enough. The smart cutting tool was simply mounted on the tool holder and it should work fine.

6.3.1 Work-piece material and cutting parameters

The smart cutting tool was tested on Moore cutting machine 250UPL with different cutting parameters. 10 cuts were performed and the force monitoring result will be discussed in the following paragraph. In summary, the cutting parameter of the Moore 250UPL turning machine is concluded in Table 6.2.

Table 6.2: Cutting parameters on Moore 250UPL lathe machine

Cutting parameter/Attempt	Spindle speed (rpm)	Feed rate (mm/min)	Depth of cut (μm)
1	1000	15	2
2	1000	15	2
3	1000	15	2
4	1000	15	4
5	1500	15	6
6	1500	15	8
7	1500	15	8
8	1500	15	6
9	1500	15	4
10	1500	15	2

6.3.2 Tool signal stability control test

The experiment process began with regular alignment and positioning of the work-piece, the tool and the motors, and also ensured that the connections of the Bluetooth port were open on both smart cutting tool and PC.

The tool signal stability was tested in this way: continuously extend the distance from the remote monitor and turning machine up to the farthest end in the laboratory. As Figure shows, the signal still is still responding well. Hence, the stability test of the signals is concluded as a very good result. However, the figure may not be very clear due to the distance from the camera.

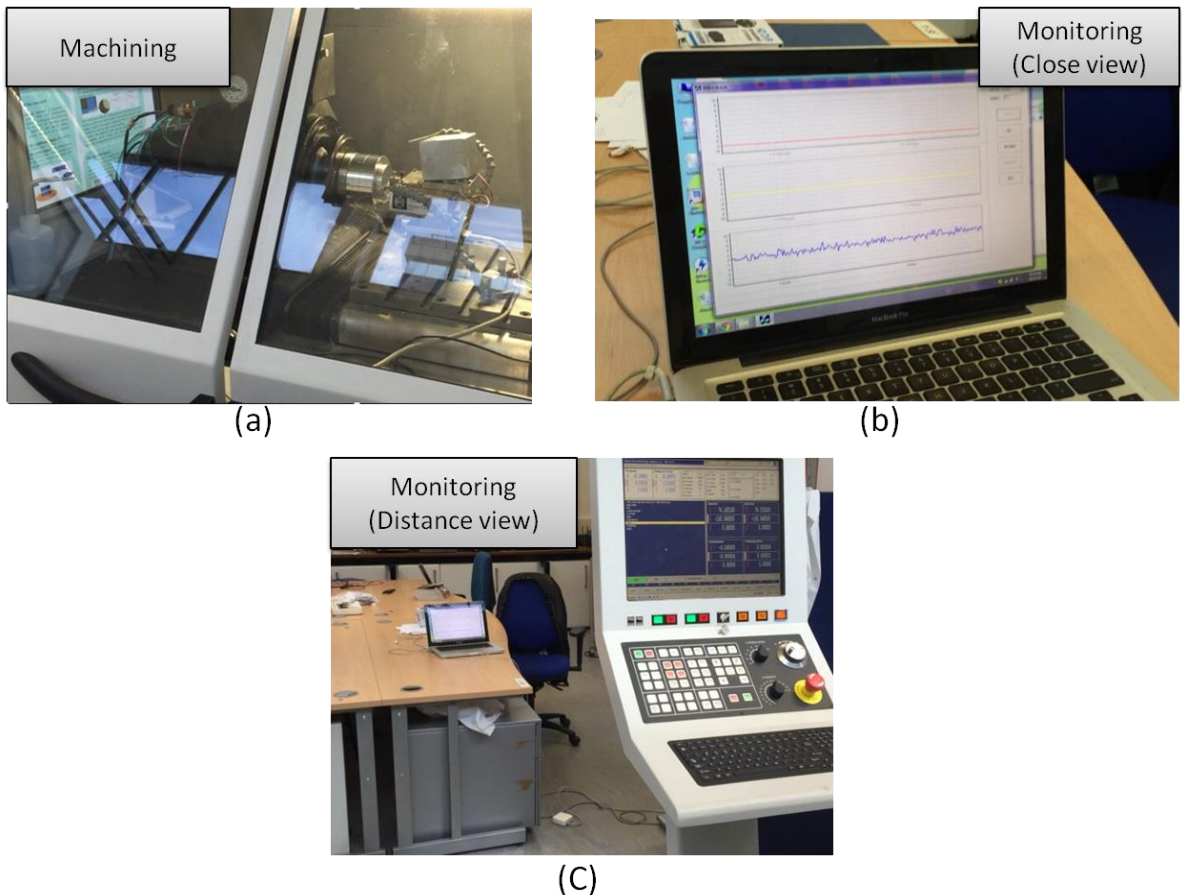


Figure 6.10: Wireless cutting force real-time monitoring

The real scenarios during smart cutting tool monitoring of the cutting process are shown in Figure 6.10 where (a) is the machining lathe machine, (b) is the close up view of receiver interface reading the real-time un-processed cutting force data from the smart cutting tool, and (c) is demonstrating the distance operation of the wireless feature of the smart cutting tool.

6.3.3 Cutting force analysis

The 1st cutting trial was performed at a self-developed three directional turning machine. The 2nd cutting trial was performed at a commercialised ultraprecision turning machine. Hence the cutting force signal is relatively small in this cutting attempt compared to the 1st cutting trial, not only because the depth of cut is smaller but also the spindle speed is much faster and there is less vibration.

The original signals saved for the smart cutting tool are raw voltage signals, because the circuitry design of the smart cutting tool was aimed to maintain lower power consumption, hence it was not designed for the full analysis force signal. This means that the collected data has to be processed and analysed after the PC received the force signal in each cut. The analysis methods are to detrend the raw force signal by averaging each sample and then plotting the result, see Figure 6.11. The program code is included in the appendix.

Figure 6.11 is the processed cutting force signal in cut number 20. It is a typical example for demonstrating the cutting process in the view of cutting forces. While the feed drive is approaching the work-piece, the sensor starts to sense a very tiny amount of vibration, just before the contact of the workpiece and diamond tool, with cutting force raised to 0.5 N. The cutting forces finished after approximately 200 seconds. The figure presents clearly that the radial force is comparatively larger than the cutting force. The reason for this could be that the depth of cut is 2 μm compared to 10 μm of the 1st cutting trial. Hence, the material removal rate is much lower and the thrust of diamond tool becomes comparatively more significant. Also a noticeable point is that the cutting

force and feed force are much smaller than in the 1st attempt of a cutting trial. The reason is probably that in an ultraprecision turning process, the commercial lathe machine is performing with a much faster spindle speed and much less vibration compared to the custom turning machine. The spindle speed is 1500 rpm compared to 600 rpm.

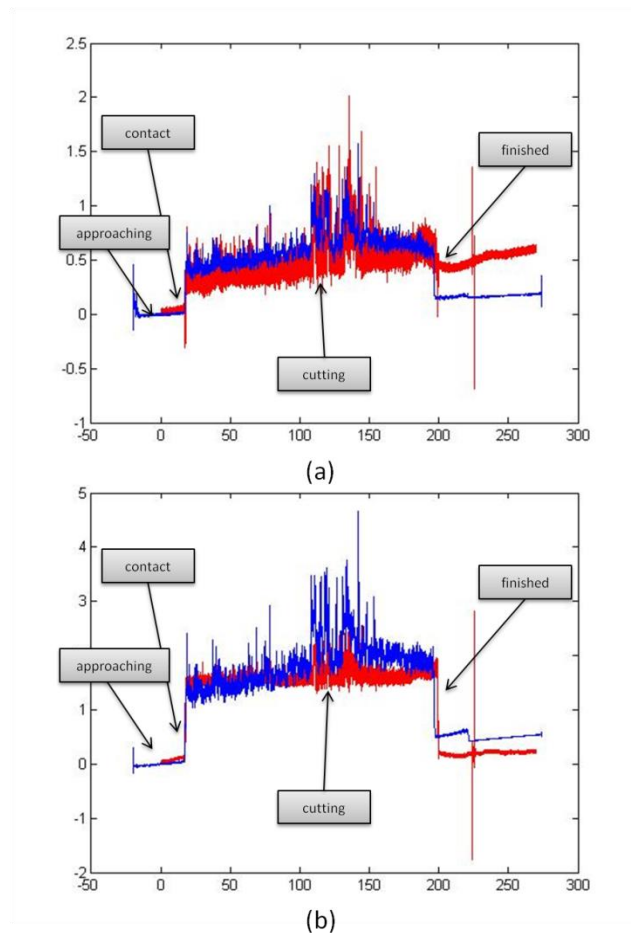


Figure 6.11: Representative comparison of the cutting force data from smart cutting tool (Blue) and Kistler dynamometer (Red) in one cut. Cutting force (a) and radial force (b)

6.3.4 Work-piece inspection

The smart cutting tool not only fulfils its sensing responsibilities but also shows good tool performance and cutting results. With the last few cuts on Moore 250UPL, the workpieces are shown in Figure 6.12.



Figure 6.12: Example of workpiece manufactured by the smart cutting tool

The figure shows clearly the workpiece has a clean mirror surface finish. The Zygo microscope is used to measure the surface roughness and the results are shown in Figure 6.13.

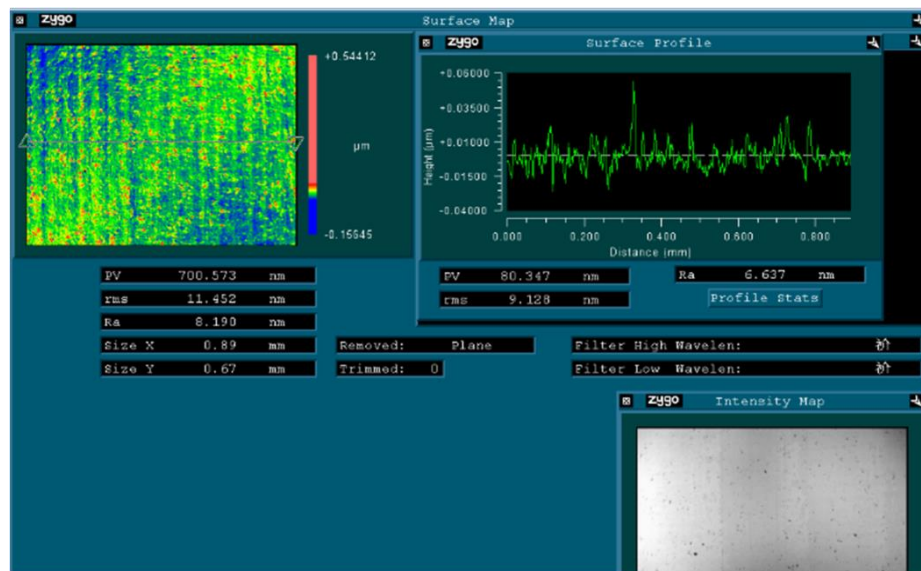


Figure 6.13: Surface roughness profile from Zygo 3D profiler

Figure 6.13 shows the measured surface roughness under a 20 times magnification on an area of 0.89 mm x 0.67 mm. The measured surface roughness is Ra 8.19 3nm, which

shows a mirror surface finish. However, by extracting the profiles along the federate direction, the periodic variation of the profile can still be clearly seen, and which represents the replication every revolution of tool geometry on the work-piece.

6.4 Summary

The smart cutting tool has been successfully calibrated after the bench test and cutting trial, and the initial aims and objectives have been achieved. The real-time monitoring system is reliable in the laboratory environment. The cutting trial experiments have provided some cutting force data to analyse and show a highly dependable cutting force signal compared with a commercial dynamometer.

Chapter 7 Conclusions and recommendations for future work

This chapter draws conclusions from the research, particularly in the light of smart cutting tools developed within this research and their comparison with the ones developed by other researchers. Furthermore, the contributions to knowledge are highlighted and recommendations for future work are provided.

7.1 Conclusions

Smart tooling is an essential subset and key enabler for smart manufacturing. Its main functions are to improve the machining process reliability and optimise the machining system's performance in process.

In this research, the smart cutting tool design concepts are proposed for ultraprecision and micro-cutting in particular. The developed prototype smart tool has a 0.1 N resolution in measuring the cutting forces and operates wirelessly in shop-floor operational distances. This smart cutting tool is thus more convenient to use and tool operation without additional cabling is also necessary for micro-cutting in-process on the machines. All the cutting force data are wirelessly transmitted under the standard Bluetooth transmitting protocol, which ensures the cutting force data are proofread and checked so as to render the accuracy of the in-process cutting force measurement.

All cutting force data captured will be stored and analysed in process in order to determine the optimum cutting conditions and thus extend the tool life through the

process optimisations. The embedded algorithms and analytics of the smart cutting tool are able to optimise cutting process parameters and control of the machine tool in process. The design of the smart turning tool is evaluated and validated through well-designed cutting trials, and which is benchmarked in comparison with the commercial cutting force measurement equipment, e.g. the Kistler Dynamometer, in terms of the measurement accuracy, application flexibility, in-process capability and stability.

Table 7.1: Assessment and comparison of three smart cutting tools

Smart cutting tool specifications	Radio frequency sensed tool	SAW-based smart cutting tool	Bluetooth smart cutting tool
Cutting force range (N)	0-100	0-100	0-100
Cutting force resolution (N)	1	1	0.1
Reliability	Poor	Good	Good
Power supply	Battery (9 V)	None	Battery (9 V)
Operation range (m)	2	0.5	20

Table 7.1 highlights the design and development of three types of smart cutting tool developed by the Brunel research team, to which this PhD research project is to some extent more or less related. The RF sensed cutting tool and SAW-based smart cutting tool are made for cutting force monitoring for conventional CNC machines, and the Bluetooth smart cutting tool aims to measure the cutting forces in ultraprecision and micro-machining. The SAW-based smart cutting tool requires no internal power source for the sensing unit, but the operating range is limited.

7.2 Contributions to knowledge

The contributions to knowledge arising directly from the following research work are as follows:

- Proposing a multi-physics-based approach to design and analysis of the smart cutting tool;

- Development of the wireless smart cutting monitoring tool (Gap tech);
- Development of the plug-and-produce concepts with application to the smart turning tool;
- Proposing in-process cutting force measurement strategies for ultraprecision and micro-machining processes; and
- Providing a feasibility study on the cutting process optimisation-based on monitoring and control of in-process cutting force data.

The contributions above are implemented and applied in the development of the prototype smart cutting tool; its main technical performance data are listed in Table 7.2.

Smart cutting tool technical data specifications:

Table 7.2: The standard technical data for the smart cutting tool

Calibrated measuring range	N	44
Overload	N	45
Sensitivity	N	0.1
Hysteresis	%FSO	≤ 2
Rigidity	N/ μm	6.5
Natural frequency	kHz	6.1; 5.9
Operating temperature range	$^{\circ}\text{C}$	$0 \rightarrow 70$
Weight	kg	1.5×10^{-6}
Dimension	mm	50x10x10
Operating range	m	20
Bandwidth	kHz	2.5

The smart cutting tool concludes with the specifications in Table 7.2 as a completed designed product. The main limitations of the tool are generally twofold. Firstly, the aimed for force range of 10 N is relatively small and can be used only on micro-machining machines. Secondly, if the target machine is a CNC conventional machine for example, this smart cutting tool is not going to be available at present; however, it is feasible by optimising the electrical design.

7.3 Recommendations for future work

The duration of the PhD study has imposed limitations on further research and development of the prototype smart cutting tool, particularly against the industrial requirement in smart ultraprecision turning applications. Therefore, the following future work is recommended:

- 1) A smart cutting tool should have the comprehensive and systematic capability to adapt itself onto any CNC controlled machine tools, i.e. possessing plug-and-produce features and adaptively interfacing with machine tools operating with any CNC controllers. With continuous working on this smart cutting tool project, the monitoring of the tool condition can be theoretically shared with any other mode of the whole production process chain and to truly work as an enabling plug-and-produce smart tooling device for the Industry 4.0 era and beyond.
- 2) In the context of precision manufacturing and engineering implementation, there are potentials for the smart cutting tools to lead to the development of an in-process or even real-time approach to the quality of the production and also to extend the cutting tool life-based on the smart cutting tool operation protocols. The approach is likely to not only include cutting force monitoring, but also cutting temperature monitoring and, or combined with, further development of real-time automation adjustment and high precision control of the machining processes.
- 3) In view of the potential of the smart cutting tools, the innovative force sensing method and implementation perspectives developed can maybe provide the possibility of applying this research outcome to other engineering applications, such as medical engineering, where the piezoelectric transducer can be applied as a micro-force sensing device for human body activities. However, the

smaller the piezoelectric device is, the harder the technological challenge will be. The research on the piezoelectric wireless sensing application is inevitably the key for future intelligent manufacturing.

References:

Adolfsson, C. and Ståhl, J. (1995) 'Cutting force model for multi-toothed cutting processes and force measuring equipment for face milling', *International Journal of Machine Tools and Manufacture*, 35(12), pp. 1715-1728.

Astakhov, V.P. and Davim, J.P. (2008) 'Tools (geometry and material) and tool wear' in *Machining*, London: Springer, pp. 29-57.

Barker, R.W., Klutke, G. and Hinich, M.J. (1993) 'Monitoring rotating tool wear using higher-order spectral features', *Journal of Engineering for Industry*, 115(1), pp. 23-29.

Bayramoglu, M. and Döngel, Ü. (1998) 'A systematic investigation on the use of force ratios in tool condition monitoring for turning operations', *Transactions of the Institute of Measurement and Control*, 20(2), pp. 92-97.

Bhattacharyya, P., Sengupta, D. and Mukhopadhyay, S. (2007) 'Cutting force-based real-time estimation of tool wear in face milling using a combination of signal processing techniques', *Mechanical Systems and Signal Processing*, 21(6), pp. 2665-2683.

Bhuiyan, M.S.H. and Choudhury, I.A. (2014) 'Review of Sensor Applications in Tool Condition Monitoring in Machining', *Comprehensive Materials Processing*, 13, pp. 539-569.

Brehl, D.E. and Dow, T.A. (2008) 'Review of vibration-assisted

References

- machining', *Precision Engineering*, 32(3), pp. 153-172.
- Byrne, G., Dornfeld, D. and Denkena, B. (2003) 'Advancing cutting technology', *CIRP Annals - Manufacturing Technology*, 52(2), pp. 483-507.
- Byrne, G., Dornfeld, D., Inasaki, I., Ketteler, G., König, W. and Teti, R. (1995) 'Tool Condition Monitoring (TCM) — The Status of Research and Industrial Application', *CIRP Annals - Manufacturing Technology*, 44(2), pp. 541-567.
- Charttopadhyay, A.B., Paul, S. and Dutta, R.K. (2000) 'Fuzzy controlled backpropagation neural network for tool condition monitoring in face milling', *International Journal of Production Research*, 38(13), pp. 2989-3010.
- Chen, X.Q. and Li, H.Z. (2009) 'Development of a tool wear observer model for online tool condition monitoring and control in machining nickel-based alloys', *The International Journal of Advanced Manufacturing Technology*, 45(7), pp. 786-800.
- Cheng, K., Rakowski, R. and Bateman, R. (2015) 'Smart Toolings and Smart Machines for High Precision Smart Machining', [PowerPoint slides]. Presented at *International Conference on Automation & Computing (ICAC2015)*, Glasgow, UK.
- Choi, D., Kwon, W.T. and Chu, C.N. (1999) 'Real-Time Monitoring of Tool Fracture in Turning Using Sensor Fusion', *The International Journal of Advanced Manufacturing Technology*, 15(5), pp. 305-310.
- Choudhury, S.K. and Rath, S. (2000) 'In-process tool wear estimation in milling using cutting force model', *Journal of Materials Processing Tech*, 99(1), pp. 113-119.

References

- Chung, K.T. and Geddam, A. (2003) 'A multi-sensor approach to the monitoring of end milling operations', *Journal of Materials Processing Technology*, 139(1), pp. 15-20.
- Dagdeviren, C., Yang, B.D., Su, Y., Tran, P.L., Joe, P., Anderson, E., Xia, J., Doraiswamy, V., Dehdashti, B., Feng, X., Lu, B., Poston, R., Khalpey, Z., Ghaffari, R., Huang, Y., Slepian, M.J. and Rogers, J.A. (2014) 'Conformal piezoelectric energy harvesting and storage from motions of the heart, lung, and diaphragm', *Proceedings of the National Academy of Sciences*, 111(5), pp. 1927-1932.
- De Filippi, A. and Ippolito, R. (1969) 'Adaptive Control in Turning: Cutting Forces and Tool Wear Relationships for P10, P20, P30 Carbides,' *Annals of the CIRP*, 17, pp. 377-379.
- Dimla Sr, D.E. and Lister, P.M. (2000) 'On-line metal cutting tool condition monitoring. I: force and vibration analyses', *International Journal of Machine Tools and Manufacture*, 40(5), pp. 739-768.
- Dirk Slama, Frank Puhlmann, Jim Morrish, Rishi M. Bhatnagar. (2015) Chapter 4. Manufacturing and Industry. In: *Enterprise IoT: Strategies and Best Practices for Connected Products and Services*. USA: O'Reilly Media Inc. E-book.
- Elangovan, M., Devasenapati, S.B., Sakthivel, N.R. and Ramachandran, K.I. (2011) 'Evaluation of expert system for condition monitoring of a single point cutting tool using principle component analysis and decision tree algorithm', *Expert Systems with Applications*, 38(4), pp. 4450-4459.
- El-Wardany, T.I., Gao, D. and Elbestawi, M.A. (1996) 'Tool condition

References

- monitoring in drilling using vibration signature analysis', *International Journal of Machine Tools and Manufacture*, 36(6), pp. 687-711.
- Girardin, F., Rémond, D. and Rigal, J.-F. (2010) 'A new method for detecting tool wear and breakage in milling', *International Journal of Material Forming*, 3(1), pp. 463-466.
- Gould, L. (1988) 'Sensing tool and drive element conditions in machine tools', *Sensors* (1988), pp. 5-13.
- Groover, M.P. (2010) *Fundamentals of modern manufacturing: materials, processes, and systems*. 4th edn. Hoboken, NJ: J. Wiley and Sons.
- Hidayah, M.T.N, Ghani, J.A, Nuawi, M.Z. and Haron, C.H.C. (2015) 'A Review of Utilisation of Cutting Force Analysis in Cutting Tool Condition Monitoring', *International Journal of Engineering and Technology IJET-IJENS*, 15(3), pp 28-35.
- Jaffe, B., Cook, W.R. and Jaffe, H.H. (1971) *Piezoelectric ceramics*. Academic Press, London.
- Jantunen, E. (2002) 'A summary of methods applied to tool condition monitoring in drilling', *International Journal of Machine Tools and Manufacture*, 42(9), pp. 997-1010.
- Jemielniak, K. (1999) 'Commercial Tool Condition Monitoring Systems', *International Journal of Advanced Manufacturing Technology*, 15(10), pp. 711-721.
- Jones, T.B. and Nenadic, N.G. (2011) *Electromechanics and MEMS*.
- Jun, M.B., Burak Ozdoganlar, O., DeVor, R.E., Kapoor, S.G., Kirchheim, A.

References

- and Schaffner, G. (2002) 'Evaluation of a spindle-based force sensor for monitoring and fault diagnosis of machining operations', *International Journal of Machine Tools and Manufacture*, 42(6), pp. 741-751.
- Martin, K.F., Brandon, J.A., Grosvenor, R.I. et al. (1986) A comparison of in-process tool wear measurement methods in turning, *Proceedings of the 26th MTDR Conference*, pp. 289-296.
- Kagermann, H., Helbig, J., Hellinger, A. et al. (2013) *Recommendations for Implementing the Strategic Initiative INDUSTRIE 4.0: Securing the Future of German Manufacturing Industry*. Final Report of the Industrie 4.0 Working Group[M]. Forschungsunion, 2013.
- Kannatey-Asibu, E. and Emel, E. (1987) 'Linear discriminate function analysis of acoustic emission signals for cutting tool monitoring', *Mechanical Systems and Signal Processing*, 1(4), pp. 333-347.
- Kious, M., Ouahabi, A., Boudraa, M., Serra, R. and Cheknane, A. (2010) 'Detection process approach of tool wear in high speed milling', *Measurement*, 43(10), pp. 1439-1446.
- Ko, T.J. and Cho, D.W. (1994) 'Cutting state monitoring in milling by a neural network', *International Journal of Machine Tools and Manufacture*, 34(5), pp. 659-676.
- Komanduri, R. and Hou, Z.B. (2001) 'A review of the experimental techniques for the measurement of heat and temperatures generated in some manufacturing processes and tribology', *Tribology International*, 34(10), pp. 653-682.
- Koren, Y. (1978) 'Flank Wear Model of Cutting Tools Using Control Theory,'

References

- ASME J. of Engineering for Industry*, 100(1), pp. 103-109.
- Korkut, İ. (2003) 'A dynamometer design and its construction for milling operation', *Materials and Design*, 24(8), pp. 631-637.
- Kurada, S. and Bradley, C. (1997) 'A review of machine vision sensors for tool condition monitoring', *Computers in Industry*, 34(1), pp. 55-72.
- Lan, M.S. and Dornfeld, D.A. (1984) 'In-Process Tool Fracture Detection', *Journal of Engineering Materials and Technology, Transactions of the ASME*, 106(2), pp. 111-118.
- Lee, E. (2008) 'Cyber physical systems: Design challenges', *ISORC '08 Proceedings of the 2008 11th IEEE Symposium on Object Oriented Real-Time Distributed Computing*, pp. 363-369.
- Lee, D.E., Hwang, I., Valente, C.M.O., Oliveira, J.F.G. and Dornfeld, D.A. (2006) 'Precision manufacturing process monitoring with acoustic emission', *International Journal of Machine Tools and Manufacture*, 46(2), pp. 176-188.
- Li, C.J. and Li, S.Y. (1993) 'New sensor for real-time milling tool condition monitoring', *Journal of Dynamic Systems, Measurement and Control, Transactions of the ASME*, 115(2A), pp. 285-290.
- Li, X. (2002) 'A brief review: acoustic emission method for tool wear monitoring during turning', *International Journal of Machine Tools and Manufacture*, 42(2), pp. 157-165. Oxford: Elsevier Ltd.
- Li, X., Djordjevich, A. and Venuvinod, P.K. (2000) 'Current-sensor-based feed cutting force intelligent estimation and tool wear condition monitoring', *IEEE Transactions on Industrial Electronics*, 47(3), pp. 697-702.

References

- Li, X., Li, H., Guan, X. and Du, R. (2004) 'Fuzzy estimation of feed-cutting force from current measurement-a case study on intelligent tool wear condition monitoring', *IEEE Transactions on Systems, Man, and Cybernetics, Part C (Applications and Reviews)*, 34(4), pp. 506-512.
- Li, X., Venuvinod, P.K. and Chen, M.K. (2000) 'Feed Cutting Force Estimation from the Current Measurement with Hybrid Learning', *International Journal of Advanced Manufacturing Technology*, 16(12), pp. 859-862.
- Liang, S.Y. and Dornfeld, D.A. (1987) 'Tool wear detection using time series analysis of acoustic emission', *Journal of Manufacturing Science and Engineering*, 111(3), pp. 199-205.
- Lin, R.J. and Lin, S.C. (1996) 'Tool wear monitoring in face milling using force signals', *Wear*, 198(1), pp. 136-142.
- Lindstrom, B. and Lindberg, B. (1987) 'Measurement of Dynamic Cutting Forces in the Cutting Process, a New Sensor for In-process Measurements', *Proc of 24th Int. MTDR Conf.*, pp. 137-142
- Lister, P.M. (1993) *On-line measurement of tool wear*. Ph.D. thesis, Manufacturing and Machine Tools Division, Department of Mechanical Engineering, UMIST, Manchester, UK.
- Liu, T.I. and Ko, E.J. (1990) 'On-line recognition of drill wear via artificial neural networks', , pp. 101-110.
- Lüthje, H., Bandorf, R., Biehl, S. and Stint, B. (2004) 'Thin film sensor for wear detection of cutting tools', *Sensors and Actuators: A. Physical*, 116(1), pp. 133-136.

References

- Ma, L., Melkote, S.N., Morehouse, J.B., Castle, J.B., Fonda, J.W. and Johnson, M.A. (2012) 'Thin-film PVDF sensor-based monitoring of cutting forces in peripheral end milling', *Journal of Dynamic Systems, Measurement and Control, Transactions of the ASME*, 134(5), pp. 51014.
- Madhava Reddy, S., Chennakesava Reddy, A. and Sudhakar Reddy, K. (2012) 'Latest developments in condition monitoring of machining operations', *Journal of Applied Sciences*, 12(10), pp. 938-946.
- Moheimani, S.O.R. and Fleming, A.J. (2006) *Piezoelectric Transducers for Vibration Control and Damping*. London: Springer.
- Moriwaki, T. and Okushima, K. (1980) 'Detection for Cutting Tool Fracture by Acoustic Emission Measurement', *CIRP Annals - Manufacturing Technology*, 29(1), pp. 35-40.
- Nouni, M., Fussell, B., Ziniti, B. and Linder, E. (2015) 'Real-time tool wear monitoring in milling using a cutting condition independent method', *International Journal of Machine Tools and Manufacture*, 89, pp. 1-13.
- O'Donnell, G., Young, P., Kelly, K. and Byrne, G. (2001) 'Towards the improvement of tool condition monitoring systems in the manufacturing environment', *Journal of Materials Processing Technology*, 119(1), pp. 133-139.
- Oraby, S.E. and Hayhurst, D.R. (1990) 'High-capacity compact three-component cutting force dynamometer', *International Journal of Machine Tools and Manufacture*, 30(4), pp. 549-559.
- Özel, T., Hsu, T. and Zeren, E. (2005) 'Effects of cutting edge geometry, workpiece hardness, feed rate and cutting speed on surface roughness and forces

References

- in finish turning of hardened AISI H13 steel', *International Journal of Advanced Manufacturing Technology*, 25(3), pp. 262-269.
- Pahl, G., Beitz, W. and Wallace, K. (1995) *Engineering design: a systematic approach*. 2nd edn, London: Springer.
- Park, H. and Tran, N. (2014) 'Development of a smart machining system using self-optimizing control', *International Journal of Advanced Manufacturing Technology*, 74(9), pp. 1365-1380.
- Pfeifer, T. and Wieggers, L. (2000) 'Reliable tool wear monitoring by optimized image and illumination control in machine vision', *Measurement*, 28(3), pp. 209-218.
- Pugh, S. (1991) *Total design: integrated methods for successful product engineering*. Harlow: Pearson Education Ltd.
- Rabinowicz, E. (1995) *Friction and wear of materials*. 2nd edn, Chichester, New York: Wiley.
- Rangwala, S. and Dornfeld, D. (1990) 'Sensor integration using neural networks for intelligent tool condition monitoring', *Transactions of ASME: Journal of Engineering for Industry*, 112(3), pp. 219-228.
- Rantatalo, M., Aidanpää, J., Göransson, B. and Norman, P. (2007) 'Milling machine spindle analysis using FEM and non-contact spindle excitation and response measurement', *International Journal of Machine Tools and Manufacture*, 47(7), pp. 1034-1045.
- Rehorn, A.G., Jiang, J. and Orban, P.E. (2005) 'State-of-the-art methods and results in tool condition monitoring: a review', *International Journal of*

References

- Advanced Manufacturing Technology*, 26(7), pp. 693-710.
- René de Jesús, R., Gilberto, H., Iván, T. and Juan Carlos, J. (2003) 'Driver current analysis for sensorless tool breakage monitoring of CNC milling machines', *International Journal of Machine Tools and Manufacture*, 43(15), pp. 1529-1534.
- Şeker, U., Kurt, A. and Çiftçi, İ. (2002) 'Design and construction of a dynamometer for measurement of cutting forces during machining with linear motion', *Materials and Design*, 23(4), pp. 355-360.
- Shaw, M.C. (1984) *Metal cutting principles*. Oxford: Clarendon.
- Shinozuka, J., Basti, A. and Obikawa, T. (2008) 'Development of cutting tool with built-in thin film thermocouples for measuring high temperature fields in metal cutting processes', *Journal of Manufacturing Science and Engineering, Transactions of the ASME*, 130(3), pp. 0345011-0345016.
- Slocum, A.H. (1992) *Precision machine design*. Society of Manufacturing Engineers, Dearborn, Michigan.
- Stein, J.L. and Huh, K. (2002) 'Monitoring cutting forces in turning: A model-based approach', *Journal of Manufacturing Science and Engineering, Transactions of the ASME*, 124(1), pp. 26-31.
- Stoney, R., Donohoe, B., Geraghty, D. and O'Donnell, G.E. (2012) 'The development of surface acoustic wave sensors (SAWs) for process monitoring', *Procedia CIRP*, 1(1), pp. 569-574.
- Stoney, R., O'Donnell, G.E. and Geraghty, D. (2013) 'Dynamic wireless passive strain measurement in CNC turning using surface acoustic wave

References

- sensors', *International Journal of Advanced Manufacturing Technology*, 69(5), pp. 1421-1430.
- Texas instrument. (2015) *History of sensor innovation*. Available at: <http://www.ti.com/corp/docs/company/history/sensortimelinelowbandwidth.shtml> (Accessed: 10 October 2015).
- Thusty, J. and Andrews, G.C. (1983) 'A Critical Review of Sensors for Unmanned Machining', *CIRP Annals - Manufacturing Technology*, 32(2), pp. 563-572.
- Unuvar, A. and Saglam, H. (2003) 'Tool condition monitoring in milling-based on cutting forces by a neural network', *International Journal of Production Research*, 41(7), pp. 1519-1532.
- Vamsi Krishna, P., Rao, D.N. and Srikant, R.R. (2009) 'Predictive modelling of surface roughness and tool wear in solid lubricant assisted turning of AISI 1040 steel', *Proceedings of the Institution of Mechanical Engineers, Part J: Journal of Engineering Tribology*, 223(6), pp. 929-934.
- Wang, L. and Gao, R.X. (2006) *Condition monitoring and control for intelligent manufacturing*. Springer Science and Business Media.
- Wang, C., Rakowski, R. and Cheng, K. (2013) 'Design and analysis of a piezoelectric film embedded smart cutting tool', *Proceedings of the Institution of Mechanical Engineers, Part B: Journal of Engineering Manufacture*, 227(2), pp. 254-260.
- Wang, C., Cheng, K., Chen, X., Minton, T. and Rakowski, R. (2014) 'Design of an instrumented smart cutting tool and its implementation and application

References

- perspectives', *Smart Materials and Structures*, 23(3), pp. 1-11.
- Wang, C., Ghani, S.B., Cheng, K. and Rakowski, R. (2013) 'Adaptive smart machining-based on using constant cutting force and a smart cutting tool', *Proceedings of the Institution of Mechanical Engineers, Part B: Journal of Engineering Manufacture*, 227(2), pp. 249-253.
- Werschmoeller, D., Ehmann, K. and Li, X. (2011) 'Tool embedded thin film microsensors for monitoring thermal phenomena at tool-workpiece interface during machining', *Journal of Manufacturing Science and Engineering, Transactions of the ASME*, 133(2), pp. 21007.
- Werschmoeller, D., Li, X. and Ehmann, K. (2012) 'Measurement of transient tool-internal temperature fields during hard turning by insert-embedded thin film sensors', *Journal of Manufacturing Science and Engineering, Transactions of the ASME*, 134(6).
- Wong, Y.S., Nee, A.Y.C., Li, X.Q. and Reisdorf, C. (1997) 'Tool condition monitoring using laser scatter pattern', *Journal of Materials Processing Technology*, 63(1), pp. 205-210.
- Yan, J., Murakami, Y. and Davim, J.P. (2009) *Tool Design, Tool Wear and Tool Life*. Machining Dynamics. London: Springer, pp. 117-149.
- Yoshioka, H., Hashizume, H. and Shinno, H. (2004) 'In-process microsensor for ultraprecision machining', *IEE Proceedings: Science, Measurement and Technology*, 151(2), pp. 121-125.
- Zhai, L.-., Er, M.-., Li, X., Gan, O.-., Phua, S.-., Huang, S., Zhou, J.-., San, L. and Torabi, A.J. (2010) 'Intelligent monitoring of surface integrity and cutter

References

degradation in high-speed milling processes' in *Annual Conference of the Prognostics and Health Management Society, 2010*.

Zhou, Q., Hong, G.S. and Rahman, M. (1995) 'A new tool life criterion for tool condition monitoring using a neural network', *Engineering Applications of Artificial Intelligence*, 8(5), pp. 579-588.

Zhu, D., Zhang, X. and Ding, H. (2013) 'Tool wear characteristics in machining of nickel-based superalloys', *International Journal of Machine Tools and Manufacture*, 64, pp. 60-77.

Zorev, N.N. (1966) *Metal Cutting Mechanics*. Oxford: Pergamon Press.

Appendix A: A list of publications arising from the research

- Chen, X., Cheng, K. and Wang, C. (2014) ‘Design of a smart turning tool with application to in-process cutting force measurement in ultraprecision and micro cutting, *Manufacturing Letters*, 2(4), pp. 112-117.
- Wang, C., Cheng, K., Chen, X., Minton, T. and Rakowski, R. (2014) ‘Design of an instrumented smart cutting tool and its implementation and application perspectives’, *Smart Materials and Structures*, 23(3), pp. 1-11.
- Wang, C., Cheng, K., Rakowski, R., Chen, X. and Cheng, M. (2013) ‘An investigation on the development of a smart cutting tool for precision machining using SAW-based force measurement’. *13th European Precision Engineering & Nanotechnology Annual Conference (EUSPEN)*, 2013, pp. 335-339.
- Chen, X. and Cheng, K. (2011) ‘Design of a pick and place delta robot: modelling, simulation and implementation perspectives’. *9th International Conference on manufacturing research 2013(ICMR)*, 6, pp. 37-43.

Appendix B: Key equipment used for this research

Technical specifications of the capacitive sensor (Microsense 5810)

5810 - Specifications

Performance

Measurement Range

± 25 µm to ± 1000 µm full scale, depending on probe selection

Measurement Resolution

Typical resolution is better than 2 nm (r.m.s.) @ 1 kHz.

Typical Resolutions (nm, r.m.s)

Sensor ø (mm)	Range (± µm)	Bandwidth (kHz)	Resolution (nm)
0.5	25	1	0.5
0.5	50	20	2.2
2.0	125	1	1.7
2.0	250	100	22.3
5.0	250	5	2.9
5.0	500	1	5.7

Linearity

Typically 0.25% over full scale range, depending on probe model and operating range.

Stability

Typically better than 200 ppm per °C over temperature range of 15°C to 35°C.

Bandwidth

Jumper selectable from:
1 kHz, 5 kHz, 20 kHz, 100 kHz

Inputs / Outputs

Probe Input

Single, accepts Series 5000 probe family

Analog Output

Single & differential, preset ± 10 volts for full scale range. Jumpers set output scaling and bipolar/unipolar output.

Limits

User adjustable digital outputs for detecting overrange and measurement limits

Adjustments / Indicators

Front Panel Adjustments

Calibration adjustment for scale factor
Offset adjustment for zero setting
Limit settings

Front Panel LED Indicators

+ Limit, - Limit

Physical Dimensions

18 cm- L x 11 cm-W x 4 cm-H
(7.0" x 4.25" x 1.5")

Weight

1 kg (2.2 lbs)

Operating Environment

Temperature

5°C to 50°C (41°F to 122°F)


Humidity

0 to 95% RH, non-condensing

Power Requirements

90-240 VAC

Standard Microsense Universal Low Noise Power Supply with IEC Connector included with Module



Microsense LLC
70 Industrial Ave E.
Lowell, MA 01852
Main Tel (978)843-7670
Fax (978)856-3375
Microsense LLC (specifications subject to change without notice)

REV 092904

www.microsense.net

Technical specifications of Moore 250UPL Ultraprecision lathe machine

1.0 Nanotech 250UPL Machine Description

The Moore Nanotech 250UPL is an ultra precision machining center used to single point diamond turn symmetric and freeform optical surfaces as well as high precision mechanical components. The machine is capable of diamond turning in a variety of materials such as Aluminum, Electroless Nickel, Brass, Copper, Germanium, ZnS, ZnSe, and Silicon. The Nanotech 250UPL standard configuration consists of two linear axes, but an optional Y-axis is available for applications requiring 3 linear axes. Our proprietary 10,000rpm Heavy Duty bi-directional air bearing workspindle is also standard. The machine is expandable to a four-axis system by combining either our optional rotary B-axis table or the above noted optional linear Y-axis with the rotary C-axis workspindle option. Several other accessories can be added to the machine including our Fast Tool Servo device. The machines modular design allows the user numerous configuration possibilities. These configurations are interchangeable at the customer site and include:

Single Point Diamond Turning	XZ
Tool Normal Diamond Turning	XZB
Diamond Ruling and Grooving	XYZC
Slow Slide Servo Machining	XZC
Fast Tool Servo Machining	XZ+FTS, XZC+FTS
Raster Machining	XYZ + Work Spindle

The Nanotech 250UPL utilizes linear motors, linear laser glass scales, oil hydrostatic box slides, and a liquid cooled temperature controlled air bearing spindle, as well as an advanced open architecture CNC control system. These elements allow the user to machine extremely accurate optical surfaces in a variety of configurations. The machine is capable of generating components with 1nm surface roughness and form accuracies below 0.1um peak-to-valley. This document describes the machine specification, capabilities, and configurations.

2.0 Machine Specification

2.1 Base & Vibration Isolation

The machine base is designed and manufactured from natural black granite with integral slide channels and a low center of gravity. The top surface of the granite along with key critical components is protected by a stainless steel apron. There is a drain hole at the center of one end of this stainless steel surface to assist in coolant recovery during machining. The entire base structure sits on an elevated air-bag vibration isolation system. The upper machine enclosure is mounted to four isolated steel posts which decouple the granite base from the enclosure. This separation between base and enclosure lowers the risk of surface vibration in the part and improves overall surface finish.

2.2 Axis Configuration and Alignment

The machine is configured with two standard linear axes, X and Z. The X and Z axes are mounted in the horizontal plane in a T-configuration. The X-axis carries the proprietary 10,000 RPM HD bidirectional work spindle. The Z-axis table top is used to mount tooling, Fast Tool Servo, rotary B-axis or our optional 100mm Oil Hydrostatic removeable Y-axis. The Z-axis has also been optimized for slow slide servo machining. With the addition of two rotary axes (B & C) or one linear and one rotary axis (Y & C), the machine becomes a 4-axis system. All linear axes are squared to one another to better than 2 arc-seconds. All linear axes have box style oil hydrostatic bearings and are driven by linear motors with linear scales for position feedback.

2.3 X & Z Linear Axes

The machine's X and Z axes are both fully constrained box-type oil hydrostatic bearing slides. The slides have an integrated linear motor centrally mounted in a horizontal (low profile) configuration with a laser linear encoder mounted on one side and a mechanical/pneumatic brake on the other side.

Appendix B

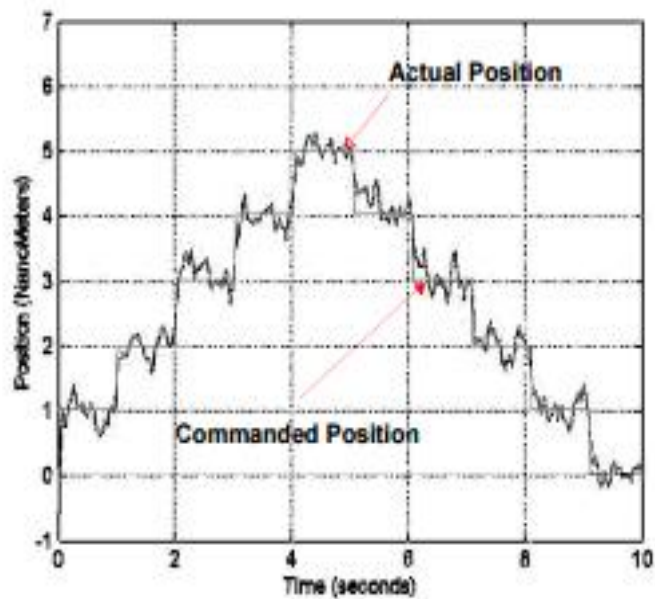
X and Z Slide Travels	200 mm
Drive System	DC Linear motor also known as AC synchronous motor
Vertical Straightness	< 0.5 μm
Horizontal Straightness	< 0.2 μm
Horizontal Stiffness	175N/ μm (1,000,000 lb/in)
Vertical Stiffness	350N/ μm (2,000,000 lb/in)
Brake	Mechanical / Pneumatic
Feedback Resolution	0.034 nm (34 Pico-meter)
Feed	4500 mm/min @ 0.034 nm



'Box-way' Style Oil Hydrostatic Slide



Glass Linear Scale and Encoder



Linear Axis 1 nanometer step response

The measurements taken at spindle center height via Laser Interferometer

Appendix B

2.4 Work Spindle and Optional C-axis

The work spindle is a groove compensated air bearing spindle. It is capable of operating up to 10,000 rpm in velocity mode and capable of operating in positioning mode or C-axis mode up to 3,000 rpm. The spindle is liquid cooled temperature controlled around both the front and back radial bearing journals and also the motor. It has error motions $\leq 12.5\text{nm}$ which are measured and qualified at several speeds from 500 to 10,000 rpm. With all Nanotech machines, one work spindle accommodates both heavy loads and high throughput applications.



The spindle can switch from spindle velocity mode to C-axis mode by the push of a button. The Nanotech 250UPL is also capable of switching from spindle velocity mode to C-axis mode during a machining cycle through the use of an M-code. M78 engages the C-axis and M79 de-engages the C-axis. In addition, there are three M-code options for homing the C-axis. The C-axis can be homed using M80 which will find the shortest distance to home, M81 which ensures that the spindle is homed CW (clock-wise) and M82 for CCW (counter clock-wise) homing.

Spindle Mode

Drive System	Brushless DC motor
Bearing Type	Groove Compensated Air Bearing
Load Capacity @ spindle nose	70 Kg (154 lbs) @ 100 psi / 85 kg (187 lbs) @ 145 psi
Axial Error Motion	< 12.5 nm
Radial Error Motion	< 12.5 nm
Axial Stiffness	228 N/ μm @ 100 psi / 260 N/ μm @ 145 psi
Radial Stiffness (at nose)	98 N/ μm @ 100 psi / 140 N/ μm @ 145 psi
Speed Range	50-10,000 RPM bi-directional

C-axis Mode

Feedback Resolution	0.07 arc-seconds
Speed	3000 RPM @ 0.07 arc-seconds
Positioning Accuracy	+/- 1 arc-seconds

Technical specifications of Kistler charge amplifier 5080A

Charge Amplifier

Type 5080A...

Multichannel Laboratory Charge Amplifier

This universal laboratory charge amplifier can be used for force and torque measurements with piezoelectric dynamometers or force plates. Piezoelectric sensors produce an electric charge which varies in direct proportion with the load acting on a sensor. The amplifier converts this charge signal into a proportional output voltage.

- Multichannel charge amplifier
- Piezotron® input (option)
- Setup of instrument is modular
- 1 ... 8 modules can be inserted
- 6-component analog summing calculation
- Wide measuring range
- USB and RS-232C interface for remote control
- Suitable for data acquisition software DynoWare Type 2825A

Description

Charge Amplifier Type 5080A... is the successor to charge amplifier Types 5017B... and Types 5019B... . Thanks to the modular design up to eight amplifier modules can be inserted. Charge modules Type 5067A0 with BNC connector are standard, as an option it is also possible to integrate Piezotron® modules Type 5067A2. A 6-component analog summing calculator Type 5245 is provided by default. This feature calculates the resulting force as well as the three components of the resulting torque real time. Dynamometer-specific values required for torque calculation can be set directly on the instrument.

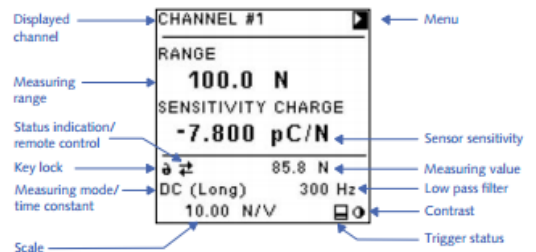
The liquid crystal display shows all channel settings. Various channels can be switched onto the display as required. The instrument is set up by means of different menus with the universal press-and-turn knob. All functions can, however, also be controlled externally via RS-232C or USB 2.0.

Application

This instrument is particularly suitable for general force measurements, cutting force measurements with Kistler dynamometers and wheel force measurements on tire test stands when a wide measuring range or high quality of signals is needed. Charge amplifier Type 5080A... finds its application in research and development.



Operation



Technical Data

Charge Input

Connector Type		BNC neg.
Measuring range FS	pC	±2 ... 2 200 000
Measuring error (0 ... 50 °C)		
FS ≥2 ... <10 pC	%	<±2
FS ≥10 ... <100 pC	%	<±0,6
FS ≥100 ... <2 200 000 pC	%	<±0,3
Drift, measuring mode DC (Long)		
at 25 °C, max. relative Humidity RH of 60 % (non-condensing)	pC/s	<±0,03
at 25 °C, max. relative Humidity RH of 70 % (non-condensing)	pC/s	typ. <±0,05
at 50 °C, max. relative Humidity RH of 50 % (non-condensing)	pC/s	<±0,3
Overload	%FS	≈±110

Technical specifications of Kistler 9256C Dynamometer

MiniDyn

Multicomponent Dynamometer up to 250 N

Multicomponent dynamometer for measuring the three orthogonal components of a force. Its very low threshold allows measuring extremely small forces.

- For cutting force measurements in ultra precise machining
- Small design
- High sensitivity and natural frequency
- Small temperature error
- Top plate made of titanium

Description

The dynamometer consists of four 3-component force sensors mounted under high preload between the cover plate and the two lateral base plates.

A low temperature error is obtained by this special mounting of the sensors. Each force sensor contains three crystal rings, of which one is sensitive to pressure in the y-direction and the two others to shear in the x- and z-directions. The forces are measured practically without displacement.

The outputs of the four mounted force sensors are fed to the 7-pole flanged socket. There are also multicomponent force-moment measurements possible.

The four sensors are fitted so that they are ground-isolated. This largely eliminates ground loop problems.

The dynamometer is corrosion-resistant and protected against penetration by splashing water or cutting fluid. The dynamometer including connecting cable Type 1696A5 or Type 1697A5 meets the degree of protection IP67.

Examples of Application

- Cutting force measurement in precision machining such as:
 - cutting wafers
 - grinding hard-disk read heads
 - diamond turning
 - high speed machining
- Ultra-high precision machining of brittle hard materials
- Multicomponent force measurement of small forces
- Force measurement in confined spaces

measured analytically

Type 9256C...



Type 9256C2

Technical Data

			9256C1	9256C2
Measuring range	F_x, F_y, F_z	N	-250 ... 250	
	M_x, M_z	Nm	-8 ... 8 -11 ... 11	
Calibrated measuring range	F_x, F_y, F_z	N	0 ... 250	
	F_x, F_y, F_z	N	0 ... 25	
Overload	F_x, F_y, F_z	N	-300/300	
Threshold		N	<0,002	
Sensitivity	F_x, F_z	pC/N	≈26	
	F_y	pC/N	≈13	
Linearity, all ranges		% FSO	±±0,4	
Hysteresis, all ranges		% FSO	±0,5	
Crosstalk		%	±±2	
Rigidity	c_x, c_z	N/μm	>250	
	c_y	N/μm	>300	
Natural frequency (mounted on rigid base)	$f_n(x)$	kHz	≈5,1	≈4,0
	$f_n(y)$	kHz	≈5,5	≈4,8
	$f_n(z)$	kHz	≈5,6	≈4,6
Operating temperature range		°C	0 ... 70	
Insulation resistance		Ω	>10 ¹⁴	
Ground isolation		Ω	>10 ⁸	
Degree of protection EN60529			IP67 **)	
Weight	Dynamometer	kg	0,75	0,87
	Top plate	kg	0,24	0,36
Clamping area		mm	39x80	55x80

**) With connecting cable Type 1696A5/1697A5

Appendix C: Components data sheet for the smart cutting tool

Technical specifications of microchip (PIC16F1827)



PIC16(L)F1826/27

18/20/28-Pin Flash Microcontrollers with nanoWatt XLP Technology

High-Performance RISC CPU:

- C Compiler Optimized Architecture
- 256 bytes Data EEPROM
- Up to 8 Kbytes Linear Program Memory Addressing
- Up to 384 bytes Linear Data Memory Addressing
- Interrupt Capability with Automatic Context Saving
- 16-Level Deep Hardware Stack with Optional Overflow/Underflow Reset
- Direct, Indirect and Relative Addressing modes:
 - Two full 16-bit File Select Registers (FSRs)
 - FSRs can read program and data memory

Flexible Oscillator Structure:

- Precision 32 MHz Internal Oscillator Block:
 - Factory calibrated to $\pm 1\%$, typical
 - Software selectable frequencies range of 31 kHz to 32 MHz
- 31 kHz Low-Power Internal Oscillator
- Four Crystal modes up to 32 MHz
- Three External Clock modes up to 32 MHz
- 4X Phase-Lock Loop (PLL)
- Fail-Safe Clock Monitor:
 - Allows for safe shutdown if peripheral clock stops
- Two-Speed Oscillator Start-up
- Reference Clock Module:
 - Programmable clock output frequency and duty-cycle

Special Microcontroller Features:

- 1.8V-5.5V Operation – PIC16F1826/27
- 1.8V-3.6V Operation – PIC16LF1826/27
- Self-Programmable under Software Control
- Power-on Reset (POR), Power-up Timer (PWRT) and Oscillator Start-up Timer (OST)
- Programmable Brown-out Reset (BOR)
- Extended Watchdog Timer (WDT):
 - Programmable period from 1ms to 268s
- Programmable Code Protection
- In-Circuit Serial Programming™ (ICSP™) via two pins
- In-Circuit Debug (ICD) via two pins
- Enhance Low-Voltage Programming
- Power-Saving Sleep mode

Extreme Low-Power Management PIC16LF1826/27 with nanoWatt XLP:

- Operating Current: 75 μ A @ 1 MHz, 1.8V, typical
- Sleep mode: 30 nA
- Watchdog Timer: 500 nA
- Timer1 Oscillator: 800 nA @ 32 kHz


Analog Features:

- Analog-to-Digital Converter (ADC) Module:
 - 10-bit resolution, 12 channels
 - Auto acquisition capability
 - Conversion available during Sleep
- Analog Comparator Module:
 - Two rail-to-rail analog comparators
 - Power mode control
 - Software controllable hysteresis
- Voltage Reference Module:
 - Fixed Voltage Reference (FVR) with 1.024V, 2.048V and 4.096V output levels
 - 5-bit rail-to-rail resistive DAC with positive and negative reference selection

Peripheral Highlights:

- 15 I/O Pins and 1 Input Only Pin:
 - High current sink/source 25 mA/25 mA
 - Programmable weak pull-ups
 - Programmable interrupt-on-change pins
- Timer0: 8-Bit Timer/Counter with 8-Bit Prescaler
- Enhanced Timer1:
 - 16-bit timer/counter with prescaler
 - External Gate Input mode
 - Dedicated, low-power 32 kHz oscillator driver
- Up to three Timer2-types: 8-Bit Timer/Counter with 8-Bit Period Register, Prescaler and Postscaler
- Up to two Capture, Compare, PWM (CCP) Modules
- Up to two Enhanced CCP (ECCP) Modules:
 - Software selectable time bases
 - Auto-shutdown and auto-restart
 - PWM steering
- Up to two Master Synchronous Serial Port (MSSP) with SPI and I²C™ with:
 - 7-bit address masking
 - SMBus/PMBus™ compatibility
- Enhanced Universal Synchronous Asynchronous Receiver Transmitter (EUSART) Module
- mTouch™ Sensing Oscillator Module:
 - Up to 12 input channels
- Data Signal Modulator Module:
 - Selectable modulator and carrier sources
- SR Latch:
 - Multiple Set/Reset input options
 - Emulates 555 Timer applications

Technical specifications of Op-amp (MCP-6023)



MICROCHIP MCP6021/1R/2/3/4

Rail-to-Rail Input/Output, 10 MHz Op Amps

Features

- Rail-to-Rail Input/Output
- Wide Bandwidth: 10 MHz (typical)
- Low Noise: 8.7 nV/√Hz, at 10 kHz (typical)
- Low Offset Voltage:
 - Industrial Temperature: ±500 μV (maximum)
 - Extended Temperature: ±250 μV (maximum)
- Mid-Supply V_{REF}: MCP6021 and MCP6023
- Low Supply Current: 1 mA (typical)
- Total Harmonic Distortion:
 - 0.00053% (typical, G = 1 V/V)
- Unity Gain Stable
- Power Supply Range: 2.5V to 5.5V
- Temperature Range:
 - Industrial: -40°C to +85°C
 - Extended: -40°C to +125°C

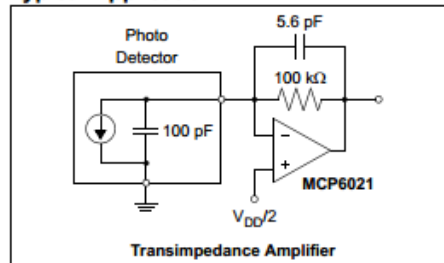
Applications

- Automotive
- Multi-Pole Active Filters
- Audio Processing
- DAC Buffer
- Test Equipment
- Medical Instrumentation

Design Aids

- SPICE Macro Models
- FilterLab® Software
- Mindi™ Circuit Designer & Simulator
- Microchip Advanced Part Selector (MAPS)
- Analog Demonstration and Evaluation Boards
- Application Notes

Typical Application



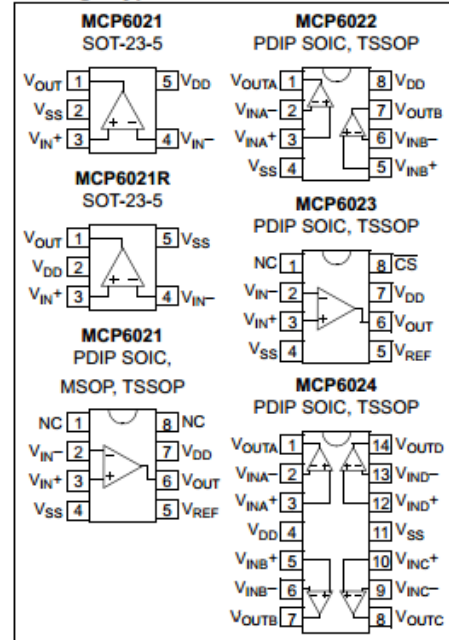
Description

The MCP6021, MCP6021R, MCP6022, MCP6023 and MCP6024 from Microchip Technology Inc. are rail-to-rail input and output op amps with high performance. Key specifications include: wide bandwidth (10 MHz), low noise (8.7 nV/√Hz), low input offset voltage and low distortion (0.00053% THD+N). The MCP6023 also offers a Chip Select pin (CS) that gives power savings when the part is not in use.

The single MCP6021 and MCP6021R are available in SOT-23-5. The single MCP6021, single MCP6023 and dual MCP6022 are available in 8-lead PDIP, SOIC and TSSOP. The Extended Temperature single MCP6021 is available in 8-lead MSOP. The quad MCP6024 is offered in 14-lead PDIP, SOIC and TSSOP packages.

The MCP6021/1R/2/3/4 family is available in Industrial and Extended temperature ranges. It has a power supply range of 2.5V to 5.5V.

Package Types



Technical specifications of Bluetooth module (HC-05)



HC-05 module is an easy to use Bluetooth SPP (Serial Port Protocol) module, designed for transparent wireless serial connection setup.

Serial port Bluetooth module is fully qualified Bluetooth V2.0+EDR (Enhanced Data Rate) 3Mbps Modulation with complete 2.4GHz radio transceiver and baseband. It uses CSR Bluecore 04-External single chip Bluetooth system with CMOS technology and with AFH(Adaptive Frequency Hopping Feature). It has the footprint as small as 12.7mmx27mm. Hope it will simplify your overall design/development cycle.

Specifications

Hardware features

- Typical -80dBm sensitivity
- Up to +4dBm RF transmit power
- Low Power 1.8V Operation ,1.8 to 3.6V I/O
- PIO control
- UART interface with programmable baud rate
- With integrated antenna
- With edge connector

Appendix D: Program codes developed for the smart cutting tool

C Codes for the microchip on the circuit board

```
#include <16f1827.h>
#fuses NOWDT,INTRC_IO, PLL, PUT, NOPROTECT, MCLR, NOCPD, BROWNOUT, NOIESO,
FCMEN
#fuses NOWRT, NOSTVREN, BORV25, NOLVP
#DEVICE ADC=10
#use delay(clock=32000000)
#use RS232(STREAM=BT, BAUD=115200,PARITY=N, ERRORS, UART1)
//#use RS232(STREAM=BT, BAUD=9600,PARITY=N, ERRORS, UART1)

int on=0;

#int_ext
void ISR_EXT(){
delay_ms(250);
on++;
if (on==5){
on=0;
}
if (on==0){
output_low(PIN_B4);
output_low(PIN_A6);
output_low(PIN_A7);
delay_ms(1000);
}

if (on==1){
output_high(PIN_A6);
output_high(PIN_B4);
output_high(PIN_A7);
}
if(on==2){
set_adc_channel(0);
delay_us(1);
output_high(PIN_B4);
output_low(PIN_A6);
output_low(PIN_A7);
}
if(on==3){
set_adc_channel(1);
delay_us(1);
```

Appendix D

```
    output_high(PIN_A6);
    output_low(PIN_B4);
    output_low(PIN_A7);
}
if(on==4){
    set_adc_channel(2);
    delay_us(1);
    output_high(PIN_A7);
    output_low(PIN_B4);
    output_low(PIN_A6);
}
}

void main(){
//setup_oscillator(OSC_16MHZ | OSC_INTRC | OSC_PLL_ON);
SETUP_TIMER_0(T0_INTERNAL | T0_DIV_1);

SETUP_ADC(ADC_CLOCK_DIV_32);

//SETUP_ADC(ADC_CLOCK_INTERNAL);
SETUP_ADC_PORTS(sAN0 | sAN1 |sAN2);

enable_interrupts(GLOBAL);
enable_interrupts(INT_EXT_H2L);
while(1){

    while(on==0){ }
    while (on==1){
        set_adc_channel(0);
        delay_us(1);
        fprintf(BT, "%Lu\n" read_adc());
        set_adc_channel(1);
        delay_us(1);
        fprintf(BT, "%Lu\v" read_adc());
        set_adc_channel(2);
        delay_us(1);
        fprintf(BT, "%Lu\r" read_adc());
    }

    while (on==2){
        fprintf(BT, "%Lu\n" read_adc());
    }

    while (on==3){
        fprintf(BT, "%Lu\n" read_adc());
    }

    while (on==4){
        fprintf(BT, "%Lu\n" read_adc());
    }

}
```


Appendix D

```
}  
  
//1000 uS / 6.25 uS = expected number of samples per millisecond  
// = 160 samples per millisecond...  
  
//Actually getting:  
  
//~150000 samples per minute  
//150000 / 60 = 2500 sps  
// /1000 = 2.5 samples per millisecond  
  
//I'm getting 2.5 samples per millisecond,  
  
//A0-->LED B4  
//A1-->LED A6  
//A2-->LEDA7
```

Program codes for undertaking cutting trials on the diamond turning machine

```
G01 G18 G40 G54 G63 G71 G90 G94 G103  
M3S1500//spindle speed 1500 rpm  
    T0101  
    X54Z25F500  
    Z-0.002F500// depth of cut  $2\mu\text{m}$   
  
    M26  
    X0Z0F15//feed rate 15mm/min  
    Z2  
    M29  
    X54Z25F500  
    M30
```

Program codes for the PC receiver interface

```
// SensorPrjDlg.cpp : implementation file  
//  
  
#include "stdafx.h"
```

Appendix D

```
#include <objbase.h>
#include "SensorPrj.h"
#include "SensorPrjDlg.h"
#include "axes.h"
#include "axis1.h"
#include "series.h"
#include "registry.h"
#include "page.h"

#ifdef _DEBUG
#define new DEBUG_NEW
#undef THIS_FILE
static char THIS_FILE[] = __FILE__;
#endif

FILE* g_pFileLog = NULL;

BOOL IsFileExist(CString strFn, BOOL bDir)
{
    HANDLE h;
    LPWIN32_FIND_DATA pFD=new WIN32_FIND_DATA;
    BOOL bFound=FALSE;
    if(pFD)
    {
        h=FindFirstFile(strFn,pFD);
        bFound=(h!=INVALID_HANDLE_VALUE);
        if(bFound)
        {
            if(bDir)
                bFound= (pFD->dwFileAttributes&FILE_ATTRIBUTE_DIRECTORY)!=NULL;
            FindClose(h);
        }
        delete pFD;
    }
    return bFound;
}

////////////////////////////////////
// CAboutDlg dialog used for App

class CAboutDlg : public CDialog
{
public:
    CAboutDlg();

protected:
    virtual void DoDataExchange(CDataExchange* pDX); // DDX/DDV support

// Implementation
protected:
    DECLARE_MESSAGE_MAP()
};

CAboutDlg::CAboutDlg() : CDialog(CAboutDlg::IDD)
```

Appendix D

```
{
}

void CAboutDlg::DoDataExchange(CDataExchange* pDX)
{
    CDialog::DoDataExchange(pDX);
}

BEGIN_MESSAGE_MAP(CAboutDlg, CDialog)

END_MESSAGE_MAP()

////////////////////////////////////
// CSensorPrjDlg dialog

CSensorPrjDlg::CSensorPrjDlg(CWnd* pParent /*=NULL*/)
    : CDialog(CSensorPrjDlg::IDD, pParent)
{
    m_nXPoints = 0;
    m_hIcon = AfxGetApp()->LoadIcon(IDR_MAINFRAME);

    pProcessThread = NULL;
    bRun = FALSE;
    hEventShut = NULL;
    hEventStop = NULL;

    memset(RxData, 0, BUF_SIZE_COMM);
    Start = 0;
    End = 0;
    BufLen = 0;

    InitializeCriticalSection(&m_cs);
}

void CSensorPrjDlg::DoDataExchange(CDataExchange* pDX)
{
    CDialog::DoDataExchange(pDX);
    DDX_Control(pDX, IDC_PROGRESS, m_Progress);
    DDX_Control(pDX, IDC_COMBO_PORT, m_ComboPort);
    DDX_Control(pDX, IDC_TCHART1, m_ctrlChart1);
    DDX_Control(pDX, IDC_TCHART2, m_ctrlChart2);
    DDX_Control(pDX, IDC_TCHART3, m_ctrlChart3);
    DDX_Text(pDX, IDC_EDIT_X_POINTS, m_nXPoints);
}

BEGIN_MESSAGE_MAP(CSensorPrjDlg, CDialog)
    ON_WM_SYSCOMMAND()
    ON_WM_PAINT()
    ON_WM_QUERYDRAGICON()
    ON_BN_CLICKED(IDC_BTN_START, OnBtnStart)
    ON_BN_CLICKED(IDC_BTN_STOP, OnBtnStop)
    ON_BN_CLICKED(IDC_BTN_VIEW, OnBtnView)
    ON_BN_CLICKED(IDC_BTN_EXIT, OnBtnExit)
    ON_WM_DESTROY()
    ON_BN_CLICKED(IDC_BTN_CLEAR_DATA, OnBtnClearData)
```

Appendix D

```
        ON_EN_CHANGE(IDC_EDIT_X_POINTS, OnChangeEditXPoints)
        ON_WM_TIMER()
        ON_MESSAGE(UM_DRAW_DATA, OnDrawData)
    END_MESSAGE_MAP()

    //////////////////////////////////////
    // CSensorPrjDlg message handlers

    BOOL CSensorPrjDlg::OnInitDialog()
    {
        CDialog::OnInitDialog();

        // Add "About..." menu item to system menu.

        // IDM_ABOUTBOX must be in the system command range.
        ASSERT((IDM_ABOUTBOX & 0xFFF0) == IDM_ABOUTBOX);
        ASSERT(IDM_ABOUTBOX < 0xF000);

        CMenu* pSysMenu = GetSystemMenu(FALSE);
        if (pSysMenu != NULL)
        {
            CString strAboutMenu;
            strAboutMenu.LoadString(IDS_ABOUTBOX);
            if (!strAboutMenu.IsEmpty())
            {
                pSysMenu->AppendMenu(MF_SEPARATOR);
                pSysMenu->AppendMenu(MF_STRING, IDM_ABOUTBOX,
strAboutMenu);
            }
        }

        // Set the icon for this dialog. The framework does this automatically
        // when the application's main window is not a dialog
        SetIcon(m_hIcon, TRUE);           // Set big icon
        SetIcon(m_hIcon, FALSE);        // Set small icon

        // Define window name: Data gathering system
        SetWindowText(_T("数据采集系统"));

        CString strPort;
        for (int i = 1; i <= 16; ++i)
        {
            strPort.Format(_T("COM%d"), i);
            m_ComboPort.AddString(strPort);
        }

        m_nXPoints = 200;
        UpdateData(FALSE);

        m_ctrlChart1.GetAxis().GetLeft().SetAutomatic(false);
        m_ctrlChart1.GetAxis().GetLeft().SetMinMax(-11.0f, 11.0f);

        m_ctrlChart1.GetAxis().GetBottom().SetAutomatic(false);
        m_ctrlChart1.GetAxis().GetBottom().SetMinMax(0 - m_nXPoints, 0);
    }
}
```

Appendix D

```
m_ctrlChart2.GetAxis().GetLeft().SetAutomatic(false);
m_ctrlChart2.GetAxis().GetLeft().SetMinMax(-11.0f, 11.0f);

m_ctrlChart2.GetAxis().GetBottom().SetAutomatic(false);
m_ctrlChart2.GetAxis().GetBottom().SetMinMax(0 - m_nXPoints, 0);

m_ctrlChart3.GetAxis().GetLeft().SetAutomatic(false);
m_ctrlChart3.GetAxis().GetLeft().SetMinMax(-11.0f, 11.0f);

m_ctrlChart3.GetAxis().GetBottom().SetAutomatic(false);
m_ctrlChart3.GetAxis().GetBottom().SetMinMax(0 - m_nXPoints, 0);

return TRUE; // return TRUE unless you set the focus to a control
}

void CSensorPrjDlg::OnSysCommand(UINT nID, LPARAM lParam)
{
    if ((nID & 0xFFF0) == IDM_ABOUTBOX)
    {
        CAboutDlg dlgAbout;
        dlgAbout.DoModal();
    }
    else
    {
        CDialog::OnSysCommand(nID, lParam);
    }
}

// If you add a minimize button to your dialog, you will need the code below
// to draw the icon. For MFC applications using the document/view model,
// this is automatically done for you by the framework.

void CSensorPrjDlg::OnPaint()
{
    if (IsIconic())
    {
        CPaintDC dc(this); // device context for painting

        SendMessage(WM_ICONERASEBKGND, (LPARAM) dc.GetSafeHdc(), 0);

        // Center icon in client rectangle
        int cxIcon = GetSystemMetrics(SM_CXICON);
        int cyIcon = GetSystemMetrics(SM_CYICON);
        CRect rect;
        GetClientRect(&rect);
        int x = (rect.Width() - cxIcon + 1) / 2;
        int y = (rect.Height() - cyIcon + 1) / 2;

        // Draw the icon
        dc.DrawIcon(x, y, m_hIcon);
    }
    else
    {
        CDialog::OnPaint();
    }
}
```

Appendix D

```
}

// The system calls this to obtain the cursor to display while the user drags
// The minimized window.
HCURSOR CSensorPrjDlg::OnQueryDragIcon()
{
    return (HCURSOR) m_hIcon;
}

void CSensorPrjDlg::OnBtnStart()
{
    // TODO: Add control notification handler code here
    ///////////////////////////////////////////////////////////////////
    UpdateData(TRUE);

    int nPort = m_ComboPort.GetCurSel();
    if (nPort == CB_ERR)
    {
        AfxMessageBox(_T("Select port! "));
        return;
    }

    if (m_nXPoints < 0)
    {
        AfxMessageBox(_T("Re-enter data! "));
        return;
    }

    StopThread();

    StartThread();

    // Situation while port already established, restart the port.
    if (m_SerialPort.IsPortOpened())
    {
        // Shut down the 'port receive' before shout down else.
        m_SerialPort.StopMonitoring();
    }

    // index ReadRecv before buffering
    m_SerialPort.OnCommRecv = OnCommReadRecv;

    ///////////////////////////////////////////////////////////////////
    m_nSensorIndex = 0;
    m_nTotalGroupCount = 0;
    m_nDrawSensorIndex = 0;
    m_nTotalGroupCountDrawed = 0;
    m_dwStartTick = GetTickCount();
    m_nDataCount = 0;
    m_strBuffLine = _T("");

    memset(RxData, 0, BUF_SIZE_COMM);
    Start = 0;
    End = 0;
    BufLen = 0;
}
```

Appendix D

```
// m_arrBuff.RemoveAll();
//
//
// GetDlgItem(IDC_EDIT_LOG)->SetWindowText(_T(""));
//
//
// CString strFileName;
// strFileName.Format(_T("%s%s"), g_strAppFolder, XLS_FILE_NAME);
// if(IsFileExist(strFileName,FALSE))
// {
//     DeleteFile(strFileName);
// }
//
// strFileName.Format(_T("%s%s"), g_strAppFolder, TXT_FILE_NAME);
// if(IsFileExist(strFileName,FALSE))
// {
//     DeleteFile(strFileName);
// }
// g_pFileLog = fopen(strFileName, "a+");
//
//
// if (!m_SerialPort.InitPort(this, nPort+1, 115200))
// {
//     AfxMessageBox(_T("Port attempt fail! "));
//     AddLog(_T("Port attempt fail! "));
//
//     return;
// }
//
// AddLog(_T("Port established! "));
//
// SetTimer(ID_TIMER_SCROLL_LEFT, ID_TIME_OUT_SCROLL_LEFT, NULL);
//
// m_SerialPort.StartMonitoring();
//
// GetDlgItem(IDC_BTN_START)->EnableWindow(FALSE);
// GetDlgItem(IDC_BTN_STOP)->EnableWindow(TRUE);
// GetDlgItem(IDC_EDIT_X_POINTS)->EnableWindow(FALSE);
// }
//
// void CSensorPrjDlg::OnBtnStop()
// {
//     // TODO: Add your control notification handler code here
//     if (m_SerialPort.IsPortOpened())
//     {
//         // Shut down the 'port receive' before shout down elsez.
//         m_SerialPort.StopMonitoring();
//     }
//
//     StopThread();
//
//     KillTimer(ID_TIMER_SCROLL_LEFT);
// }
```

Appendix D

```
        if (g_pFileLog != NULL)
        {
            fflush(g_pFileLog);
            fclose(g_pFileLog);

            g_pFileLog = NULL;
        }

        GetDlgItem(IDC_BTN_START)->EnableWindow(TRUE);
        GetDlgItem(IDC_BTN_STOP)->EnableWindow(FALSE);
        GetDlgItem(IDC_EDIT_X_POINTS)->EnableWindow(TRUE);
    }

void CSensorPrjDlg::OnBtnView()
{
    // TODO: Add your control notification handler code here
    CWinThread* pWriteThread = AfxBeginThread(WriteProcessProcFunc, this,
    THREAD_PRIORITY_NORMAL);
    if (pWriteThread == NULL)
    {
        return;
    }
}

void CSensorPrjDlg::OnBtnExit()
{
    // TODO: Add your control notification handler code here
    OnOK();
}

void CSensorPrjDlg::OnDestroy()
{
    CDialog::OnDestroy();

    // TODO: Add your message handler code here
    if (m_SerialPort.IsPortOpened())
    {
        // Shut down the 'port receive' before shout down else.
        m_SerialPort.StopMonitoring();
    }

    StopThread();

    if (hEventShut != NULL)
    {
        CloseHandle(hEventShut);
    }

    if (hEventStop != NULL)
    {
        CloseHandle(hEventStop);
    }
}
```


Appendix D

```
        DeleteCriticalSection(&m_cs);
    }

void CALLBACK CSensorPrjDlg::OnCommReadRecv(DWORD UserParam, BYTE *buf, DWORD
buflen)
{
    CSensorPrjDlg *pDlg = (CSensorPrjDlg *)UserParam;

    // Point the received data to buffering
    if (buflen > 0)
    {
        DWORD i = 0;
        for (i = 0; i < buflen; i++)
        {
            pDlg->AddLog(buf[i]);

            pDlg->RxData[pDlg->End] = buf[i];
            pDlg->End = (pDlg->End + 1) % BUF_SIZE_COMM;
            if (pDlg->End == pDlg->Start)
            {
                pDlg->Start = (pDlg->Start + 1) % BUF_SIZE_COMM;
                // AfxMessageBox("rx data over");
            }
        }
    }
}

int CSensorPrjDlg::StartThread()
{
    int nRet = 0;

    ASSERT(pProcessThread == NULL);
    ASSERT(bRun == FALSE);

    // create or reset event handle
    if (hEventShut == NULL)
    {
        hEventShut = CreateEvent(NULL, TRUE, FALSE, NULL);
    }
    else
    {
        ResetEvent(hEventShut);
    }

    if (hEventStop == NULL)
    {
        hEventStop = CreateEvent(NULL, TRUE, FALSE, NULL);
    }
    else
    {
        ResetEvent(hEventStop);
    }

    pProcessThread = AfxBeginThread(BuffProcessProcFunc, this,
THREAD_PRIORITY_NORMAL);
}
```

Appendix D

```
        if (pProcessThread == NULL)
        {
            nRet = 1;
            goto RET;
        }

        return nRet;

RET:
    return nRet;
}

int CSensorPrjDlg::StopThread()
{
    if (pProcessThread != NULL && bRun)
    {
        SetEvent(hEventShut);
        if (::WaitForSingleObject(hEventStop, 1500) == WAIT_TIMEOUT)
        {
            DWORD dwExitCode;
            BOOL bThreadStatus;
            bThreadStatus = GetExitCodeThread(pProcessThread->m_hThread, &dwExitCode);
            if ((dwExitCode == (DWORD)STILL_ACTIVE) && (bThreadStatus))
            {
                TerminateThread(pProcessThread->m_hThread, 101);
            }
        }
    }

    pProcessThread = NULL;
    bRun = FALSE;

    return 0;
}

UINT CSensorPrjDlg::BuffProcessProcFunc(LPVOID lParam)
{
    TRACE("BuffProcessProcFunc is started\n");

    UINT nRet = 0;
    long i = -1;
    CSensorPrjDlg *pThread = (CSensorPrjDlg*)lParam;
    BOOL bExit = FALSE;

    pThread->bRun = TRUE;

    while(!bExit)
    {
        if (WaitForSingleObject(pThread->hEventShut, 30) == WAIT_OBJECT_0)
        {
            bExit = TRUE;
            nRet = 0;           // manual terminate
            break;
        }
    }
}
```

Appendix D

```
        }

        pThread->BuffProcessProc();
        //Allow CPU cool down
    }

    SetEvent(pThread->hEventStop);

    pThread->pProcessThread = NULL;
    pThread->bRun = FALSE;

//    CoUninitialize();

    TRACE("BuffProcessProcFunc is ended with code %d\n", nRet);
    return nRet;
}

void CSensorPrjDlg::BuffProcessProc() //Analysis code for port data
{

    CString strLabelX;
    int nCount = 0;

    while(TRUE)
    {
        if (Start < End)
        {
            //Normal order
            BufLen = End - Start;
        }
        else if (Start > End)
        {
            //Last come first out
            BufLen = BUF_SIZE_COMM - Start + End;
        }
        else
        {
            //Data not recived
            BufLen = 0;
        }

        //For large data
        if (BufLen <= 0)
        {
            break;
        }

        int i = 0;
        int j = 0;
        int nSensorFlag = -1;

        //Looking for the very first '\n'
        for (i = 0; i < BufLen; ++i)
        {
            if (RxData[(Start + i) % BUF_SIZE_COMM] == 0x0A)
```

Appendix D

```
{
    nSensorFlag = 0;
    break;
}
else if (RxData[(Start + i) % BUF_SIZE_COMM] == 0x0B)
{
    nSensorFlag = 1;
    break;
}
else if (RxData[(Start + i) % BUF_SIZE_COMM] == 0x0D)
{
    nSensorFlag = 2;
    break;
}
}

// Looking for the header
if (i < BufLen)
{
    TRACE(_T("Find header...\r\n"));

    m_strSensorOriginHex = _T("");
    m_strSensorDec = _T("");

    CString strTemp = _T("");
    for (j = 0; j < i; ++j)
    {
        strTemp.Format(_T("%02X"), RxData[(Start + j) %
BUF_SIZE_COMM]);
        m_strSensorOriginHex += strTemp;

        strTemp.Format(_T("%c"), RxData[(Start + j) %
BUF_SIZE_COMM]);
        m_strSensorDec += strTemp;

        if (j != i - 1)
        {
            m_strSensorOriginHex += _T(" ");
        }
    }

    // renew header pointer
    // i represents ' \n' bits
    Start = (Start + i + 1) % BUF_SIZE_COMM;

    if (nSensorFlag == 0)
    {
        m_strSensorOriginHex += _T(" 0A");
    }
    else if (nSensorFlag == 1)
    {
        m_strSensorOriginHex += _T(" 0B");
    }
    else

```

Appendix D

```
        {
            m_strSensorOriginHex += _T(" 0D");
        }

        m_fSensorData = 0.02f * (atoi(m_strSensorDec) - 512);

        _DATA_BUFFER* pBuff = new _DATA_BUFFER;
        pBuff->nSensorIndex = nSensorFlag;
        pBuff->nTotalGroupCount = m_nTotalGroupCount;
        pBuff->fSensorData = m_fSensorData;
        pBuff->strSensorOriginHex = m_strSensorOriginHex;
        pBuff->strSensorDec = m_strSensorDec;
        PostMessage(UM_DRAW_DATA, 0, (LPARAM)pBuff);

        if (nSensorFlag == 2)
        {
            ++m_nTotalGroupCount;
        }
    }
    else
    {
        break;
    }
}

}

void CSensorPrjDlg::OnBtnClearData()
{
    // TODO: Add your control notification handler code here
    m_ctrlChart1.Series(0).Clear();
    m_ctrlChart2.Series(0).Clear();
    m_ctrlChart3.Series(0).Clear();
}

void CSensorPrjDlg::OnChangeEditXPoints()
{
    // TODO: If this is a RICHEDIT control, the control will not
    // send this notification unless you override the CDialog::OnInitDialog()
    // function and call CRichEditCtrl().SetEventMask()
    // with the ENM_CHANGE flag ORed into the mask.

    // TODO: Add your control notification handler code here
    UpdateData(TRUE);

    if (m_nXPoints > 0)
    {
        m_ctrlChart1.GetAxis().GetBottom().SetAutomatic(false);
        m_ctrlChart1.GetAxis().GetBottom().SetMinMax(0 - m_nXPoints, 0);

        m_ctrlChart2.GetAxis().GetBottom().SetAutomatic(false);
        m_ctrlChart2.GetAxis().GetBottom().SetMinMax(0 - m_nXPoints, 0);

        m_ctrlChart3.GetAxis().GetBottom().SetAutomatic(false);
        m_ctrlChart3.GetAxis().GetBottom().SetMinMax(0 - m_nXPoints, 0);
    }
}
```

Appendix D

```
    }  
}  
  
void CSensorPrjDlg::AddLog(CString strLog)  
{  
    CString strText;  
    GetDlgItem(IDC_EDIT_LOG)->GetWindowText(strText);  
    strText += strLog;  
    strText += _T("\r\n");  
    GetDlgItem(IDC_EDIT_LOG)->SetWindowText(strText);  
}  
  
UINT CSensorPrjDlg::WriteProcessProcFunc(LPVOID lParam)  
{  
    CSensorPrjDlg *pDlg = (CSensorPrjDlg*)lParam;  
  
    return 0;  
}  
  
LRESULT CSensorPrjDlg::OnDrawData(WPARAM wParam, LPARAM lParam)  
{  
    _DATA_BUFFER* pBuffer = (_DATA_BUFFER*)lParam;  
    if (!pBuffer)  
    {  
        return -1;  
    }  
  
    CString strLabelX;  
    if (pBuffer->nTotalGroupCount % 100 == 0)  
    {  
        strLabelX.Format(_T("%d"), pBuffer->nTotalGroupCount);  
    }  
    else  
    {  
        strLabelX = _T("");  
    }  
  
    if (pBuffer->nSensorIndex == 0)  
    {  
        m_ctrlChart1.Series(0).AddXY(pBuffer->nTotalGroupCount, pBuffer->fSensorData,  
            strLabelX, (ULONG)pBuffer->nTotalGroupCount);  
    }  
    else if (pBuffer->nSensorIndex == 1)  
    {  
        m_ctrlChart2.Series(0).AddXY(pBuffer->nTotalGroupCount, pBuffer->fSensorData,  
            strLabelX, (ULONG)pBuffer->nTotalGroupCount);  
    }  
    else if (pBuffer->nSensorIndex == 2)  
    {  
        m_ctrlChart3.Series(0).AddXY(pBuffer->nTotalGroupCount, pBuffer->fSensorData,  
            strLabelX, (ULONG)pBuffer->nTotalGroupCount);  
    }  
  
    m_nTotalGroupCountDrawed = pBuffer->nTotalGroupCount;  
}
```

Appendix D

```
if (pBuff->nSensorIndex == 0 ||
    pBuff->nSensorIndex == 1 ||
    pBuff->nSensorIndex == 2)
{
    m_strBuffLine += pBuff->strSensorOriginHex;
    m_strBuffLine += _T(";");

    m_strBuffLine += pBuff->strSensorDec;
    m_strBuffLine += _T(";");

    if (pBuff->nSensorIndex == 2)
    {
        m_strBuffLine += _T("\n");

        if (g_pFileLog != NULL)
        {
            int nLength = m_strBuffLine.GetLength();
            fwrite(m_strBuffLine.GetBuffer(nLength), 1, nLength, g_pFileLog);
            m_strBuffLine.ReleaseBuffer();
        }

        // fflush(g_pFileLog);

        m_strBuffLine = _T("");
    }
}

delete pBuff;
pBuff = NULL;

////////////////////////////////////
////////////////////////////////////
return 0;
}

void CSensorPrjDlg::OnTimer(UINT nIDEvent)
{
    // TODO: Add your message handler code here and/or call default
    if (ID_TIMER_SCROLL_LEFT == nIDEvent)
    {
        m_ctrlChart1.GetAxis().GetBottom().SetMinMax(m_nTotalGroupCountDrawed -
m_nXPoints, m_nTotalGroupCountDrawed);
        m_ctrlChart2.GetAxis().GetBottom().SetMinMax(m_nTotalGroupCountDrawed -
m_nXPoints, m_nTotalGroupCountDrawed);
        m_ctrlChart3.GetAxis().GetBottom().SetMinMax(m_nTotalGroupCountDrawed -
m_nXPoints, m_nTotalGroupCountDrawed);

        int i = 0;
        int nCount = m_ctrlChart1.Series(0).GetCount();

        for (i = 0; i < (nCount - 1000); ++i)
        {
```

Appendix D

```
        m_ctrlChart1.Series(0).Delete(0);
    }

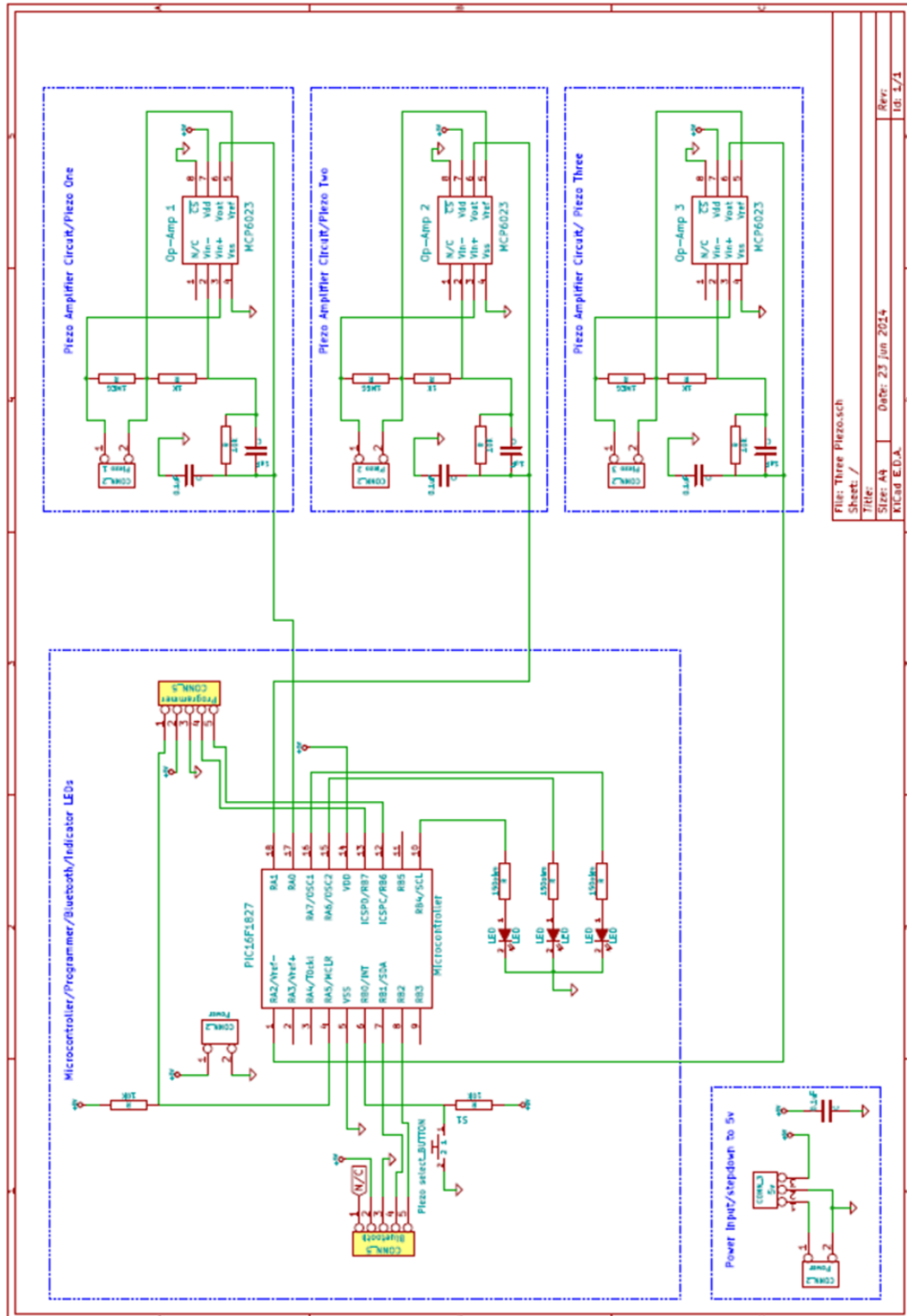
    nCount = m_ctrlChart2.Series(0).GetCount();
    for (i = 0; i < (nCount - 1000); ++i)
    {
        m_ctrlChart2.Series(0).Delete(0);
    }

    nCount = m_ctrlChart3.Series(0).GetCount();
    for (i = 0; i < (nCount - 1000); ++i)
    {
        m_ctrlChart3.Series(0).Delete(0);
    }
}

CDialog::OnTimer(nIDEvent);
}
```


Appendix E: Schematic diagram for the smart cutting tool

Electrical circuitry schematic diagram



Appendix F: Pro-Engineer CAD plotting for the smart cutting tool - top and bottom parts

